Test-cell & On-wing Turbofan Performance Comparison at KLM Engine Services

B. Röell

Delft University of Technology

TU Delft

Test-cell & On-wing Turbofan Performance Comparison at KLM Engine Services

by

B. Röell

to obtain the degree of Master of Science
at the Delft University of Technology,
to be defended publicly on Friday November 29, 2019 at 14:00 AM.

Student number:	4226224	
Project duration:	January, 2019 – November, 2019	
Thesis committee:	Prof. dr. ir. P. Colonna,	TU Delft, chair
	Dr. ir. W. P. J. Visser,	TU Delft, supervisor
	Ir. P. C. Roling,	TU Delft
	Dr. ir. A. Apostolidis,	KLM Engine Services, supervisor

This thesis is confidential and cannot be made public until November 29, 2024

TU Delft

Executive summary

Turbofan engines systematically require Maintenance, Repair & Overhaul (MRO) at specialised shops such as KLM Engine Services. Afterwards, a performance acceptance test in KLM's indoor test-cell is performed, to demonstrate that safety requirements and corrected performance thresholds are met.

After on-wing installation, the same corrected performance indicators are monitored. However, despite correcting for operating conditions and test-cell (TC) or on-wing (OW) specific installation losses, significant differences are observed between official TC and subsequent OW performance. The objective of this research is to identify the main root causes for that discrepancy and to assess the feasibility to reduce it.

The focus is on KLM's CF6-80E1 turbofans, which are monitored on the basis of performance snapshots recorded during takeoff. The key performance indicator is Exhaust Gas Temperature hot day Margin (EGTM), which is a measure of overall thermal efficiency in case of fan speed controlled engines. New test-cells need to be correlated to evaluate the empirical facility modifiers that account for the specific TC related effects. Nevertheless, the OW-TC EGTM differences ($\Delta\mathrm{EGTM}_{\mathrm{OW-TC}}$) are distributed with significant variance and a negative mean.

Gas turbine modelling and a previously developed Gas turbine Simulation Program (GSP) CF6-80 model were studied in preparation. Also a comprehensive list of to-be-analysed potential root causes was composed based on literature research.

First, the correction equations and tables used for OW and TC EGTM were elaborately studied. A comparison of corrections, theory and simulations revealed the physical origin of the TC absolute humidity (AH) corrections and that TC condensation correction precision is questionable. The facility modifier accuracy could not be quantified, but no impact on $\Delta\mathrm{EGTM}_{\mathrm{OW-TC}}$ variance is expected.

Concerning OW EGTM, the data was first adjusted for faults. Then engine-specific non-linear correlations between EGTM and corrected fan speed (N1K) were observed, resulting from ineffective throttle corrections due to engine-to-engine variation of the physical EGT-N1K relation. After merging airport humidity and OW data, engine-specific temperature (TT2) and AH correlations were identified as well. Simulations confirmed that engine condition affects the physical EGT-N1K, -AH and -TT2 relations.

Therefore improvements to the OW EGTM calculations were proposed, based on engine-specific, data-driven customisation of the N1K- and TT2-corrections and an additional AH-correction. A fleet-average 27.5% EGTM scatter reduction was achieved, combined with an average 13°C EGTM reduction because the official corrections are non-conservative. All in all, the method and results are a successful proof of concept for engine-specific corrections, nevertheless the $\Delta\mathrm{EGTM}_{\mathrm{OW-TC}}$ variance was almost unaffected.

The impact of other OW-related causes on $\Delta\mathrm{EGTM}_{\mathrm{OW-TC}}$ was also investigated with statistical analyses backed by theory and simulations. It was concluded that despite inherent unpredictability, condensation and non-gaseous water ingestion are not main root causes for $\Delta\mathrm{EGTM}_{\mathrm{OW-TC}}$. It was found that current corrections over-compensate for customer bleed and under-compensate for anti-ice bleed, but nevertheless the predicted impact on $\Delta\mathrm{EGTM}_{\mathrm{OW-TC}}$ is negligible. Power off-take is implicitly accounted for with the customised corrections, because its use is correlated to N1K and TT2.

The fact that OW performance is recorded before the engine is fully warmed up reduces its EGTM with up to 10°C, therefore thermal effects – amplified by Active Clearance Control – are a primary cause for the mean and variance of $\Delta\mathrm{EGTM}_{\mathrm{OW-TC}}$. The initial rapid EGTM degradation due to seal run-in is also a primary cause for $\Delta\mathrm{EGTM}_{\mathrm{OW-TC}}$. Both thermal and seal run-in effects are unpredictable, therefore effectively correcting for them is impossible with the currently available data.

Finally, a considerable residual gap exists between predicted and observed mean $\Delta\mathrm{EGTM}_{\mathrm{OW-TC}}$, which is allocated to inaccurate facility modifiers, aircraft TT2-sensor bias and the cowling adjustment. Comparison of the predicted and observed variance of $\Delta\mathrm{EGTM}_{\mathrm{OW-TC}}$ also revealed that some scatter is unaccounted for, which is expected to result from unknown aircraft TT2-sensor bias differences, under-predicted thermal effects and combined effect of minor unquantified causes such as condensation.

Preface

This thesis report is the culmination of a year long research at KLM Engine Services, a seven year long time as a student of Aerospace Engineering at Delft University of Technology and a life-long fascination for aviation and technology.

Doing the research has given me a comprehensive introduction to aircraft engine performance and systems. Furthermore the chance to perform my research at KLM Engine Services has helped to put my academic knowledge and skills into practice within an operational engine MRO environment. I want to thank all my colleagues at KLM for their expertise and support as well as the working atmosphere I always felt at home in. The daily walks though the shop and hangars – amid the engines I have been working on – were also highly motivating and never ceased to amaze.

More specifically, I would first of all like to thank my KLM supervisor Asteris Apostolidis for his support, critical feedback, flexibility and sharing a passion for aviation. Furthermore I would like to thank Wilfried Visser for the academic supervision and entrusted freedom. Also I want to thank Rob Duivis for his inexhaustible knowledge of aero-engines, Michel Nollet for his test-cell expertise and my direct colleagues Martijn van der Werf, Albert Timmer and Mike Brull for their daily support. Lastly, I want to thank fellow interns Stijn van Vuuren and Tim Rootliep for the theoretical discussions and making the daily traffic jams a lot more enjoyable.

B. Röell
Delft, November 2019

Contents

List of Figures

List of Tables

Nomenclature

Abbreviations

ACC	Active Clearance Control
AF	Air France
AGARD	Advisory Group for Aerospace Research and Development
AM	Adaptive Modelling
CAS	Calibrated AirSpeed
CEOD	Continuous Engine Operating Data
DP	Design Point (*equivalent: GSP model design point*)
ECU	Engine Control Unit
EDP	Engine Driven Pump
EPR	Engine Pressure Ration
ESM	Engine Shop Manual
FAA	Federal Aviation Administration
FADEC	Full-Authority Digital Engine Control
FM	Facility Modifier (*equivalent: test-cell correction factor*)
GE	General Electric Aviation
GPA	Gas Path Analysis (*equivalent: engine condition/health monitoring*)
GSP	Gas turbine Simulation Program
HD	Hot Day (*definition: ISA+, i.e. T_{flat}, 101,325 Pa & 0% RH*)
HPC	High Pressure Compressor
HPT	High Pressure Turbine
IAS	Indicated AirSpeed
IDG	Integrated Drive Generator
IGV	Inlet Guide Vane
ISA	International Standard Atmosphere
KLM	Royal Dutch Airlines (*Dutch: Koninklijke Luchtvaart Maatschappij*)
KLM ES	KLM Engine Services
LPC	Low Pressure Compressor
LPT	Low Pressure Turbine
MC	Maximum Continuous
METAR	Meteorological Aerodrome Report
MRO	Maintenance, Repair & Overhaul
NAI	Nacelle Anti-Ice
NDE	Non-linear Differential Equation
NLR	Netherlands Aerospace Centre (*Dutch: Nederlands Lucht- en Ruimtevaartcentrum*)
OD	Off-Design
OEM	Original Equipment Manufacturer
OW	On-Wing (*NB: only abbreviated as adjective*)
PTO	Power off-take
RMS	Root Mean Square
SAE	Society of Automotive Engineers
SD	Standard Day (*definition: ISA, i.e. 15°C, 101,325 Pa & 0% RH*)
SL	Sea-Level
SMA	Simple Moving Average
TC	Test-Cell (*NB: only abbreviated as adjective*)
TO	Take-Off (*NB: only abbreviated as adjective*)
VBV	Variable Bleed Valve
VSV	Variable Stator Vane
WAI	Wing Anti-Ice

Greek symbols

γ	Isentropic exponent (*equivalent: ratio of specific heats*)
Δ	Change or difference (*usage: Δx is x change*)
δ	Actual-to-SD pressure correction ratio
η_{is}	Isentropic efficiency
μ	Mean (*usage: $\mu(x)$ is mean of x*)
σ	Standard deviation (*usage: $\sigma(x)$ is standard deviation of x*)
σ^2	Variance
Θ	Actual-to-SD temperature correction ratio

Roman symbols

A	Area (*unit: [m^2]*)
AH	Absolute Humidity (*unit: mass ratio [g/kg]*)
C_p	Isobaric specific heat (*unit: [J kg^{-1} K^{-1}]*)
C_v	Isochoric specific heat (*unit: [J kg^{-1} K^{-1}]*)
CEGT	Condensation correction factor for EGT
CN1	Condensation correction factor for EGT
$\Delta\mathrm{EGTM}_{\mathrm{OW-TC}}$	On-wing to test-cell EGTM difference (*unit: [°C]*)
EGT	Exhaust Gas Temperature (*equivalent: TT45 & units: [K] or [°C]*)
EGTFM	Facility modifier for EGT
EGTK	Standard day corrected EGT (*units: [K]*)
EGTHDK	Hot day corrected EGT (*units: [°C]*)
EGTMDEV	EGTM deviation
EGTM	Hot Day EGT Margin (*in full: EGTHDM & unit: [°C])*
FN	Net thrust (*unit: [kN]*)
h_{ISA}	Pressure altitude (*unit: [m]*)
HEGT	AH-correction factor for EGT
HFN	AH-correction factor for FN
HN1	AH-correction factor for N1
$\dot{m}$	Mass flow (*unit: [kg/s]*)
M	Mach number
$\dot{m}_c$	Corrected mass flow
$\dot{m}_f$	Fuel flow
N1i	Indicated N1 (*units: [rpm] or [%])*
N1	Fan rotational speed (*units: [rpm] or [%] & note: see conventions*)
N2	Core rotational speed (*units: [rpm] or [%] & note: see conventions*)
PR	Pressure Ratio
PSn	Static Pressure at station n (*units: [Pa] & note: see conventions*)
PTn	Total Pressure at station n (*units: [Pa] & note: see conventions*)
R	Specific gas constant (*unit: [J kg^{-1} K^{-1}]*)
$\Re$	Universal gas constant (*unit: [J mol^{-1} K^{-1}]*)
RH	Relative Humidity (*unit: [%]*)
SF	Shunted Factor
SH	Specific Humidity (*unit: mass fraction [%]*)
t	Time (*units: [s] or [minutes]*)
TDEW	Dew point temperature (*unit: [°C]*)
$\mathrm{T}_{\mathrm{flat}}$	Flat-rating temperature (*equivalent: corner point temperature*)
TIT	Turbine Inlet Temperature (*unit: [K] or [°C]*)
TOIL	Oil temperature (*unit: [°C]*)
TTn	Total Temperature at station n (*units: [K] or [°C] & note: see conventions*)
WA	Mass flow (*unit: [kg/s] & note: see conventions*)
WB	Customer bleed flow (*unit: [kg/s]*)
WF	Fuel flow (*unit: [kg/s] & note: see conventions*)
XN1	Temperature correction exponent for N1
XT	Temperature correction exponent for EGT

Parameter naming & numbering conventions

Engine components & station numbering

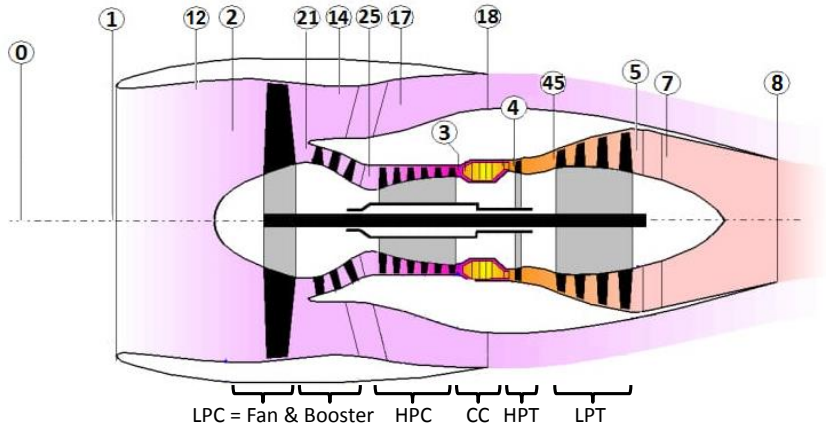

Parameter naming convention

Two parameter naming conventions are described in the table below, which can be defined as:

- ***Component-level:*** Used for individual component performance (e.g. η_{is} for HPC efficiency) and theoretical parameters for isolated components (e.g. $T_{t,\mathrm{in}}$ for turbomachine total inlet temperature)
- ***Engine-level:*** Used for ambient and gas path station conditions (e.g. TT3 for HPC discharge total temperature), measured system parameters (e.g. N2 for core spool speed) and corrected performance indicators (e.g. N2K for corrected core speed and EGTK for Standard Day EGT)

Engine-level and component-level parameter naming conventions

	Engine-level			**Component-level**	
	Measured	*Corrected*	*Margin*	*Measured*	*Corrected*
Rotor speed	N1 N2	N1K & N1Kc [(a)] N2K	- N2M (HD)	N	N_c
Mass flow	WA	WAK	-	$\dot{m}$	$\dot{m}_c$
Fuel flow	WF	WFK	WFM (SD)	$\dot{m}_f$	-
Net thrust	FN	FNK	FNM (SD)	F_{net}	-
Isentropic efficiency	-	-	-	-	η_{is}
Total temperature	TTn [(b)]	TTnK & TTnKHD [(c)]	TTnM (HD) [(d)]	T_t	-
Total pressure	PTn [(b)]	-	-	P_t	-
Static pressure	PSn [(b)]	-	-	P_s	-
Mach number	Mn [(b)]	-	-	M	-

[(a)] *Basic* (N1K) and *fully* (N1Kc) corrected fan speed, see Subsection 4.1.3 for definitions

[(b)] At station number n

[(c)] Only used for EGT (TT45), where EGTK is the Standard Day EGT and EGTKHD is the Hot Day EGT

[(d)] Only used for EGT (TT45), where EGTM is the Hot Day EGT margin

1 Introduction

This chapter introduces the thesis on comparison on-wing and test-cell turbofan performance indicators that culminated to this report. First of all, the industrial context and problem at the foundation of the work are discussed in Section 1.1. Subsequently, Section 1.2 presents how the problem statement was formalised into the thesis research question and objectives and Section 1.3 delimits the research scope. The final section provides an overview of this report's structure.

1.1. Context & problem

Over the last decades turbofans have become the standard propulsion technology for civil aviation, powering millions of daily passengers to their destinations across the globe [1]. Doing so turbofans have proven to be highly reliable machines, often spending thousands of hours and cycles on-wing without major maintenance [2]. Nevertheless, inevitably a turbofan's performance will deteriorate through continuous processes like mechanical wear, fouling and corrosion [3, 4]. Furthermore foreign object ingestion might result in acute engine failure.

In order to guarantee safe operation and sufficient service life turbofan engines will therefore require occasional inspection or Maintenance, Repair & Overhaul (MRO), which is performed by specialised MRO shops given the required expertise for such tasks. An airline's competitiveness greatly depends on cost-effective MRO because the corresponding costs can amount up to 10% of their total direct operating costs [5]. Additionally, effective maintenance will contribute to savings through improved fuel consumption as well [2].

The need for predictable and cost-effective maintenance has gradually turned engine MRO into a competitive market. KLM Engine Services (KLM ES), a major subsidiary of Air France Industries KLM Engineering & Maintenance (AFI KLM E&M), is one of the main engine shops in Europe. It is certified to handle a range of popular General Electric Aviation (GE) engines, among others the CFM56-7B, the CF6-80 family and the GEnx-1B. Current capacity is approximately 200 engine shop visits per year, about half of which are for external clients from all over the world. The facilities based at Schiphol Airport also include a test-cell, facilitating engine testing in a controlled environment.

Following a shop visit, regulations demand KLM ES to demonstrate that overhauled engines meet performance thresholds during a test in the test-cell. Typically the requirements for engine acceptance include meeting net thrust requirements at rated fan speed while maintaining sufficient margins with respect to Exhaust Gas Temperature (EGT) and core speed limits. These measured performance indicators are commonly adjusted to ISA Hot Day conditions through extensive corrections in order to eliminate the effects of operating conditions [6–8]. The resulting corrected performance indicators, such as the EGT Hot Day Margin (EGTM), should therefore be worldwide reproducible. Furthermore they should serve as an accurate prediction for subsequent on-wing performance, which is assessed and monitored based on the same corrected parameters.

The thresholds for the corrected performance indicators are set by the Original Equipment Manufacturer (OEM) and the contract with the client, where the latter often poses the steepest requirements to guarantee sufficient margins - particularly the EGTM - for the planned time on-wing until subsequent

shop visits. A failure to meet set requirements entails considerable costs for KLM ES, on the one hand due to requirement for additional maintenance and tests, on the other hand due to the contractual obligations to provide a replacement engine and pay penalties. Both stressing the importance of accurate measurement and adjustment of the performance margins.

However, despite correcting for operation conditions and test-cell or on-wing specific installation losses, significant discrepancies between test-cell and subsequent on-wing performance have been observed at KLM ES over the last decades. Attempts to define factors for consistent test-cell to on-wing margin conversions and vice versa have proven futile due to the inconsistent nature of the discrepancies, with mean and standard deviation values also varying with engine type.

As a result, engines with insufficient test-cell performance might show sufficient on-wing performance, in which case KLM ES might want to negotiate to disregard the test-cell margins. The other way around, engines with sufficient test-cell performance might show insufficient on-wing performance, in which case KLM ES might expect complaints. Either way the observed differences between on-wing and test-cell performance can put pressure on client-relations, with the ultimate risk of loosing clients. The recognisable need to develop a comprehensive understanding of the observed corrected performance discrepancies is what sparked the thesis assignment on *Test-cell & On-wing Turbofan Performance Comparison at KLM Engine Services* and the subsequent research provided in this report.

1.2. Research question & objectives

Despite the extensive corrections, including terms to account for operating conditions as well as test-cell and on-wing installation losses, comparison of test-cell and subsequent on-wing corrected performance indicators by KLM ES has revealed an inconsistent and significant discrepancy. The facts that a similar problem is encountered at AFI-KLM E&M's Paris test-cell and that GE recently modified the CFM56-7B's shop manual by including a simple term in the EGTM calculations to decrease its average discrepancy, substantiate that undesired corrected performance discrepancies are an industry-wide challenge rather than an isolated incidence. The high variance of the discrepancy has rendered application of straightforward correction factors to predict on-wing margins based on the test-cell acceptance test results impossible.

Therefore, an in-depth analysis of the underlying root causes for the observed discrepancy is needed to fill the gaps in the understanding of the phenomena. Accordingly the research question for the thesis, discussed in this report, that originated from that need is defined as follows.

Research question
What phenomena cause the discrepancy between on-wing and test-cell corrected turbofan performance indicators?

The primary objective for this research, directly related to the above research question, is formulated as follows.

Primary research objective
To identify the main root causes for the discrepancy between on-wing and test-cell corrected turbofan performance indicators by data- and simulation-driven analyses of potential root causes.

Achievement of the above research objective would be considered of great value to KLM ES, potentially serving as a starting point for additional research to eliminate the observed discrepancy. Nevertheless, from a commercial perspective the ultimate goal would be to have full comparability of on-wing and test-cell corrected turbofan performance. Therefore the secondary objective for this research is formulated as follows.

Secondary research objective
To assess the feasibility of reducing the discrepancy between on-wing and test-cell corrected turbofan performance indicators by improving and extending performance indicator corrections.

The actual research work related to either the primary or secondary research objective will be very similar, since achievement of either one will greatly contribute to the other.

The full proposed workload was split into several subsequent task blocks in order to structure the research, all of which can be summarised by one of the corresponding sub-objectives below. These sub-objectives also form the baseline for this report's structure as will be discussed in Section 1.4.

- Investigate current on-wing and test-cell practices.
- Identify potential root causes for the performance discrepancy based on literature research.
- Assess test-cell performance indicator accuracy.
- Assess and improve on-wing performance indicator accuracy.
- Quantify and account for remaining on-wing and test-cell performance indicator discrepancy.

1.3. Research scope

The aforementioned discrepancy is observed for a range of engine types and performance indicators. Answering the research question and achieving set objectives for all those types and indicators might culminate in an amount of work far beyond a masters thesis commitment, especially when considering component-level indicators as well. Therefore this research was scoped in the proposal phase to fit the expected amount of work and depth required for a master's thesis, while also taking into account the availability of required data and commercial opportunities within KLM ES. The scope or delimitation considered during this research is given and substantiated below.

- ***Performance indicators:*** This research focuses on the Exhaust Gas Temperature Hot Day Margin (EGTM), which is the margin of the take-off EGT, corrected to Hot Day conditions, with respect to the EGT limit. This margin is considered the key performance indicator for monitoring on-wing engine performance because it is a direct proxy for overall engine thermal efficiency in case of fan speed controlled engines. Consequently, for the remainder of this thesis report terms regarding engine performance or performance discrepancy will refer to EGTM unless specified otherwise. Subsection 2.2.2 will elaborate on the significance and principle of EGTM as primary engine performance indicator in more detail. Lastly, although corrected thrust margin is also considered a key engine performance indicator during acceptance tests in the test-cell, thrust is not measured on-wing.

- ***Engine types:*** Regarding the engine types, the research will only consider the CF6-80E1A3, used on the Airbus A330-200 and -300 by both AFR and KLM, and the CF6-80C2B1F, used on the Boeing 747-400 by KLM. The research priority lies with the CF6-80E1 because its maintenance is typically performance-driven wherefore accurate performance indicators are critical. Given its similarity with the CF6-80E1, the CF6-80C2 is included in the research on an as-needed basis for validation purposes, either based on additional data-driven analyses or on performance simulations with KLM's validated CF6-80C2 Gas turbine Simulation Program (GSP) model [2]. Section 2.1 will discuss the CF6-80 family in more detail.

- ***Test-cells:*** Since engine MRO shops understandably regard their test-cell engine performance data as confidential, this research will only regard the test-cell facility at Schiphol Airport from KLM ES. Any conclusions on test-cell specific corrections like the so-called facility modifiers will therefore only hold for this specific test-cell. The methods to assess those corrections should however also be applicable to other test-cells with similar protocols if the data would become available.

- ***Data:*** In terms of test-cell acceptance test data all available official performance logs since 2013 will be used. Accordingly, only on-wing data from the same time period will be considered as obtained from the in-house monitoring tool *PROGNOS* and the OEM's monitoring tool *myGEAviation (myGE)*. The on-wing data consist of a single take-off performance snapshot per flight, include corrected performance indicators as well as a set of measured (gas path) parameters.

1.4. Report structure

Now that the context, objectives and scope of the research are defined, this section briefly addresses how the methods, results and conclusions that followed are structured in this report. The overall structure is connected to the sub-objectives that were stated in Section 1.2.

First of all Chapter 2 starts with providing relevant background information, which constitutes to a familiarisation with the General Electric CF6-80 family, an introduction to test-cell and on-wing operation related practices at KLM ES and an overview of the currently observed differences between on-wing and test-cell turbofan performance.

Then Chapter 3 presents an overview of the literature research that was conducted in preparation of the research in later chapters. The chapter includes a review of related work and corrected turbomachinery performance. Gas turbine modelling, including related diagnostics concepts and a previously developed CF6-80C2 model that was used during the research, is also discussed. The core of Chapter 3 consists of composing a comprehensive list of the potential root causes for the observed performance differences that were later investigated.

Thereafter Chapter 4 starts with the assessment of test-cell performance indicator accuracy in order to identify the impact of the test-cell operation related potential causes on the performance discrepancy. The definitions of the official engine performance indicators resulting from test-cell performance testing are also discussed.

In similar fashion Chapter 5 continues by addressing on-wing operation related potential causes. First the official definitions for on-wing performance monitoring are discussed. Then data-driven analyses, supported by theory and simulations, are used to assess the accuracy of those on-wing performance correction methods and the related impact on the on-wing to test-cell performance differences. Chapter 5 also proposes a methodology to improve on-wing performance monitoring accuracy based on engine-specific customised corrections in Section 5.5. The corresponding results are provided in Section 5.6.

Subsequently Chapter 6 provides an updated overview of the on-wing to test-cell performance discrepancy based on the results from Chapters 4 and 5. It also addresses the remaining potential root causes for that discrepancy and finishes off with the overall discussion of results by doing a side-by-side comparison of the predicted and observed performance discrepancy distribution.

Finally, Chapter 7 addresses all conclusions and recommendations resulting from the research. It effectively assembles all sub-conclusions and recommendations from the research chapters into an accessible stand-alone document.

2

Background information

This chapter endeavours to provide a brief but comprehensive overview of the background and setting of this thesis. The reader is familiarised with the relevant MRO-related facilities and practices at KLM ES that form the outlook for the research. A significant share of the information in this chapter was passed onto the author via word of mouth. Important formal sources include a selection of facility and engine manuals [9–14] and previous theses at KLM ES [2, 15–20].

First of all, Section 2.1 provides an overview of the GE CF6-80 engine family. Subsequently Sections 2.2 and 2.3 treat relevant on-wing (OW) and test-cell (TC) related MRO practices. Lastly, Section 2.4 gives an insight into the scale of the current performance discrepancy problem.

2.1. General Electric CF6-80

The long history of the GE CF6 family started in the 1960s with GE's military TF39 and CF6-6 commercial derivatives, which are considered the first high-power, high-bypass turbofans [18, 21, 22]. Continuous demands for performance and fuel consumption improvements resulted in the CF6-50, used on McDonnell Douglas DC-10, Airbus A300 and Boeing 747-300, and subsequently CF6-80. The CF6-80C2 was introduced as early as 1985 and became a very popular choice for Boeing 747-400 and 767, McDonnell Douglas MD-11 and Airbus A310. The CF6-80E1 resulted from a further evolution of the CF6-80C2's design to enable sufficient thrust delivery for Airbus's A330 twin-jet wide-body. It is the most powerful member of the CF6-80 family and entered service in 1993.

Below the general characteristics, important subsystems and onboard sensors are discussed briefly. Please note that the ARP755A turbofan station numbering conventions [23] are used, as depicted by the figure in the conventions in the front matter.

2.1.1. General design & characteristics

The CF6-80C2B1F and CF6-80E1A3, which are the respective ratings used within AF-KLM's fleet, are both categorized as twin-spool, high-bypass and axial flow turbofans. Their primary characteristics are provided in Table 2.1 alongside the cross-section in Figure 2.1. Regarding the table some noteworthy details are:

- ***TO power time limit:*** The provided rated thrust and EGT limits are for TO power setting, which can be maintained for a maximum of 5 minutes. The slight lower Maximum Continuous (MC) power setting can be maintained significantly longer if required.
- ***Flat-rated temperature:*** The flat-rated temperature (T_{flat}) is the maximum ambient temperature TT0 for which the engine can deliver its maximum thrust. If TT0 is above T_{flat}, N1 and consequently thrust are derated to prevent EGT limit exceedance.
- ***Control system:*** Both engine types are N1-controlled using a Full-Authority Digital Engine Control (FADEC) system consisting of an Engine Control Unit (ECU) and accessory actuators and sensors.
- ***EGT shunt:*** Within a single engine type, each rating can have its own physical EGT limit. It is common to use an EGT shunt, which augments the measured value to the indicated EGT such that

the indicated EGT limit is not rating-specific. For example, the indicated EGT redline for the CF6-80E1 is 975°C, while the physical EGT limit for the A3-rating is 1060°C hence a maximum 85°C shunt is applied. The CF6-80E1 uses an analogue shunt, consisting of an electrical resistance that converts sensor output.

- ***EGT sensors:*** In case of the CF6-80, EGT is measured by 8 sensors between the turbines (i.e. TT45). The average value is subsequently reported as the official EGT.
- ***Engine differences:*** Both models are very similar in terms of general characteristics and dimensions, nevertheless modifications were made to achieve the higher thrust rating of the CF6-80E1 including a larger fan diameter, redesigned booster for increased core mass flow and new turbine materials and cooling techniques for increased maximum temperatures [18].

Table 2.1: Engine characteristics of CF6-80E1A3 and CF6-80C2B1F [10–13]

	CF6-80E1A3	**CF6-80C2B1F**
Dimensions		
Diameter	2.9 m	2.7 m
Length	4.3 m	4.3 m
Bypass ratio (TO)	5.1	5.0
Performance & limits		
Rated thrust	69,830 lbf (305 kN)	57,160 lbf (250 kN)
Flat-rated temperature	30°C	32.2°C
Max. pressure ratio	34.8	31.8
Max. indicated EGT	975°C	960°C
Max. EGT shunt	85°C	60°C
Max. N1	3,835 rpm (115.5%)	3,854 rpm (117.5%)
Max. N2	11,105 rpm (113%)	11,055 rpm (112.5%)
Design		
LPC	1 fan, 4 booster stages	1 fan, 4 booster stages
HPC	14 stages	14 stages
HPT	2 stages	2 stages
LPT	5 stages	5 stages
Combustor	Annular	Annular
Controlled parameter	N1	N1
Control system	FADEC	FADEC
EGT sensor station	45	45

2.1.2. Subsystems & important features

A brief numeration of the important subsystems shown in Figure 2.1 is provided below. More in-depth analyses of subsystems are provided in the research chapters when needed.

- ***VBVs:*** The Variable Bleed Valve system enables bleeding of booster discharge air into the bypass duct, which helps to prevent HPC surge during unstable, low N1 conditions such as start-up. All VBVs are closed during takeoff.
- ***IGVs & VSVs:*** The Inlet Guide Vanes and Variable Stator Vanes are used to control the HPC mass flow and flow angles to optimize compression efficiency and reduce risk of compressor surge.
- ***Bleed manifolds:*** Bleed air is extracted from stages 7, 8, 11 and 14, the latter being HPC discharge. The stage 7, 11 and 14 bleed flows are used internally for cooling. During OW operation customer bleed air for pneumatic and cabin conditioning functions is extracted from stage 8, with additional stage 14 flow being mixed in if the stage 8 delivery pressure is insufficient at low power. Furthermore, wing and nacelle anti-ice systems extract stage 11 air for inlet nacelle and wing leading-edge heating.

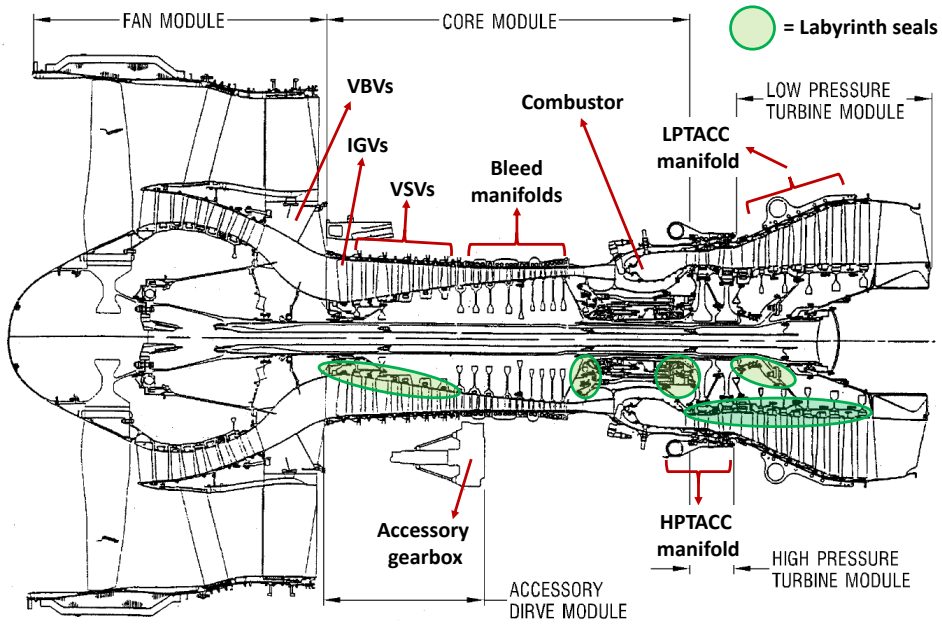

Figure 2.1: Schematic CF6-80E1 cross section (adapted from [14])

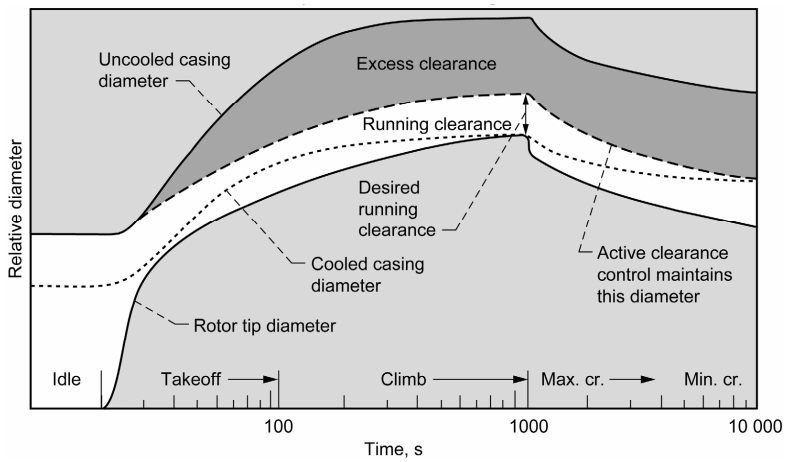

Figure 2.2: Effect of thermal expansion and Active Clearance Control (ACC) on turbine rotor tip clearance (reprinted from [24])

- ***Accessory gearbox:*** This gearbox is connected to the high pressure spool (N2) and drives the Integrated Drive Generator (IDG) and Engine Driven Pump (EDP), which are responsible for electrical and hydraulic power delivery to the aircraft. During test-cell operation the IDG and EDP are not connected to the gearbox.
- ***ACC:*** The Active Clearance Control system uses bypass air for cooling of the HPT and LPT casings. The mass flow that is directed to the HPTACC and LPTACC manifolds is controlled to achieve shrinkage of the casings and consequently minimise turbine tip clearances. The typical effect of thermal expansion on turbine rotor tip and casing diameter, including the effect of ACC on the latter is depicted by Figure 2.2.
- ***Seals:*** Although not distinguishable module, sealing contributes considerably to aero-thermodynamic efficiency by decreasing parasitic flows. Figure 2.3a shows typical sealing locations within a compressor stage, including interstage seals and rotor tip clearance seals. The latter consist of a shroud of abradable material around the rotor blades that is design to withstand occasional rubbing without causing immediate damage.

  Most other seals can be categorised as labyrinth seals, consisting of abradable honeycomb material

as shown in Figure 2.3c and multiple seal teeth as shown in Figures 2.3a and 2.3b). These labyrinth seals are used throughout the engine to prevent leakage between rotating and stationary or other rotating parts.

After replacement of the honeycomb, the seal teeth will start to cut channels. This process is referred to as seal break- or run-in and induces considerable performance deterioration over approximately the first 10 cycles. Afterwards seal clearance and hence deterioration stabilises. As is discussed in Section 3.3, seal run-in is a potential cause for OW-TC EGTM differences.

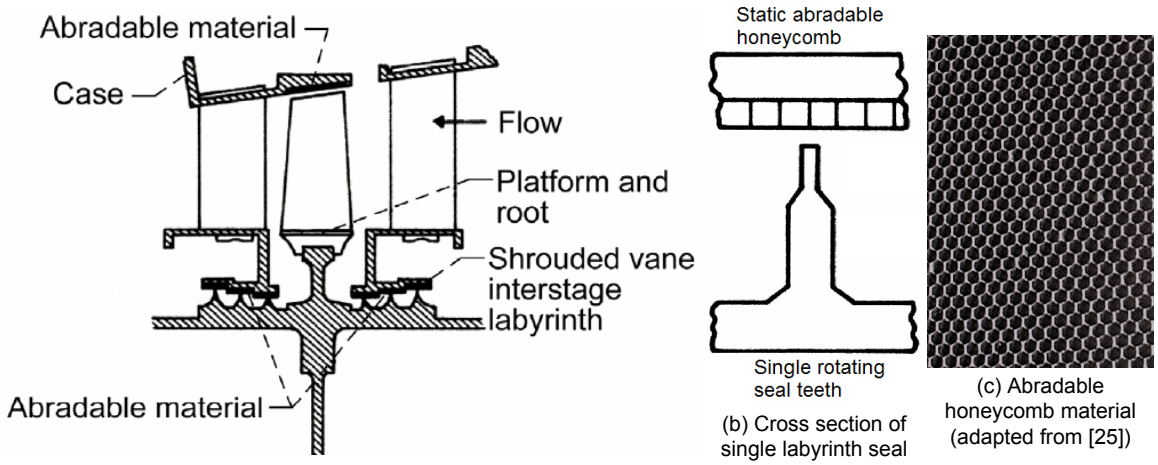

(a) Cross section of compressor seals (reprinted from [24])

(b) Cross section of single labyrinth seal (adapted from [24])

(c) Abradable honeycomb material (adapted from [25])

Figure 2.3: Turbomachinery sealing components and geometry

2.1.3. Sensors

Table 2.2 gives an overview of the most important measured parameters on the CF6-80E1 and CF6-80C2, including relevant aircraft parameters. Some comments regarding the engine and aircraft sensors are given below:

- ***Gas path sensors:*** The main difference in terms of the available gas path sensors originates from the extended sensor package fitted to KLM's CF6-80C2s. The extended sensor package has proven extremely valuable for GPA and modelling purposes [2, 18, 26], while lacking gas path parameters on the CF6-80E1 and GEnX-1B are known to introduce uncertainties [19]. During test-cell operation engines are fitted with additional pressure and temperature sensors such that component performance can be deduced.
- ***Inlet conditions:*** In order to derive corrected performance such as EGTM, the fan inlet pressure (PT2) and temperature (TT2) are required. During on-wing operation, the PT0 and TT0 measured by the aircraft are used for PT2 and TT2. The CF6-80E1 nacelle is fitted with two dedicated TT12 sensors, which are used only if there is a significant TT0-TT12 discrepancy. Lastly PS0 can be derived from aircraft's pressure altitude (h_{ISA}), which is a direct measure of ambient static pressure.
- ***Variable geometry systems:*** The variable geometry and ACC actuator positions, which can be converted to valve and vane angles using known relations [10, 11], are included in OW data.
- ***Bleed & power extraction:*** Customer bleed mass flow (WB) and electrical power off-take (PTO) are measured on the CF6-80E1, although PTO is not included in OW EGTM calculations. Also the selection status (i.e. on or off) of the nacelle (NAI) and wing anti-ice (WAI) systems are included in the data.

2.2. On-wing monitoring practices

Accurate engine monitoring during on-wing operation is of paramount importance to an airline to guarantee safe and efficient operation. The growing popularity of so-called 'power-by-the-hour' contracts

Table 2.2: Engine and aircraft sensors on CF6-80E1 and CF6-80C2
(see nomenclature and conventions for parameter definitions)

Aircraft sensors	**CF6-80E1**	**CF6-80C2**
Aircraft ambient	TT0, PT0, PS0	TT0, PT0, PS0
Aircraft general	Mach (M0), IAS, CAS, h_{ISA}	Mach (M0), IAS, CAS, h_{ISA}
Engine & nacelle sensors		
Gas path temperatures	TT12, TT25, TT3, TT45/EGT	TT25, TT3, TT45/EGT, TT5
Gas path pressures	PS3	PS17, PT25, PS3, PT49
Control and spools	N1i, N1, N1K, WF, N2	N1i, N1, N1K, WF, N2
Variable geometry systems	VSV, VBV, HPTACC, LPTACC	VSV, VBV, HPTACC, LPTACC
Bleed & power extraction	NAI, WAI, WB, PTO	NAI, WAI, WB
Oil system	POIL, TOIL	POIL, TOIL

[27, 28], where clients pay a fixed price for a complete engine MRO package, has engaged shops to develop their monitoring capabilities into an integral part of their provided fleet management program.

Two important distinguishable aspects of engine monitoring are: 1) engine performance monitoring by trending measured and corrected performance indicators like EGTM, N2 and fuel flow; and 2) engine health monitoring by trending derived condition indicators like HPC efficiency [2]. The latter requires the additional process of component condition computation and is often referred to as Gas Path Analysis (GPA).

The remainder of this section will provide a baseline understanding of relevant protocols and practices. Section 3.4 discusses GPA and modelling developments in open literature.

2.2.1. Data management & trending

On-wing performance monitoring of the CF6-80 engines is done primarily based on performance snapshots taken once per flight during takeoff. Snapshot recording is done automatically by the ECU. The ECU takes the snapshot between 40 and 60 seconds after TO power is selected, which should correspond with peak EGT values [29]. The snapshot itself is taking by averaging sensor output over a 10 s period to reduce the impact of sensor noise. The measured values are uploaded for analysis immediately after.

More modern engine types like the GEnX-1B and CFM LEAP-1B also record Continuous Engine Operating Data (CEOD) throughout the flight, which enables more advanced diagnostics in some cases. A drawback of the CEOD is that it is only uploaded after landing.

The measured performance snapshots are retrieved by diagnostics tools that calculate the corrected indicators like EGTM. With respect to this thesis, snapshot data could be collected from two separate source:

- ***PROGNOS:*** Used in-house by KLM ES for monitoring. The tool has diagnostics and prognostics as key features, enabling trending and engine-specific deviation identification. The latter employs Simularity-Based Modelling to identify deviant behaviour. PROGNOS data querying is limited to a single engine's data at once and the database time range is limited to the current install period[(1)].
- ***myGE:*** A web-portal provided by GE, used primarily for (big) data querying at KLM ES. A query widget lets the user specify queries for multiple engine serials, types or families at once, with the database going back to 2001 for most types.

Both tools include the list of measured parameters and several derived indicators such as EGTM and N2 margin. Although EGTM is calculated by the tools separately, as discussed in Section 5.1 it has been concluded that both tools use exactly the same equations and empirical correction tables.

[(1)] *Install period*: the time on-wing between two consecutive overhauls or the time since the last overhaul

2.2.2. EGT margin

The EGT margin (EGTM), short for Hot Day Exhaust Gas Temperature margin, is the primary focus of this research concerning OW-TC performance comparison. First of all arising from the commercial importance of EGTM, because desired improvements are often contractually defined in terms of minimal post-overhaul EGTM. This section provides a physics-based substantiation for the industry's practice to monitor EGTM [29].

EGT & engine efficiency

GE engines measure their EGT between the HPT and LPT (TT45) to serve as an indicator for the Turbine Inlet Temperature (TIT or TT4), which is the highest temperature in the engine cycle. The TIT is not measured directly because this is simply not possible at the high temperature achieved in modern turbofans [30, 31]. For a given engine type, TIT can be considered an indication of how efficient the engine delivers its thrust because component-level deterioration will decrease system efficiency such that it burns more fuel and runs hotter to deliver the same amount of thrust [32]. GE engines are N1-controlled, where similarly less efficient engines require more fuel and run hotter to maintain N1.

Alternatively one could consider the effects at component level. Equation 2.1 gives the isentropic relation for compression, where TR is the Temperature Ratio, PR the pressure ratio, η_{is} the isentropic efficiency and γ the isentropic exponent. HPC deterioration will therefore: 1) increase its discharge temperature (TT3), which will increase EGT if WF is conserved; and 2) increase the HPT mechanical work, which will increase WF and subsequent EGT even more. Figure 2.4 shows the effects of HPC deterioration on the thermodynamic cycle and EGT.

$$\text{TR} = \frac{1}{\eta_{\text{is}}}\left(\text{PR}^{(\gamma-1)/\gamma} - 1\right) \tag{2.1}$$

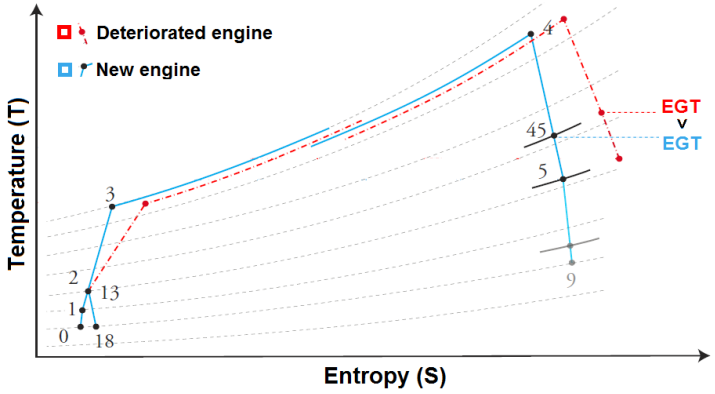

Figure 2.4: Effect of HPC efficiency deterioration on EGT in T-S diagram (adapted from [18])

Correcting for operating conditions

Other than engine aero-thermodynamic condition, the observed EGT is very sensitive to ambient conditions and power setting. Therefore measured EGT is adjusted to acquire the Standard Day EGT (EGTK) and Hot Day EGT (EGTKHD). The EGTK and EGTKHD should be interpreted as the EGT values that would have been measured if the same engine would instead have taken off at rated corrected fan speed (N1K) in SD or HD conditions. Here SD is defined as dry sea-level ISA conditions, while HD conditions are similar except that the engine's flat-rating temperature is used. The exact corrections equations are discussed in Chapters 4 and 5 for TC and OW operation respectively.

Margin

The EGT margin is the difference between the EGT limit and EGTKHD. The advantages of monitoring the margin compared to EGT itself are: 1) an accessible scale where higher values are better; and 2) a straightforward indication of remaining on-wing life for a given stabilised deterioration rate.

Merely to familiarise the reader with EGTM monitoring, Figure 2.5 presents typical scatter and deterioration of EGTM of an single CF6-80E1 over a period of 2000+ cycles. Considering the full fleet, values range between 15°C and 80°C for the CF6-80C2 and between −6°C and 33°C for the CF6-80E1.

Note that negative EGTM is not necessarily a reason to remove an engine, as actual EGT exceedance can be averted by avoiding full rated takeoffs in HD conditions.

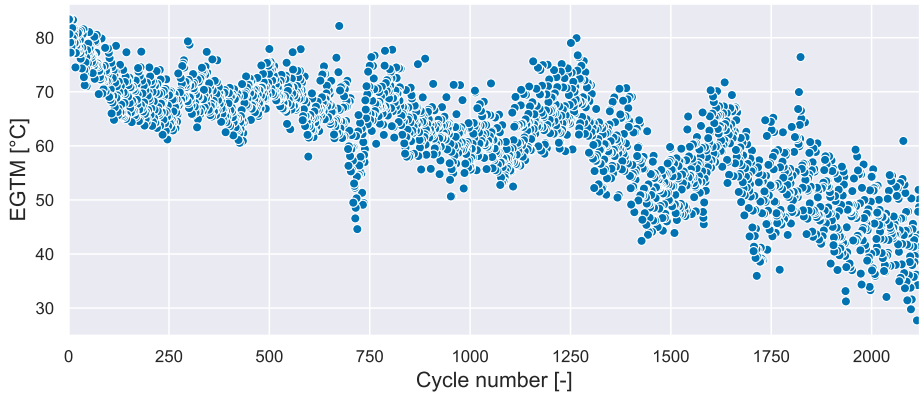

Figure 2.5: EGTM scatter and deterioration for a CF6-80E1 example

Regarding the different aspects of engine monitoring, EGTM can be categorized a performance and a condition indicator simultaneously. It is a dependent parameter that accurately reflects the combined effect of the underlying independent parameters such as component conditions [2, 15]. For example, a study on large civil turbofan life extension techniques showed that EGTM and Specific Fuel Consumption (SFC) are clearly correlated, as a 1°C EGTM decrease was found to be equivalent to a 0.1% increase of SFC [33].

2.3. Test-cell facility & practices

Before being mounted back onto an aircraft for operation, turbofan engines need to demonstrate safe operation while meeting strict performance thresholds. Indoor test-cells are commonly used to provide a quasi-controlled environment to perform these so-called acceptance performance tests. Any uncontrolled influences like atmospheric pressure are carefully measured and then used to correct the measured performance towards well-defined SD and HD conditions.

This section addresses KLM's test-cell at Schiphol Airport, starting with its design and instrumentation in Subsections 2.3.1 and 2.3.2. Subsequently test-cell correlation is discussed in Subsection 2.3.3 and engine testing protocols are discussed in Subsection 2.3.4.

2.3.1. Facility design

KLM ES operates an U-type test-cell, which was commissioned in 1972 [9]. Design and construction were performed by Aero Systems Engineering (ASE) conform GE's requirements [18]. An schematic overview of the facility's design is provided in Figure 2.6.

The flow is first drawn in vertically at the inlet section which subsequently rotates the flow 90° using the turning vanes. The flow passes a screen to reduce flow distortion as it enters the engine section. This section has a 10 by 11 meter cross sectional area, which enables certification of engine delivering up to 100.000 lbs or 450 kN of thrust. The engine is fitted to a frame capable of accurately measuring the thrust force exerted by the engine during operation. The engine's exhaust gas is directed into the augmenter section, which includes metal frames to diffuse the jet with minimum noise production before being expelled in the vertical exhaust section. Preparations and monitoring is done in a separate building which is build detached to prevent propagation of vibrations and noise during testing.

2.3.2. Facility instrumentation

Where possible, the engine's sensors are used during testing. A noticeable exception is thrust, which is not measured directly by the engine. Also parameters depicting TC ambient conditions that might affect performance, such as TT2, PT2 and humidity, are measured by dedicated TC sensors. The key dedicated TC sensors and their positions are discussed below using Figure 2.6. All of these sensors require calibration at regulated intervals of 6 or 12 months to prevent sensor drift [17].

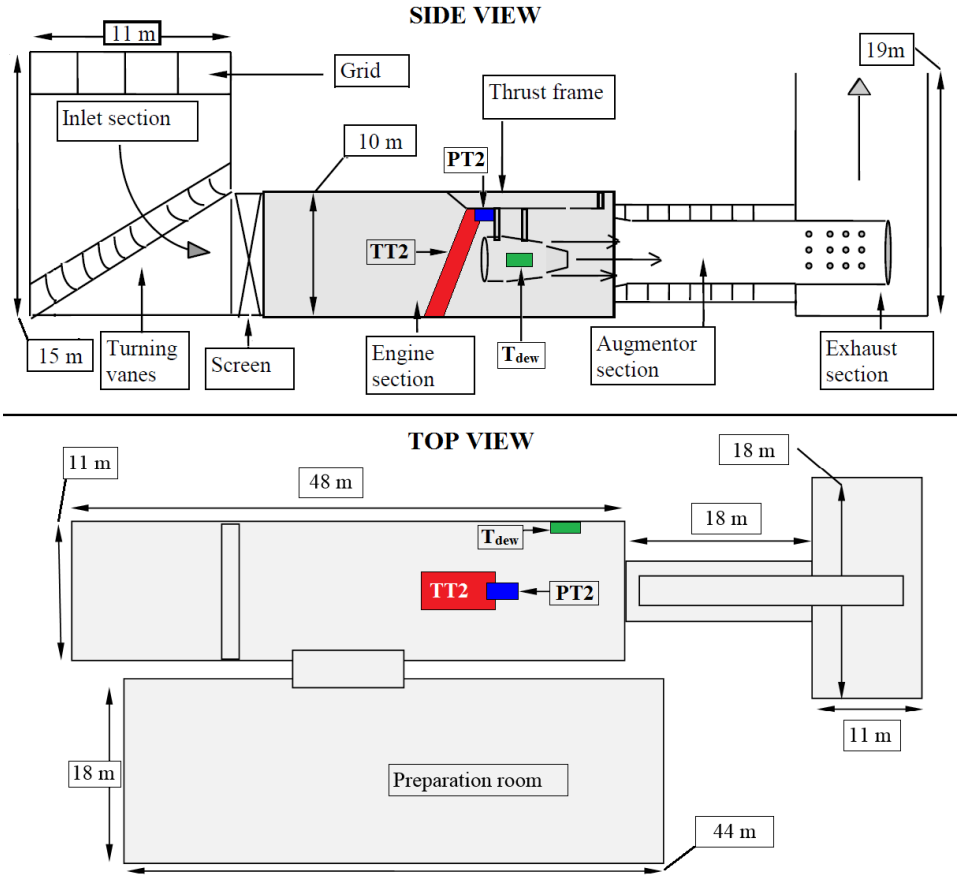

Figure 2.6: Side- and top-view of KLM's test-cell facility including dedicated TC sensor locations (adapted from [9, 17])

- ***Thrust load cell:*** A set of strain gauges is used to measure the thrust force produced by the engine. Elaborate preceding calibration is used to convert the measured strains into the corresponding net force component parallel with the engine's centreline. That net force is affected by indoor testing related drag forces such as ram, entrainment and pressure drag [17]. The empirical corrections to convert measured FN into corrected FN (FNK) are determined using test-cell correlating as discussed in Subsection 2.3.3.

- ***Inlet temperature sensors:*** Temperature measurements are performed by multiple sensors fitted to a metal frame that is fitted in front of the inlet. The average measured temperature is used as TT2. Inlet condensation can change effective TT2, but is accounted for with empirical corrections [10, 11].

- ***Inlet pressure sensor:*** A static pressure sensor fitted to the TC ceiling above the engine inlet measures PS0, which is also used for PT0 and PT2 based on the negligible total pressure losses within the bell-mouth inlet fitted to the engine. Bell-mouth inlets are used in test-cells to prevent the inlet lip separation and improve flow uniformity at the fan face. Although slight errors propagating from incorrect assumptions are theoretically accounted for using the empirical facility modifiers discussed in the next subsection, the position of the PT2-sensor at KLM's facility is undoubtedly questionable.

- ***Humidity sensor:*** Through gas properties changes and potential inlet condensation, atmospheric humidity can have a significant effect on engine performance. To correct for those effects, a humidity sensor is fitted to the side of the engine section next to the engine.

- ***Gas path sensors:*** In order to enable accurate diagnostics of individual component conditions, engines are fitted with additional gas path temperature and pressure sensors if needed.

2.3.3. Test-cell correlation

Indoor testing affects engine performance with respect to outdoor or on-wing operation. To eliminate test-cell specific effects on the corrected performance indicators, GE introduced additional correction factors within the correction calculations. These factors are commonly referred to as Facility Modifiers (FMs) and determined empirically by test-cell correlation.

Initial test-cell correlation

The main steps performed during initial test-cell correlation are summarized below [34, 35].

1. Selection of a single engine for the correlation procedures. In order to eliminate the influence of engine deterioration, it is preferred to use an engine that has flown a considerable number of cycles since overhaul or manufacturing with stable performance.
2. Testing of the engine at GE's baseline outdoor test facility over a wide range of N1-values. The same test is repeated until a sufficient amount of measurements fall within maximum tolerances. For test-cell correlation for CF6-80E1 engines, the corresponding tolerance for EGT is set at 3°C.
3. Testing of the engine at the test-cell that needs to be correlated following the same protocols.
4. Plot the relevant performance indicators with respect to FNK (without the FN-modifier) and determine the FMs to account for any differences. The FMs are programmed into the data acquisition system as polynomials and automatically used when measured performance is corrected.

The correlation reports for KLM's test-cell facility for the CF6-80E1 and CF6-80C2 were issued in 2006 and 1994 respectively and are considered confidential. The examples in Figure 2.7 originate from other outdated correlation reports. There are modifiers for thrust (FNFM), EGT (EGTFM, but still T5FM in the example), fuel flow (WFFM), core speed (N2FM), engine pressure ratio (EPRFM) and mass flow (WAFM). These are applied as a correction factor on the related SD values before being converted to HD conditions. Section 4.1 will elaborate on the TC EGTM calculations, including the use of EGTFM.

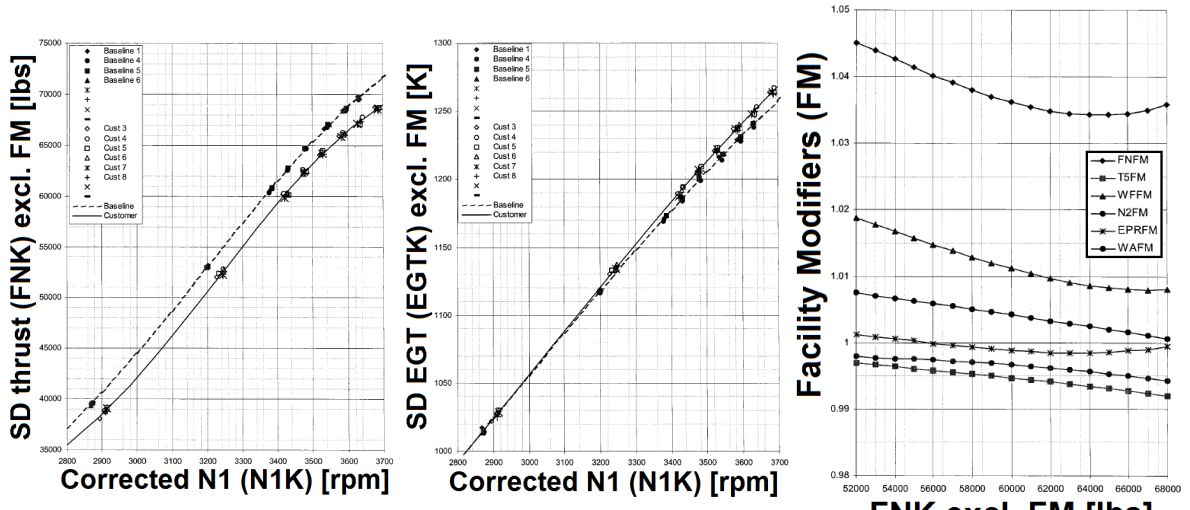

(a) KLM and GE FNK, excluding facility modifier, w.r.t. N1K

(b) KLM and GE EGTK, excluding facility modifier, w.r.t. N1K

(c) Facility modifiers w.r.t. FNK, excluding facility modifier

Figure 2.7: Content from outdated CF6-80E1 test-cell correlation report

Back-to-back testing

Back-to-back testing is used to certify the applicability of the facility modifiers after small modifications to the test-cell's flow path or relocation or replacement of test-cell sensors. First of all, a stable engine is tested until sufficient data within the set tolerances is gathered in the original test-cell without modifications. The same procedure is repeated after the modifications to evaluate if full re-correlation is required. Effects on the corrected performance indicators are considered significant if their changes

exceed pre-defined tolerances [34], such as 5.0°C for EGTK. If significant changes are evaluated, full re-correlation is required or the modification need to be reversed.A single successful back-to-back test is considered valid for all other engine types as well as.

Given the EGTK tolerance of 5.0°C, it is possible that over the course of several back-to-back tests the combined effect of modifications is significant. Given the costs related to a full re-correlation, it is typically avoided. Understandably great efforts are made to design modifications with minimal effect on the validity of the facility modifiers. Agencies like SAE Aviation have published advisory reports on maintaining and trending accurate TC correlation [36] or related topics [35, 37, 38].

2.3.4. Testing procedures

Overhauled engines are first fitted with the test-cowling which consists of a bell-mouth inlet, fan cowling, core-cowling, bypass nozzle and core nozzle. For some engine types this nozzles might have different dimensions than their on-wing counterpart, but with the CF6-80 this is not the case. Next, the engines are attached to the thrust frame and positioned in the testing section using rails on the ceiling.

The full post-overhaul acceptance test procedure can be divided into several distinct phases with distinct goals. The corresponding procedures in terms of power schedule, required inspections and key measured parameters are strictly defined in each Engine Shop Manual (ESM) [10, 11, 39]. Below the main phases are briefly enumerated in the common order, though other orders could also be used if convenient.

1. ***Seal run-in:*** This first phase is required if the abradable material of any seal has been replaced. The phase consist of a gradual step-by-step increase of throttle to gently break-in the seals without risking significant damage. Less gradual engine heating during OW takeoffs typically results additional seal run-in, resulting in rapid performance deterioration over the first ± 10 cycles.

2. ***Vibration check:*** Given the high spool speeds typical for turbofan operation, any imbalance of the rotating components might result in engine vibrations. These vibrations are often continuously measured during testing given the potential damage. A specific acceleration test is performed for analysis of engine vibrations as well as variable geometry operation. In case of intolerable vibrations, trimming is required before the tests are continued.

3. ***Performance check:*** The official TC performance snapshot, at takeoff (TO), maximum continuous (MC), flight idle and ground idle power, are recorded during this test phase. The first snapshot is at TO power, which is recorded after consecutive 5-minute stabilisation at MC and TO power. The other snapshots are taken at 5-minute intervals after stabilisation at the corresponding setting.

   The ECU records the snapshot by averaging sensor output over a 10-second period. The averaging, which is also used for OW snapshots, reduces the effects of sensor noise on the accuracy. During the performance check, the test-cell systems will also accurately monitor oil consumption for potential anomalies. Occasionally the performance testing phase is also used for pre-overhaul inbound testing, but due to cost considerations this is very uncommon.

   The test-cell's data acquisition system calculates the corrected performance indicators based on the snapshot measurements. The results are reported in official performance logs. These performance logs were used during this thesis to link OW and TC data and quantify the resulting EGTM discrepancies.

2.4. Current performance discrepancy

This section provides a baseline for the OW-TC EGTM discrepancy ($\Delta\mathrm{EGTM}_{\text{OW-TC}}$) based on the original data without any improvements, substantiating the scale of the problem faced at KLM ES.

Given the lack of an official protocol for comparing OW and TC performance, first of all two definitions for $\Delta\mathrm{EGTM}_{\text{OW-TC}}$ were chosen in consultation with KLM engineers.

$\Delta\mathrm{EGTM}^{\text{tc}}_{\text{OW}-\text{TC}}$ The difference between the cycle 11-20 average OW EGTM and the official TC EGTM.

$\Delta\mathrm{EGTM}^{\text{ow}}_{\text{OW}-\text{TC}}$ The difference between the cycle 11-20 average OW EGTM and the OW-method-based TC EGTM. That OW-method-based TC EGTM is calculated by applying the OW EGTM calculations on the official TC measurements. Therefore differences between the OW

and TC EGTM calculation methodology are eliminated such that $\Delta\mathrm{EGTM}^{\mathrm{ow}}_{\mathrm{OW-TC}}$ can be allocated to physical differences between OW and TC operation.

First of all TC data was successfully linked with the corresponding OW data for 62 CF6-80E1, 67 CF6-80C2 and 66 CFM56-7B installations. The CFM56-7B and CF6-80C2 are only included in the baseline discrepancy overview to substantiate the scope of the problem.

The resulting baseline differences are visualised by histograms in Figure 2.8. The figure is structured with a row per engine type and a column per TC EGTM definition (i.e. the official or OW-method-based TC EGTM). Furthermore, Table 2.3 summarises the distributions in terms of the corresponding mean values (μ)[2] and standard deviations (σ)[3].

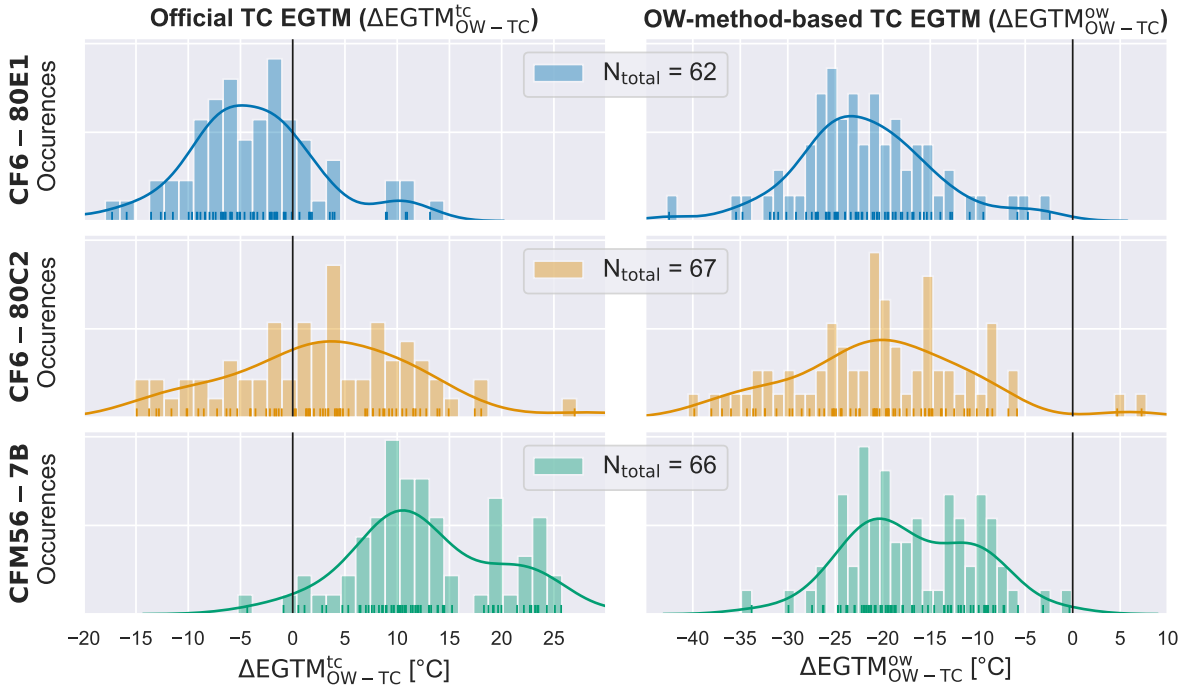

Figure 2.8: Distribution of baseline OW-TC EGTM discrepancy for CF6-80E1 (top), CF6-80C2 (middle) and CFM56-7B (bottom) based on official (left) or OW-method-based (right) TC EGTM

Table 2.3: Baseline differences between OW and TC EGTM, where μ is the average and σ is the standard deviation

Family	Count	Official TC EGTM $\Delta\mathrm{EGTM}^{\mathrm{tc}}_{\mathrm{OW\text{-}TC}}$ [°C]		OW-method-based TC EGTM $\Delta\mathrm{EGTM}^{\mathrm{ow}}_{\mathrm{OW\text{-}TC}}$ [°C]	
		μ	σ	μ	σ
CF6-80E1	62	-3.81	6.69	-21.80	7.28
CF6-80C2	67	3.15	9.17	-20.20	9.36
CFM56-7B	66	12.95	7.28	-16.84	6.78

The main insights to take from the baseline discrepancy are:

- Regardless of its definition and engine family, $\Delta\mathrm{EGTM}_{\mathrm{OW\text{-}TC}}$ is very scattered with standard deviations ranging from 6.78°C to 9.36°C.
- The discrepancy distributions based on the OW-method-based TC EGTM ($\Delta\mathrm{EGTM}^{\mathrm{ow}}_{\mathrm{OW\text{-}TC}}$) all have negative means with only outlier values above zero, therefore suggesting that all engine types normally run cooler in the test-cell than on-wing for the same operating conditions. The differences

[2] *Mean values:* the symbol μ is used throughout the report, additionally $\mu(x)$ represents *the mean of* x
[3] *Standard deviation:* the symbol σ is used throughout the report, additionally $\sigma(x)$ represents *the standard deviation of* x

between OW and TC operation are partly accounted for in the official TC EGTM, based on the fact that the mean values of $\Delta\mathrm{EGTM}^{\mathrm{tc}}_{\text{OW-TC}}$ are higher than $\Delta\mathrm{EGTM}^{\mathrm{ow}}_{\text{OW-TC}}$ for all engine types. On average the additional terms in the official TC EGTM over-correct the OW-TC differences for the CF6-80C2 and CFM56-7B and under-correct for the CF6-80E1.

3

Literature research

In preparation for the research work to identify the root causes for the discrepancy between on-wing and test-cell corrected turbofan performance indicators, a literature study was performed. This chapter handles the topics from the literature research that are relevant to the research discussed in subsequent chapters.

First Section 3.1 starts with a brief introduction to the theoretical non-dimensional and corrected parameters. Subsequently, Section 3.2 continues with an review of related research in open literature and Section 3.3 provides a comprehensive overview of the potential root causes for the performance discrepancy, focussing on the Hot Day EGT margin (EGTM). Lastly, Section 3.4 discusses gas turbine diagnostics and modelling methods in open literature, the methods and features of NLR's Gas turbine Simulation Program (GSP) and the CF6-80C2 GSP model at KLM ES.

3.1. Non-dimensional & corrected performance

The general principle of corrected engine performance indicators is to eliminate the effects of ambient and operating condition, consequently enabling day-to-day and engine-to-engine comparison of those indicators. The origin of corrected engine performance indicators can be found in the use of non-dimensional, quasi-dimensional and corrected parameters in turbomachinery theory. This section briefly introduces the theory of corrected turbomachinery performance and the corresponding parameters at a component and an engine level.

3.1.1. Component parameters

Derivation of corrected parameters at a component level can be based on either a dimensional analysis approach or Mach number similarity approach, both of which are discussed in this subsection.

Dimensional analysis approach

Assuming constant gas properties, the behaviour of a turbomachinery component can be fully described by its geometry, mass flow, rotational speed and total inlet and outlet conditions [40]. The symbolic representation is given below, where D is the characteristic diameter and N the rotational speed [40].

$$\text{Function}\left(D, N, \dot{m}, p_{t,\text{in}}, p_{t,\text{out}}, T_{t,\text{in}}, T_{t,\text{out}}\right) \tag{3.1}$$

Determining the component-specific relations between all those quantities over the full operational range therefore demands an excessive number of experiments, while also making efficient visualisation of those relations impossible [40]. Application of Buckingham Pi's theorem on dimensional analysis enables the derivation of four dimensionless groups: the pressure ratio, temperature ratio, non-dimensional mass flow and non-dimensional rotational speed [40] all of which are defined in Table 3.1. The subgroup $RT_{t,\text{in}}$ is conveniently used instead of $T_{t,\text{in}}$ to ease *non-dimensionalising* [40].

The quasi-dimensionless groups are derived by assuming constant geometry and subsequently the corrected parameters are derived by substituting $p_{t,\text{in}}$ and $T_{t,\text{in}}$ with δ and Θ, which are the ratios between the actual and reference values. The reference values are typically sea-level ISA conditions with the exception of engine-level Hot Day values.

To conclude, theoretically the aero-thermodynamic state of a compressor or turbine can fully described by the corrected mass flow, corrected rotor speed, pressure ratio and temperature ratio, where often isentropic efficiency (η_{is}) replaces the latter. The relations between the 4 parameters can be captured by a performance map, where specification of two parameters directly specifies the remaining two.

Table 3.1: Component-level parameter groups (adapted from [23])

	Theoretical			*Experimental*
	Non-dimensional group	**Quasi-dimensional group**	**Corrected parameter**	**Corrected parameter**
Mass flow ($\dot{m}$)	$\frac{\dot{m}\sqrt{RT_{t,\text{in}}}}{D^2 p_{t,\text{in}}\sqrt{(\gamma)}}$	$\frac{\dot{m}\sqrt{T_{t,\text{in}}}}{p_{t,\text{in}}}$	$\dot{m}_c = \frac{\dot{m}\sqrt{\Theta}}{\delta}$	$\dot{m}_c = \frac{\dot{m}\Theta^a}{\delta^b}$
Rotor speed (N)	$\frac{ND}{\sqrt{\gamma RT_{t,\text{in}}}}$	$\frac{N}{\sqrt{T_{t,\text{in}}}}$	$N_c = \frac{N}{\sqrt{\Theta}}$	$N_c = \frac{N}{\Theta^a}$
Temperature ($T_{t,\text{out}}$)	$\frac{T_{t,\text{out}}}{T_{t,\text{in}}}$	$\frac{T_{t,\text{out}}}{T_{t,\text{in}}}$	$\frac{T_{t,\text{out}}}{\Theta}$	$\frac{T_{t,\text{out}}}{\Theta^a}$
Pressure ($p_{t,\text{out}}$)	$\frac{p_{t,\text{out}}}{p_{t,\text{in}}}$	$\frac{p_{t,\text{out}}}{p_{t,\text{in}}}$	$\frac{p_{t,\text{out}}}{\delta}$	$\frac{p_{t,\text{out}}}{\delta^b}$

Mach number similarity approach

An alternative perspective on corrected parameters arises from the fundamental concept of Mach number similarity, which means that correction to reference ambient conditions should be done in such a way that the Mach number velocity triangles within the turbomachinery component are maintained [6, 41]. If Mach number similarity is achieved, compressibility effects, work and losses are maintained such that the pressure ratio and temperature ratio are also the same [6, 41]. The previously defined corrected mass flow and rotor speed can also be derived on the basis of maintaining Mach number similarity when correcting, as is shown in [41].

To demonstrate that the derivation based on dimensional analysis indeed also implicitly guarantees flow similarity, consider the derivations in Equations 3.2a and 3.2b below where ρ_{in} is the density, A the cross sectional area, C and M_C the axial flow velocity and Mach number and U and M_U the circumferential blade velocity and Mach number.

$$\frac{\dot{m}\cdot\sqrt{RT_{t,\text{in}}}}{D^2\cdot p_{t,\text{in}}\sqrt{(\gamma)}} = \frac{\rho_{\text{in}}\cdot A\cdot C\sqrt{RT_{t,\text{in}}}}{D^2\cdot p_{t,\text{in}}\sqrt{(\gamma)}} = \frac{p_{t,\text{in}}\cdot A\cdot C\sqrt{RT_{t,\text{in}}}}{R\cdot T_{t,\text{in}}\cdot D^2\cdot p_{t,\text{in}}\sqrt{(\gamma)}} = \frac{A\cdot C}{\sqrt{\gamma RT_{t,\text{in}}}\cdot D^2} \propto \frac{C}{\sqrt{\gamma RT_{t,\text{in}}}} = M_{C,\text{in}} \quad \text{[40]} \tag{3.2a}$$

$$\frac{ND}{\sqrt{\gamma RT_{t,\text{in}}}} = \frac{U}{\sqrt{\gamma RT_{t,\text{in}}}} = M_{U,\text{in}} \quad \text{[40]} \tag{3.2b}$$

Therefore maintaining both the non-dimensional mass flow and rotational speed is equivalent to maintaining equal axial and blade Mach number, hence Mach number similarity.

Experimental approach

The practical use of the theoretical corrected parameters is limited by the underlying assumptions [41]. The most restrictive assumptions that typically cannot be replicated during actual operation and will influence Mach number similarity include:

- ***Constant gas properties:*** The gas constant (R) and ratio of specific heat (γ) are both functions of atmospheric humidity, but also vary with temperature and pressure. Therefore atmospheric humidity affects the complete flow field [6]. Theoretical and empirical humidity corrections will be addressed in Section 4.2.

- ***Constant Reynold number:*** The fifth - so far unmentioned - non-dimensional group is the Reynolds number, which is often conveniently ignored because its contribution to turbomachinery behaviour is typically negligible [40]. Nevertheless variation of the Reynolds number will affect Mach number similarity slightly [6, 41].
- ***Constant geometry:*** Although variable geometry systems like Variable Stator Vanes should not affect Mach number similarity if their position is scheduled with respect to N_c [6], other deformations such as thermal expansion will invalidate the constant geometry assumption.

A well-described solution to the above invalidation of the assumptions is the application of empirical exponents a and b. The last column of Table 3.1 shows the assumed definitions for the corrected parameters. Using experiments or simulations the values of a and b can be determined empirically per corrected parameter [6]. Depending on the desired accuracy, the exponents can be defined as constants or as functions of other parameters such as N_c.

Table 3.2: Engine-level parameter groups (adapted from [23])

	Theoretical			*Experimental*
	Non-dimen. group	**Quasi-dimen. group**	**Corrected parameter**	**Corrected parameter**
Mass flow (WA)	$\frac{\mathrm{WA}\cdot\sqrt{R\cdot\mathrm{TT2}}}{D2^2\cdot\mathrm{PT2}\cdot\sqrt{(\gamma)}}$	$\frac{\mathrm{WA}\cdot\sqrt{\mathrm{TT2}}}{\mathrm{PT2}}$	$\mathrm{WAK}=\frac{\mathrm{WA}\cdot\sqrt{\Theta_{2,\mathrm{SD}}}}{\delta_{2,\mathrm{SD}}}$	$\mathrm{WAK}=\frac{\mathrm{WA}\cdot\Theta_{2,\mathrm{SD}}^{a}}{\delta_{2,\mathrm{SD}}^{b}}$
Fan speed (N1)	$\frac{\mathrm{N1}\cdot D}{\sqrt{\gamma R\cdot\mathrm{TT2}}}$	$\frac{\mathrm{N1}}{\sqrt{\mathrm{TT2}}}$	$\mathrm{N1K}=\frac{\mathrm{N1}}{\sqrt{\Theta_{2,\mathrm{SD}}}}$	$\mathrm{N1K}=\frac{\mathrm{N1}}{\Theta_{2,\mathrm{SD}}^{a}}$
Core speed (N2)	$\frac{\mathrm{N2}\cdot D}{\sqrt{\gamma\cdot R\cdot\mathrm{TT25}}}$	$\frac{\mathrm{N2}}{\sqrt{\mathrm{TT25}}}$	$\mathrm{N2K}=\frac{\mathrm{N2}}{\sqrt{\Theta_{25,\mathrm{SD}}}}$	$\mathrm{N2K}=\frac{\mathrm{N2}}{\Theta_{25,\mathrm{SD}}^{a}}$
Fuel flow (WF)	$\frac{\mathrm{WF}\cdot\mathrm{FHV}\cdot\sqrt{(R)}\cdot\eta_{CC}}{c_p\cdot D^2\cdot\mathrm{PT2}\sqrt{\gamma\cdot\mathrm{TT2}}}$	$\frac{\mathrm{WF}}{\mathrm{PT2}\sqrt{\mathrm{TT2}}}$	$\mathrm{WFK}=\frac{\mathrm{WF}}{\delta_{2,\mathrm{SD}}\cdot\sqrt{\Theta_{2,\mathrm{SD}}}}$	$\mathrm{WFK}=\frac{\mathrm{WF}}{\delta_{2,\mathrm{SD}}^{b}\cdot\Theta_{2,\mathrm{SD}}^{a}}$
Temperate (TTn)	$\frac{c_p\cdot\left(\frac{\mathrm{TTn}}{\mathrm{TT2}}-1\right)}{\gamma\cdot R}$	$\frac{\mathrm{TTn}}{\mathrm{TT2}}$	$\mathrm{TTnK}=\frac{\mathrm{TTn}}{\Theta_{2,\mathrm{SD}}}$	$\mathrm{TTnK}=\frac{\mathrm{TTn}}{\Theta_{2,\mathrm{SD}}^{a}}$

3.1.2. Engine parameters

Similarly to the previous subsection, definitions can be derived for a complete gas turbine or turbofan. An overview of these parameter groups and corrected parameters, both theoretical and as a function of empirical exponent, are provided in Table 3.2. Full derivation of the non-dimensional groups is considered beyond the scope of this research because only corrected performance parameters, such as EGTM, are used at KLM ES. Regarding engine corrected parameters, some considerations and explanation:

- ***Spool speeds:*** When a compressor and turbine component are mechanically coupled by a shaft, the definition of engine corrected speed (NK) becomes non-trivial. Defining NK based on compressor inlet conditions does not result in turbine flow similarity because the combustion chamber performance is not constant with Mach number similarity [6]. Nevertheless, corrected spool speed is often defined by the compressor inlet temperature, thus TT2 for N1K and TT25 for N2K for a twin-spool engine. This can be explained by the compressor's variable geometry that should be scheduled with respect its own N_c.
- ***Empirical coefficients:*** Similarly to component corrected parameters, often empirical Θ and δ exponents are used [6] because the assumed constant gas properties, Reynolds number and geometry limit the applicability of the theory. Also, as mentioned above, maintaining Mach similarity within the complete engine is impossible.
- ***EGTM:*** The theoretical Hot Day EGT (EGTKHD) margin can calculated using the engine's EGT redline and filling in TT45 and $\Theta_{2,\mathrm{HD}}$ instead of TTn and $\Theta_{2,\mathrm{SD}}$ in the corrected temperature definition.

In practice, a lot more correction factors and adjustments are used as is addresses in Sections 4.1 and 5.1.

3.2. Related research

Despite the significance of the test-cell and on-wing corrected performance discrepancy, no notable open academic literature asserting the issue has been found. A substantial body of knowledge exists concerning either OW or TC operation of gas turbines as will become evident in subsequent sections. Nevertheless the fundamental causes for an engine to behave differently, in terms of thrust and internal gas path parameters, when comparing indoor TC and OW operation have received no notable attention other than some unsubstantiated remarks. The few advisory reports on accurate test-cell correlation [35, 42] do mention the need to correct for TC effects considering thrust and other performance indicators, but fail to mention the underlying reasons to do so.

Intuitively the absence of notable literature raises one question: *why?*. A probable hypothesis concerns the stiff requirement for a large set of OW as well as TC data, both of which are often considered confidential by the engine or test-cell operator. Therefore universities are generally not able to perform this research. Accordingly, KLM ES is one of the limited institutes including the OEM and other MRO shops with OW data availability that possesses the required data. It is admittedly possible that other commercial corporations have made efforts to solve the apparent problem but have kept the results confidential.

Currently engineers at KLM ES deal with the discrepancy based on previous experience and engineering sense. Accurate prediction of the to-be-expected discrepancy based on previous experience or statistical data is challenging, given the large scatter of the discrepancy. Therefore the scientific value of this research, which aims to identify the fundamental root causes and study the feasibility of parameter corrections to predict discrepancies, is evident.

Given the availability of OW and TC data, some previous studies at KLM ES [2, 16, 19, 43] utilized OW gas path and performance data in conjunction with TC data. For instance for engine performance model calibration at derated power settings. In those studies the model errors induced by the discrepancy were considered acceptable, particularly for Adaptive Modelling (AM) Gas Path Analysis (GPA) purposes [19].

3.3. Potential causes for performance discrepancy

Finding an explanation for the observed OW-TC discrepancy demands familiarisation with the potential underlying root causes and their influence on turbofan performance. This section summarises the literature study on potential root causes. Some of the causes are already accounted for in the current corrections but are nevertheless included for completeness and for later accuracy evaluation. The purpose of this overview is to provide a brief introduction, more details are provided later in the report where required.

3.3.1. Ambient conditions

Ambient pressure and temperature are corrected for, but the effects of humidity and water ingestion are potential causes for a performance discrepancy between on-wing and indoor test-cell operation.

Humidity

Humidity effects can be categorized into condensation effects and gas property effects [44].

- ***Condensation effects:*** These effects depend primarily on how close an air-water mixture is to saturation, which is expressed by Relative Humidity (RH) that typically varies between 100% and value close to 0%. Inlet condensation is complex and unpredictable phenomena [23, 45], occurring typically at very low flight Mach numbers when flow is accelerated into the inlet resulting in a local decrease of static temperature and pressure. In combination with high ambient RH, part of the water vapour can condensate in the inlet which increases the actual inlet conditions at the fan. The affect of condensation can be interpreted as an adverse shift of corrected performance [46] or as an increase of gas path temperatures due to the irreversible nature of condensation (and subsequent evaporation) [23, 45]. Furthermore, inlet condensation can also affect long-term deterioration [47].

- ***Gas property effects:*** The effects on engine performance effects through gas property changes scale with absolute (AH) or specific humidity (SH), both of which are a measure of the water mass content in an air-water mixture [46]. For a given RH percentage, AH will increase with ambient temperature. For example, at ISA+15°C and 100% RH the absolute humidity equals 27.2 g/kg.

  The net effect of AH is a decrease of EGT and FN [44, 46, 48], which can mainly be contributed to the decrease of the effective corrected fan speed and mass flow [46, 49, 50]. Correcting for the gas property effects of humidity has been demonstrated to improve modelling [44] and diagnostics accuracy [48]. An example hereof with an industrial gas turbine is depicted by Figure 3.1. A cyclic variation of compressor corrected mass flow ($\dot{m}_c$) is observed if humidity is not accounted for.

Test-cells are fitted with a humidity sensor to correct the performance to dry conditions [10, 11, 39]. Due to the challenges related to accurate measurement of humidity [51], humidity is not measured during OW operation such that the humidity effects potentially contribute to the OW-TC EGTM discrepancy.

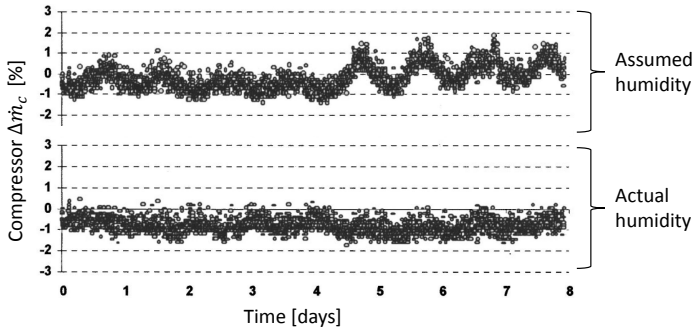

Figure 3.1: Effect of assuming standard humidity (60% RH) or accounting for actual humidity on compressor corrected mass flow ($\dot{m}_c$) evaluation of power-controlled industrial gas turbine (adapted from [48])

Non-gaseous water ingestion
The effects of ingestion of non-gaseous water on engine performance can have an aerodynamic (e.g. water films on blades), thermodynamic (e.g. water evaporation within the engine) and mechanical (e.g. water centrifuging by fan blades) nature [46, 52]. The relative impact of the different contributions depends on many parameters, including the water-to-air ratio, droplet size and flight speed. Although general trends can be identified, reliable corrections for water ingestion are deemed unrealistic due to the high complexity and poor scalability [46, 52, 53].

Nevertheless non-gaseous water ingestion is a potential cause for OW-TC EGTM discrepancy because it does potentially affect OW EGTM and does not affect indoor TC EGTM.

3.3.2. On-wing installation

Some aspects of OW installation are distinctly different from TC operation and therefore potential causes for the discrepancy.

Inlet & flow distortion
Inlet flow distortion can originate from atmospheric distortion or inlet flow separation. Despite the impact of flow distortion on compressor stability, both experiments [38] and simulations [54] have revealed small effects on overall aero-thermodynamic engine performance at high power settings. Flow distortion can also influence corrected performance when a distorted pressure reading is used as the ambient pressure for corrections [41, 54].

Acceptance tests are performed with a dedicated bell-mouth inlet, which is specifically designed to deliver non-distorted flow to the fan given the stationary conditions [19]. On-wing inlet geometry is significantly different to assure efficient operation in high speed conditions as well. While flow distortion effects on engine performance are expected to be negligible [54], the inlet pressure losses at TO conditions could introduce a discrepancy between assumed and actual fan inlet pressure [55]. The combination of flight speed and power setting will dictate the inlet capture ratio (A0/A1). If A0 > A1 than

flow separation dominates overall pressure losses, otherwise if A0 < A1 duct skin friction dominates pressure losses as shown in Figure 3.2 [41]. The expected effect of sub-optimal inlet pressure recovery on EGTM is small because theoretical [6] and actual EGTM calculations are independent of PT2.

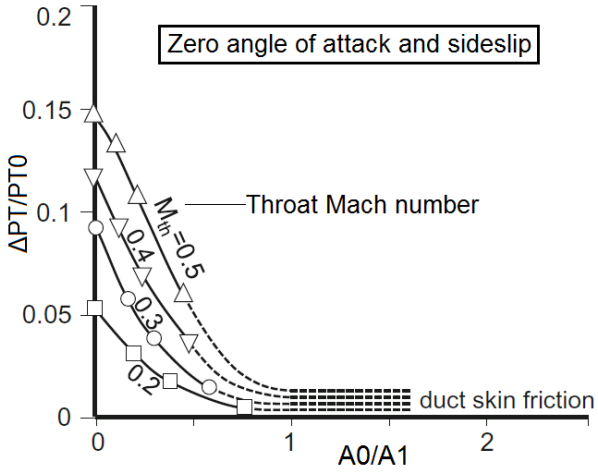

Figure 3.2: Theoretical variation of inlet total pressure loss with throat Mach number and inlet capture ratio (adapted from [41])

Nozzle geometry
Similarly to the inlet, some engine types are tested with dedicated TC core nozzles. In that case the geometrical differences between the TC and OW nozzle are a potential cause for performance discrepancy. Thrust is certainly the most affected performance indicator, while the effect on EGTM primarily depends on whether the core nozzle and LPT are choked [42, 56, 57]. In case of both CF6-80 types there is no known difference between OW and TC nozzles and therefore this cause will not be addressed later in the report.

Unsteady operation
As has been discussed in Subsection 2.3.4, TC performance data is measured when the engine is in aerodynamic, thermal and mechanical steady-state which is certainly not the case for OW snapshots. Despite the 10-second averaging, the unsteady nature of OW operation will affect OW performance to some degree and hence potentially contributes to OW-TC EGTM discrepancy.

The ECU typically records the OW snapshot just before or after lift-off close to peak EGT [29] when full steady-state is impossible. The combination of aircraft acceleration, climbing and manoeuvring as well as ground effects and flow distortion will continuously change the engine operation conditions during this flight phase [2].

Furthermore the lack of thermal equilibrium means the engine itself is also (slightly) changing due to thermal expansion of its components and parts. Before thermal equilibrium is reached clearances are often larger such that cycle thermal efficiency is temporarily decreased [24]. Active clearance control potentially behaves differently in an unsteady thermal state as well, which could amplify the OW-TC differences.

Customer bleed & anti-ice
Customer bleed refers to bleed air extraction for use by various aircraft systems, including nacelle and wing anti-ice, cabin pressurisation and the pneumatic pumps. As has been discussed in Section 2.1, customer bleed is extracted at stage 8 of the HPC during takeoff in the CF6-80 engines.

The effects of customer bleed on compressor and engine performance are well-defined by open-literature research [2, 15, 58–62]. Customer bleed will adversely affect EGT, in essence because the difference between compressor and turbine mass flow requires the engine to burn more fuel and run hotter to maintain the selected N1. Figure 3.3 depicts the *signature* effects for extracting 1% of compressor discharge mass flow ($\dot{m}_3$) from a power-controlled, single-spool industrial gas turbine. Assuming EGT values in the order of 1000 K, the magnitude of the bleed effect on EGT is at least in the order of 13°C.

To conclude, customer bleed affects turbofan operation and is therefore a potential cause for the performance discrepancy. As will be discussed in Section 5.1 current OW EGTM calculations include a term to correct for bleed effects, assessing the accuracy of that method is part of the research.

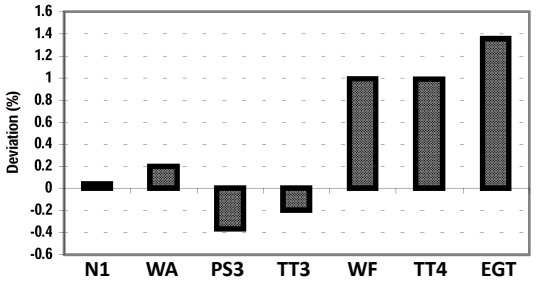

Figure 3.3: Relative effects of 1% compressor discharge flow extraction (at PS3 and TT3) on gas path parameters for an industrial power-controlled, single-spool gas turbine (adapted from [60])

Power Off-Take (PTO)
During OW operation mechanical work for generation of electrical power and hydraulic power is extracted from the engine. The effect of PTO on turbofan performance specifically has received little academic attention. Perhaps a consequence of the fact that most effect-studies are based on industrial gas turbines where PTO is not a disturbance. The fact that previous studies at KLM ES assumed constant PTO [2, 19] suggests a small influence on performance.

Similar to customer bleed, PTO theoretically adversely affects engine performance because the engine will burn more fuel and run hotter to deliver the required mechanical work while maintaining N1 [63].

Seal run-in
As discussed in Section 2.1, engines use seals to minimise undesired spillage air flows. Replacement of the abradable materials of those seals is a typical part of engine performance overhaul [24], but is associated with rapid EGTM deterioration during approximately the first 10 OW cycles due to seal run-in. In contrast to all other potential causes, seal run-in is therefore related to a physical change of the overall condition of the engine between the compared TC and OW snapshots while all other potential causes are related to operational changes.

The varying magnitude of initial EGTM degradation due to seal run-in almost certainly contributes to the mean and variance of $\Delta\mathrm{EGTM}_{\mathrm{OW-TC}}$.

3.3.3. Test-cell effects

Indoor testing primarily affects the measured thrust, which is discussed in the first paragraph below. The physical meaning of the facility modifier for EGTK is addresses subsequently.

Test-cell effects on thrust
The aerodynamics of indoor testing produce drag forces on the engine that primarily affect the net thrust. A comprehensive overview of those drag forces in provided in Figure 3.4. The aerodynamics of these drag forces have received considerable academic attention in work such as [7, 64–67]. The main force acting on the engine is the propulsive jet thrust in combination with potential pressure thrust due to under-expansion of the jet (i.e. exit buoyancy force in Figure 3.4). The major drag forces can be categorised as either: 1) forces resulting from acceleration of engine and test-cell bypass flow, such as intake momentum drag, cowling friction drag and cradle drag; and 2) forces resulting from static pressure gradients in flow direction, such as engine and bell-mouth buoyancy forces [7].

As discussed in Section 2.3.3 on test-cell correlation procedures, GE accounts for these effects by testing an engine at both their outdoor facility and the to-be-correlated indoor facility. The so-called facility modifiers, which should capture all indoor testing related effects, are hence determined purely empirically.

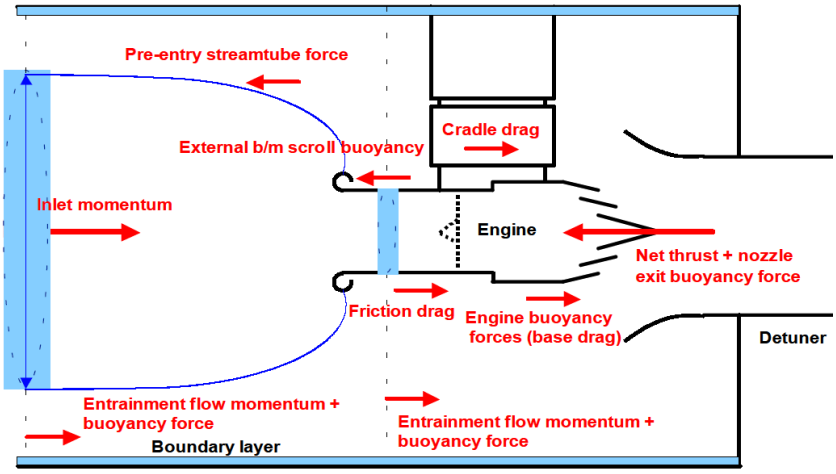

Figure 3.4: All thrust and drag forces related to indoor test-cell operation that are included in the full *first principles* thrust correction method (original from [7])

Various alternatives to an empirical method have proposed, primarily to circumvent the need for the costly free-field outdoor testing [7]. Due to inherent sensitivity to outdoor conditions like atmospheric conditions, micro-climate and pollution, it has also become increasingly challenging to achieve the required consistency for empirical correlation with outdoor test facilities [7]. Several physics-based methods based solely on indoor test-cell measurements have been proposed [7, 64], among others Rolls-Royce's patented *first principles* method [7] which combines facility and engine geometry with an anemometer and pressure sensors to calculate the magnitude of each of the drag forces shown in Figure 3.4. Detailed CFD-based corrections have also received attention [66].

Test-cell effects on EGTK

The physical reasoning for other corrections, such as the EGTK and N2K modifiers at KLM's facility, have received no notable academic attention. Advisory reports from the FAA [42] and SAE [35] both mention that typically only FNK should be modified when the core exhaust nozzle is choked, while otherwise more performance indicators require slight correcting. Some potential physical explanations for the application of an EGTK facility modifier (EGTFM) are listed below.

- ***Inlet condition sensors:*** The facility modifiers are applied to Standard Day EGT (EGTK), which is a function of the observed EGT as well as other terms including the inlet temperature (TT2) correction. Therefore differences between the indoor and outdoor facility TT2-sensors will result in different EGTK even is the observed EGT is unaffected. Apart from sensor positioning, sensor characteristics like the total temperature recovery factor (r) can also influence the recorded temperature. This factor is defined by Equation 3.3 and can vary slightly with inlet Mach number as shown in Figure 3.5 [41].

$$r = \frac{\mathrm{TT}_{\mathrm{measured}} - \mathrm{TS}}{\mathrm{TT}_{\mathrm{true}} - \mathrm{TS}} \tag{3.3}$$

- ***Jet flow restrictions:*** The engine's propulsive jets are directed into the augmenter section that is designed to decelerate the flow, which restricts the jet compared to outdoor testing. With an unchoked nozzle, any effects the flow restriction has on the jet itself could propagate back into the engine. Although unconfirmed, it is suspected that this principle explains why FAA and SAE only advice to correct EGTK if the core nozzle is not choked [35, 42]. In the CF6-80 family the EGT sensor is however located between the turbines, therefore the effects should not be able to propagate back through the choked LPT and affect EGT or N2.
- ***Re-ingestion:*** Although the likelihood is not disclosed, Ramos [65] mentions re-ingestion of exhaust gas as a potential contributor to the need for EGTFM. Re-ingested hot exhaust gases through circulation in the test-cell could significantly increase the effective TT2 and therefore EGTK, that is if TT2 sensor rakes do not capture the changing inlet conditions and hence the effects are not corrected for.

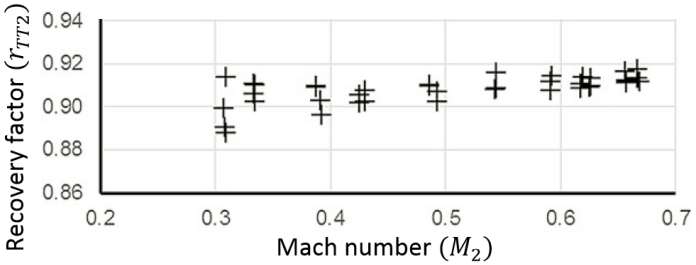

Figure 3.5: Inlet total temperature recovery (r_{TT2}) variation with respect to inlet Mach number (M_2) from CFM56-7B testing at TAP's indoor test-cell in Portugal (adapted from [41])

3.3.4. Sensors

Every sensor is characterized by measurement bias and noise, furthermore sensor positioning greatly affects what is actually measured. Effective TC instrumentation guidelines are documented in reports from SAE [37], FAA [42] and AGARD [68], many of which also apply to OW operation. By automatically averaging values over a 10-second period, the effects of high-frequency sensor noise are already reduced considerably.

Nevertheless sensors can contribute to the observed OW-TC performance discrepancy if some parameters are not measured by the same sensors or at the same location. Where possible, TC performance measurements are made using the engine's onboard sensors such that sensor bias and noise are unlikely to contribute to the observed performance discrepancy. Given that the OW-TC EGTM comparison is based on OW cycle 11-20, the same holds for sensor drift. The most notable exceptions are the inlet conditions and fuel flow, which are measured by aircraft sensors.

On-wing PT2 and TT2 are assumed equal to PT0 and TT0, which are measured at the nose of the aircraft. Therefore sensor drift, bias and noise can all contribute to OW-TC EGTM discrepancy The Airbus A330 CF6-80E1 engine nacelle is also fitted with two TT12 sensors on the inside of the inlet cowling, which is only used for corrections if there is a significant difference between TT0 and T12. Since theoretical corrections of EGT are insensitive to PT2, it is expected that inaccuracy in PT2 should not affect EGTM considerably. The effects on FNK will be more considerable, but thrust is not measured during OW operation.

Test-cells are typically fitted with dedicated fuel flow sensors [37, 42, 68], so sensor bias and noise potentially contributes to OW-TC WFK discrepancy which substantiates the industry's practice to focus on EGTM instead of WFK.

3.3.5. Correction calculations

The above subsections have discussed physics-based potential causes for OW-TC EGTM differences. However, the correction methods used to translate measured performance into the corresponding Hot Day (HD) equivalent can also contribute to the discrepancy.

- ***Numerical differences:*** With different OW and TC EGTM calculation methods, the same measured EGT produces different EGTM values. In case of correction terms like the facility modifiers, the numerical difference is included on purpose.

- ***Inaccurate corrections:*** Alternatively inaccurate corrections can impact OW-TC discrepancy even if the method and relations are exactly the same. Failure of the corrections to capture physical relations, either by inaccurate empirical tables or incorrect mathematical models, is a contributor to OW EGTM scatter and potentially contributes to the OW-TC discrepancy as well.

  For example, consider the throttle push correction used to account for de-rated (i.e. N1K < $\mathrm{N1K_{rated}}$) takeoffs by adjusting EGT accordingly. If inaccurate, there will be a residual correlation between EGTM and N1K due to under- or overcompensating. Adding the fact that TC snapshots are taken at higher N1K than the average OW snapshot, such an EGTM-N1K correlation will contribute to the OW-TC EGTM discrepancy.

The definition and quality of the correction equations will receive ample attention in this report. Sections 4.1 and 5.1 will elaborate on the current TC and OW EGTM methods respectively, while the

considerable data-driven efforts to improve OW EGTM accuracy are discussed in the remainder of Chapter 5.

3.4. Gas turbine modelling

Gas turbine modelling and simulation have been used throughout the research. Although KLM's license for the Gas turbine Simulation Program (GSP) from the Netherlands Aerospace Centre (NLR) determined what tool was to be used, a literature study was nevertheless performed to familiarise with modelling methods and their corresponding advantages and limitations. Initially, engine diagnostics or Gas Path Analysis (GPA) was also expected to contribute considerably to the research work, therefore the principle of GPA and the corresponding methods will be discussed in subsequent subsections. Since GPA methods are distinguished in terms of the underlying modelling techniques [5, 69], most of the subsequent review is also relevant purely considering gas turbine modelling without the diagnostic principles of GPA.

3.4.1. GPA principle

GPA is used to identify or quantify component condition problems [2] by evaluating independent, unmeasurable variables based on the dependent, measurable variables. Common independent, condition parameters are corrected mass flow ($\dot{m}_c$), isentropic efficiency (η_{is}) and Pressure Ratio (PR) [2]. Often engine condition is expressed in terms of condition deviations (i.e. *deltas*) with respect to reference conditions. Therefore, $\Delta\eta_{\mathrm{is}}$ specifies how much the efficiency deviates from reference map η_{is} at the measured component corrected spool speed (N_c)[(1)] and pressure ratio.

Since the first introduction of GPA by L.A. Urban in 1967 [70], a wide range of GPA methods has been developed [5, 69]. Some methods were designed specifically for fault diagnostics, therefore prioritising component fault identification with minimal risk of false alarms. Other methods were designed for deterioration monitoring, therefore prioritising component condition quantification with minimal uncertainty. The relation between the required number of measured parameters (N_P) and the calculated number of condition deltas (N_Δ) also differs between methods. The next paragraph briefly discusses the most popular GPA approaches. GPA methods based on transient data, as reviewed in [69], are out of scope since the thesis only considers (almost) steady state performance snapshots.

3.4.2. Modelling & GPA methods

This subsection briefly discusses the most important categories in Gas Path Analysis (GPA), typically distinguished in terms of the underlying modelling methods.

Linear model-based GPA

First introduced by Urban in 1967 [70] and based on linearisation of the engine model to produce the Influence Coefficient Matrix (ICM). The inverted ICM, often called the Fault Coefficient Matrix (FCM), is then used to derive the independent condition parameters from the measurements. The method is deterministic and requires $N_\Delta \leq N_P$ [5]. Although Kalman-filter and weighted least squares methods have been used for noise handling improvements, they also introduced new drawbacks like smearing [5, 69]. Most importantly, the assumed linearity is only valid in a small region around the chosen point for linearisation [2, 5, 19, 69].

Non-linear model-based GPA

Non-linear model-based methods were developed to take into account the non-linearity of gas turbine and component performance [69]. Two popular methods to utilise the non-linear models for GPA are discussed here, although many related methods are described in GPA reviews [5, 69].

- ***Adaptive Modelling (AM):*** Introduced by Stamatis in 1990 [71], AM is based on iterative adaption of an engine model until it accurately describes measured performance [15, 19]. Effectively, AM determines the actual engine condition by iteratively adapting the model and applying the above mentioned linear GPA method [2, 71]. Since AM produces deltas rather than absolute component

(1) N_c *vs N1K:* Two parameter naming conventions are used in this report: 1) component-level parameters are represented by mathematical symbols (e.g. N_c and $\dot{m}_c$, where subscript c denotes SD-corrected value); and 2) engine-level parameters are represented by abbreviations (e.g. N1K, WAK and EGTM) based on GE's nomenclature

condition values, model errors that affect both the analysed and reference engine are mostly cancelled out [19]. Furthermore AM can identify and quantify faults and deterioration with respect to the reference condition. Typically AM is limited by the $N_\Delta \leq N_P$ requirement and its deterministic nature [5]. Convergence issues can also hamper AM-based GPA.

- ***Genetic Algorithm (GA):*** Model-based GPA can also be interpreted as an optimisation problem, where the objective is to minimize the discrepancy between the predicted and measured performance at the given operating point [5, 69] or set of operating points [72]. Application of a GA[(2)] to solve the optimisation problem has several distinguishable advantages, foremost the ability to deal with noise [2, 5, 69]. Noteworthy drawbacks are the computational cost and the effort to set-up a GA [5].

Empirical GPA

These methods, also referred to as data-driven or Artificial Intelligence (AI) methods, do not require knowledge of the underlying aero-thermodynamic principles or engine performance models [2]. Despite the wide range of empirical methods, there is a shared overall concept: a large dataset of engine faults including the corresponding performance deviation is used to train the AI system, afterwards the system is used to predict the likelihood of a fault when new inputs are provided. Therefore empirical GPA methods are most useful for fault identification by being able to *concentrate* rather than *smear* [5]. Popular categories of empirical GPA include Artificial Neural Networks (ANN), Expert Systems (ES), Bayesian Belief Networks (BBN) and fuzzy-logic method [5, 69].

Common main advantages of AI methods are the low operational computational cost and the ability to deal with data bias and noise [2, 5, 19, 69]. Additionally, Expert Systems are praised for their ability to include additional types of diagnostic data (e.g. vibrational data) in the fault analysis [2]. The disadvantages include [2, 5, 19, 69]: 1) time-consuming learning phase; 2) requirement for large learning dataset; and 3) only accurate in range specified by learning dataset.

Theoretically an AI network could also be trained to model the physical relations between component conditions (i.e. the independent parameters) and gas path parameters (i.e. the dependent parameters) for given inlet conditions. The case where the empirical gas turbine model is then used for GPA purposes should actually be considered another method within the non-linear model-based GPA category.

Empirical or black-box modelling of gas turbines has gradually received more academic attention over the last decades [73]. Nevertheless physics-based or white-box modelling is still the standard because it is well-understood and sufficiently accurate for the purpose of system and component-level aero-thermodynamic diagnostics, even when zero-dimensional component models are used. Black-box modelling is primarily used in cases where the underlying physics are not understood or too computationally expensive to simulate efficiently [73].

3.4.3. Gas turbine Simulation Program (GSP)

All gas turbine modelling and GPA at KLM ES so far has been performed with GSP and its Adaptive Modelling (AM) module, which are discussed in this subsection. The CF6-80C2 GSP model that was used throughout this thesis is discussed in the subsequent subsection.

Modelling and diagnostics in GSP

The development of GSP is fully described in the 2015 PhD thesis by Visser [15]. The subsequent 2017 PhD thesis by Verbist [2] provides more details on improvements and proof-of-concepts considering the AM module, often demonstrated at KLM ES. Over the last decade several MSc theses have been dedicated to demonstrate GSP functionality and synthesise various engine-specific performance models at KLM ES [16–20, 43]. In light of this thesis engine modelling should be considered a means rather a goal, therefore the reader is referred to these reports for more detailed information if desired.

At its core GSP is a tool for modelling and simulation of gas turbine performance. It is based on zero-dimensional (0-D) component sub-models capable of predicting average inlet and outlet gas path

(2) The literature specifically refers to this method as model-based GA GPA, although theoretically alternative global optimisation algorithms like Simulated Annealing (SA) and Particle Swarm Optimisation (PSO) can also be used for the actual minimisation

parameters using aero-thermodynamic equations and user-specified characteristics, including component performance maps. The generic object-based programming enables the user to configure a wide range of gas turbine systems using any desired sequence of gas path components like compressors, turbines, ducts and nozzles.

After configuration of a model, GSP automatically: 1) determines state and (conservation) error variables; 2) combines the chosen variables into a system of Non-linear Differential Equations (NDEs); and 3) numerically solves the NDEs using Newton-Raphson's method. A distinction is made between: 1) Design Point (DP) analysis, where user-specified component performance and operating conditions inputs are used to set the model design point; and 2) Off-Design (OD) analysis, where performance at OD conditions is simulated for the model set by the DP analysis. Several noteworthy additional features within GSP include:

- ***Steady-state series:*** Multiple steady-state, either DP or OD, performance simulations are performed according to user-specified parameter sweep. For aero-engines there is also the option to analyse performance for a complete flight envelope.
- ***Transient analysis:*** Enables transient response analysis for specified operating point changes, for instance to determine compressor surge margin during acceleration, by activating the derivative terms for the momentum conservation equations. The gas dynamics within the components are assumed instantaneous such that technically the analyses are quasi-transient.
- ***Combustion modelling:*** In light of enabling accurate emission predictions as function of gas and fuel properties, GSP includes comprehensive 1-D combustion models.
- ***Heat transfer modelling:*** Enables configuration of a thermal network to simulate heat transfer between components in addition transient analysis.

Given the original expectation that GPA would contribute considerably to the research work of this thesis, the implementation, application and limitations of GSP's adaptive modelling GPA module from an aero-engine industry perspective receive specific attention here. AM within GSP requires the specification of measured or simulated performance data of two snapshots: 1) the to-be analysed snapshot, which will be referred to as the diagnosed snapshot; and 2) the reference snapshot, which sets the baseline for the component conditions and maps. The internal steps within AM include:

1. ***Model calibration:*** The model is calibrated with calibration factors, which adjust the measured reference performance such that the simulated and measured performance are in agreement for the reference snapshot.
2. ***Model adaption:*** Convergence is based on iteratively changing component condition deltas until the simulated and measured performance for the diagnosed snapshot are within the specified tolerances. Given GSP's flexible object-oriented architecture, the actual model adaptation problem is solved internally by adding AM-related states and error equations to the system of non-linear differential equations such that continuity and adaptation are solved simultaneously.

Limitations of diagnostics in GSP

The potential limitations of GSP's diagnostics capabilities are briefly enumerated below.

- ***Inputs and outputs:*** The module is programmed to determine an equal amount of deltas (N_Δ) as the number of provided measured parameters (N_P). During on-wing operation the lack of sensors therefore limits the possibility to determine all main gas path component conditions of interest (often η_{is} and $\dot{m}_c$).
- ***Deterministic:*** The method for AM in GSP is fully deterministic. Within the domain of physically feasible results, each set of performance data only has one corresponding combination of condition deltas.
- ***Ill-conditioning:*** The user can freely specify a set of performance measurements and to-be adapted variables. However, some combinations might result in ill-conditioned or unsolvable systems of NDEs. For example, specifying two closely correlated, noisy measurements can result in an unsolvable AM problem.

- ***Smearing:*** Closely related to the previous limitations, adapting a set of engine component that does not included the faulty (or deteriorated) component results in smearing, which means that the performance drop caused by the faulty component is inappropriately assigned to the remaining components. A possible solution is a combinatorial approach [74] by performing multiple runs with varying the to-be-adapted component conditions for AM and subsequently post-process the results to identify the actual root cause.
- ***Calibration:*** The use calibration factors is a simple, effective method to calibrate the baseline model to the provided reference snapshot. However, if considerable calibration factors are evaluated and the diagnosed operating point differs considerably from the reference snapshot, the (unknown) confidence bounds of the AM results could become significant [2].

3.4.4. CF6-80C2 model

During this thesis, the previously configured and tuned model for the CF6-80C2B1F has been used for simulated sensitivity analyses and effect studies. The full development of the model, summarised below, is discussed in the PhD thesis by Verbist [2]. Additionally some recommendations and limitations of the model are provided in the last paragraph.

Baseline model configuration

The configuration of the CF6-80C2 model available at KLM ES is shown in Figure 3.6. The design point inputs, such as the operating conditions, pressure and temperature ratios and component efficiencies and losses, were all based on a single CF6-80C2 test-cell acceptance test snapshot at TO power setting. Below the components are very briefly discussed.

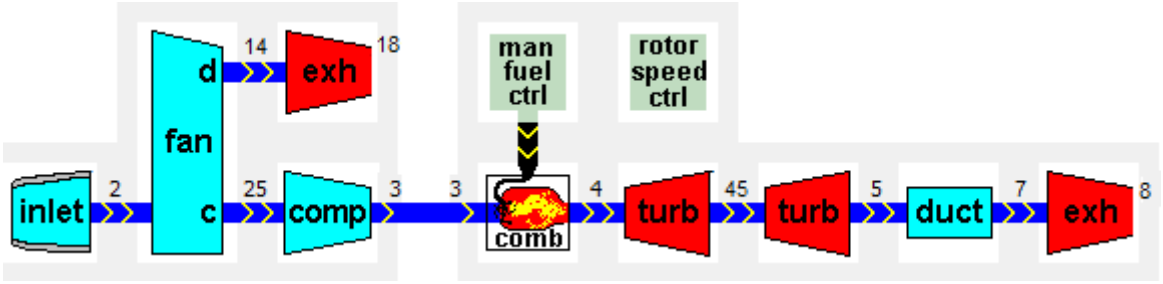

Figure 3.6: Component and control configuration of baseline CF6-80C2 model at KLM ES developed in [2, 18]

- ***Inlet:*** The inlet only serves aesthetic purposes, because its design losses are all set to zero. The area (A2) is added to enable analysis of pre-fan Mach number (M_2) and capture ratio (A0/A2).
- ***Fan & booster:*** This component resembles the combination of the fan and the booster (or LPC). The component's performance is specified by two separate design conditions and compressor maps: 1) the fan bypass map for the behaviour between stations 2 and 14; and 2) the fan core and booster map for the behaviour between stations 2 and 25. The fan and booster component is mechanically linked to the LPT.
- ***HPC:*** This compressor component is specified by a single design point and map. The internal bleed flows from stage 7, 11 and 14 are modelled by mass fractions that were chosen to guarantee design point consistency with the corresponding snapshot. The bleed extraction location is specified by an enthalpy fraction (e.g. 7/14 = 0.5 for the stage 7 bleed flow). Customer bleed from stage 8 and PTO are set to zero for the design point. The HPC is mechanically linked to the HPT.
- ***Combustor & control:*** The combustor design point is specified by a combination of fuel flow, combustion efficiency and pressure loss, where the latter two are assumed constant for off-design analysis as well. For off-design analysis the fuel flow is controlled by the fuel control component, which itself is controlled by the (N1) rotor speed component.
- ***HPT & LPT:*** Both turbines are defined by design isentropic efficiencies and a turbine map. The temperature and pressure ratio are defined by matching of compressor and turbine work. The cooling

flows are also modelled by specifying combinations of bleed flow fraction for the mass flow and an enthalpy fraction for the stage number.

- ***Nozzles:*** Both nozzles are fixed-geometry convergent nozzles. The on- and off-design properties are specified by throat discharge coefficient and exit velocity and thrust coefficients. Which were derived to match the design acceptance test snapshot thrust.

The baseline model was configured with off-the-shelf compressor and turbine performance maps from GSP's BIGFAN library. These standard maps are automatically scaled by GSP using scaling factors on the Pressure Ratio (PR) and efficiency (η_{is}) such that the map is consistent with the design point inputs [2, 15, 41, 75] as shown in the compressor map example in Figure 3.7. Since component maps are a direct representation of aero-thermodynamic design, they are considered confidential by the OEM. The subsequent part discusses the process of map tuning to fit actual CF6-80C2 performance.

Model performance tuning

Both turbines are typically (almost) choked when the engine is producing TO thrust, therefore the variation of η_{is} and $\dot{m}_c$ with changing PR and N_c are typically small [23]. The latter is visualised in the example turbine map in Figure 3.8, which shows that in the operating region surrounding the model design point efficiency and corrected – not physical [40] – mass flow are fairly constant. Consequently, the simulation error contribution from the inaccurate turbine maps shapes is often negligible. The magnitudes in the map should however be representable of the actual engine, which GSP achieves by scaling the generic turbine maps to the model's design point.

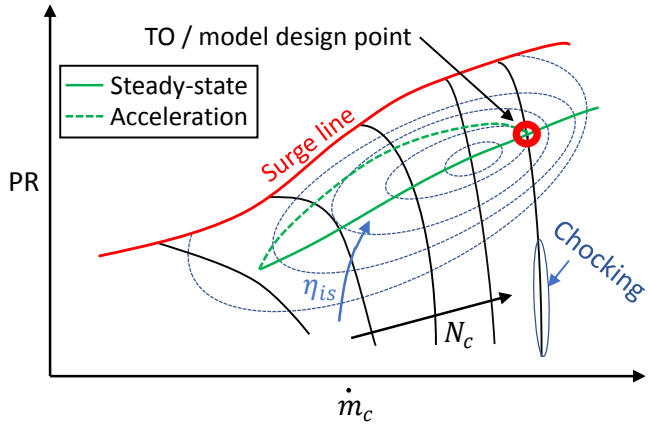

Figure 3.7: Schematic compressor map with PR, $\dot{m}_c$, N_c and η_{is} relations and typical TO/model design point (adapted from [76])

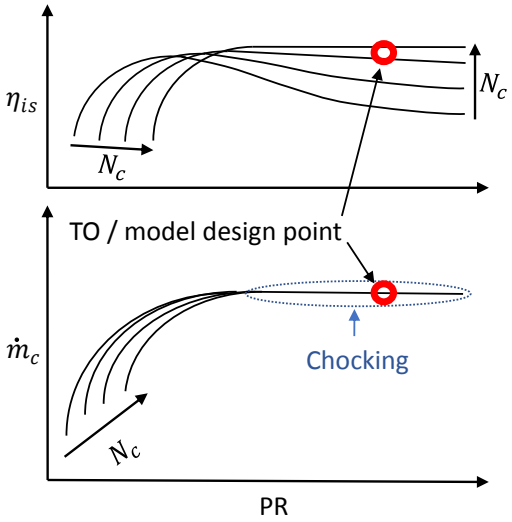

Figure 3.8: Schematic turbine map with PR, $\dot{m}_c$, and N_c relations and typical TO/model design point (adapted from [76])

The three compressor maps were tuned as described by Verbist [2], expanding on previous academic publications [71, 77], using the first 90 post-overhaul on-wing TO snapshots from a single CF6-80C2B1F. Zero customer bleed and constant PTO was assumed. The relative humidity (RH) was set to 60% for all snapshot.

The map tuning used GSP's AM module and was based on the assumption that the component conditions (η_{is} and $\dot{m}_c$) are constant over the chosen 90 snapshots. Therefore, when adapting cycles 2-90 with cycle 1 as reference, any non-zero deltas were attributed to inaccuracies in the component maps. Consequently the objective of the tuning process was defined as the minimisation of the condition delta Root Mean Square (RMS) per component.

The design variables for the minimisations of delta RMS were the corrected rotor speed values (N_c) belonging to the constant speed lines, which is often referred to as speed line re-labelling [2, 71, 77]. By changing the corresponding label of a speed line in the map, the relations between η_{is}, $\dot{m}_c$ and N_c

are effectively changed. For the actual minimisation, the RMS was determined iteratively for several speed line label values per speed line and subsequently fitted with a quadratic polynomial as shown in Figure 3.9. The final values for the speed line labels were set to the location of the polynomial's minimum, respectively 0.87 and 0.94 in the example figure.

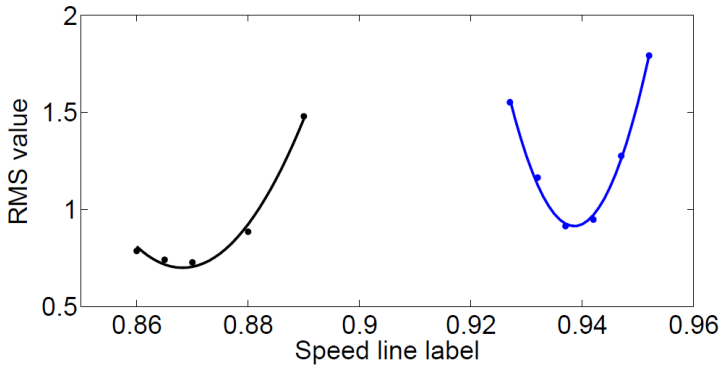

Figure 3.9: Effect of speed line labels on component condition delta RMS including quadratic best-fit (original from [2])

The effectiveness of map tuning is illustrated by Figure 3.10 with fan and booster $\Delta\dot{m}_c$ as example [2]. Additionally the plots indicate that the component condition deltas still have unexplainable scattered. It was concluded that the apparent scatter should be contributed to sensor noise, humidity variation and bleed and PTO systems.

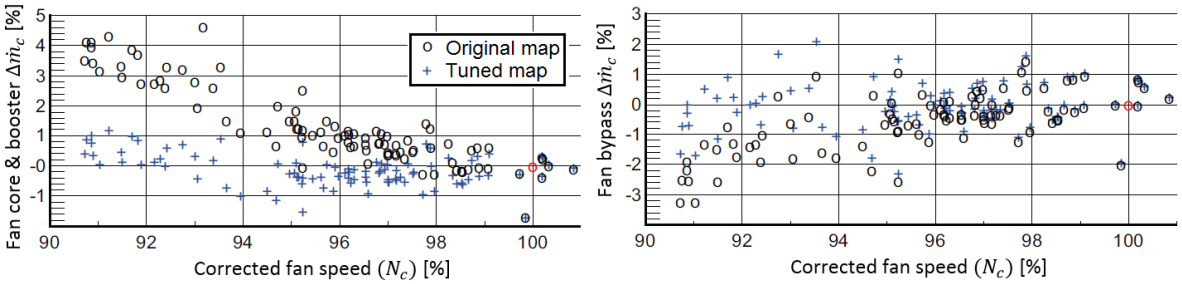

Figure 3.10: Effect of tuning on fan bypass and fan core & booster mass flow capacity deltas ($\Delta\dot{m}_c$) (adapted from [2])

Limitations & recommendations

Improving the GSP CF6-80C2 model at KLM ES is beyond the scope of this research. Nevertheless based on the experience with the model during this thesis, some brief recommendations and limitations that were discovered are summarised below.

- ***Seal run-in:*** The model was tuned using the initial 90 TO snapshots after OW installation from a single engines, if that engine did have a performance overhaul the assumption that the component conditions are constant over those 90 cycles is invalidated given the known deterioration related to seal run-in.
- ***Tuned operating region:*** The speed line re-labeling was only performed on speed lines within the operating range spanned by the unknown tuning data, therefore the maps are also only accurate for a limited but unknown operating range. A recommendation would be to exclude the speed lines that where not tuned, such that the model cannot simulate performance beyond the tuned map region.
- ***EGT shunt:*** It is unknown to check whether the physical or shunted EGT was used in the tuning process. The CF6-80C2B1F EGT shunt functions as a constant conversion factor on degrees Celsius values instead of the absolute Kelvin scale. Although EGT values are in the order of 1000°C,

if shunted EGT values were used for the tuning, both absolute as well as relative simulated EGT values could be slightly erroneous.

- ***Model design point:*** Efforts to track down the origin of the model design point revealed that the corresponding test run was performed with a CF6-80C2A5. The latter has almost identical gas path geometry such that the overall shape of the compressor maps should be comparable. However, the CF6-80C2A5 did have a different shunt which could cause a discrepancy with respect to the on-wing tuning data from a CF6-80C2B1F.
- ***Engine-to-engine variations:*** Engine-to-engine variations are significant while the model was tuned using data from a single engine. Through the use of the aforementioned calibration factors, the model can be calibrated to other engines when using adaptive modelling. However, that procedure is based on the assumption that the compressor maps are similarly shaped. Although beyond the scope of this research, a study to investigate the engine-to-engine map differences by tuning the model for multiple engines separately could validate that assumption.
- ***Tuning procedure:*** With respect to the tuning procedure, several recommendations can be constructed. A more recent study at KLM ES applied speed line relocation in addition to re-labeling and mentioned the concept of speed line morphing [19]. The latter gives full control to construct the exact map of the component. These concepts were not applied for the CF6-80C2 tuning. Furthermore, formalising and automating the tuning process with the use of off-the-shelf optimisation algorithms could improve the tuning quality and subsequently enable engine-specific tuning as mentioned above.

4

Test-cell engine performance assessment

The observed discrepancy between on-wing and test-cell performance can originate from either test-cell (TC) or on-wing (OW) causes and either physical or numerical causes. Therefore a thorough understanding of corrected test-cell engine performance is required.

This chapter first elaborately covers the official definition of test-cell EGTM according to GE manuals in Section 4.1. Then Sections 4.2 and 4.3 elaborate on the humidity and condensation corrections, including a comprehensive comparison with theory and simulations in order to familiarise with the underlying principles and prepare for later work on OW corrections. Lastly, the influence of the empirical facility modifiers on TC EGTM are briefly addresses in Section 4.4.

4.1. EGT margin calculations

The TC EGTM calculations are defined per engine type in the applicable Engine Shop Manual (ESM) [10, 11]. This section will present the equations of all relevant corrections and discuss the purpose of the terms. Calculation of EGTM is split into computation of Standard Day EGT (EGTK) and subsequently Hot Day EGT (EGTKHD) and the margin (EGTM). Since the ESMs are considered GE proprietary information, the the underlying empirical look-up tables are not fully disclosed and only discussed quantitatively if relevant for the research. The top-level correction terms are similar for the CF6-80E1 and CF6-80C2, with slight differences in the underlying empirical tables and methods.

Apart from the EGTM calculations, the TC definition for corrected fan speed (N1K) is discussed afterwards as well because it is used as input for EGTM. Lastly, the definitions for TT2 and PT2 correction ratios that are used throughout this chapter are provided in Equation 4.1.

$$\Theta_{2,\mathrm{SD}} = \frac{\mathrm{TT2}}{\mathrm{T_{ISA}}}\ ; \qquad \Theta_{\mathrm{HD}} = \frac{\mathrm{T_{ISA}}}{\mathrm{T_{flat}}}\ ; \qquad \delta_{2,\mathrm{SD}} = \frac{\mathrm{PT2}}{\mathrm{P_{ISA}}} \tag{4.1}$$

4.1.1. Standard Day EGT (EGTK)

Most of the actual *correcting* is included in the conversion of measured EGT to EGTK. Because EGT values are typically shunted as discussed in Subsection 2.1.1, the official EGTK values reported by GE are the shunted values on the Celsius-scale rather than the unshunted values on the Kelvin-scale. For the remainder of this report EGTK refers to the physical value in Kelvin to enable comparison with simulations, which can be converted to its shunted value using Equation 4.2.

$$\mathrm{EGTK_{shunted}}\ [°\mathrm{C}] = (\mathrm{EGTK}\ [\mathrm{K}] - 273.15) \cdot \mathrm{SF} \tag{4.2}$$

Where SF is the shunt factor, defined as the ratio between shunted EGT redline and physical EGT limit in °C as shown in Equation 4.3. For example, considering the CF6-80E1A3 with a maximum 85°C shunt and 975°C indicated EGT limit, the SF is approximately 0.92 as shown in the equation.

$$\mathrm{SF} = \frac{\mathrm{EGT}_{\mathrm{redline}}}{\mathrm{EGT}_{\mathrm{redline}} + \Delta\mathrm{EGT}_{\mathrm{shunt}}} \xrightarrow{\text{CF6-80E1A3}} \mathrm{SF} = \frac{975°\mathrm{C}}{975°\mathrm{C} + 85°\mathrm{C}} \approx 0.92 \tag{4.3}$$

The full definition of TC unshunted EGTK in K is given in Equation 4.4.

$$\mathrm{EGTK[K]} = \mathrm{EGT} \cdot \left(\frac{1}{\Theta_{2,\mathrm{SD}}}\right)^{\mathrm{XT}} \cdot \mathrm{HEGT} \cdot \mathrm{CEGT} \cdot \mathrm{EGTFM} + \Delta\mathrm{EGT}_{\mathrm{cowl}} + \Delta\mathrm{EGT}_{\Delta\mathrm{N1K}} \tag{4.4}$$

Where:

EGT The unshunted EGT in K, defined by linearly interpolating in the shunt table given the analogue shunt on the CF6-80E1

XT The temperature correction exponent, defined as a function of N1 by linearly interpolating XT for the measured N1 in the temperature exponent table. The theoretical value for XT is 1, but the tabulated values were determined empirically and range between approximately 0.97 and 0.94 for the CF6-80E1 for the 90% to 110% N1 range.

HEGT The Absolute Humidity (AH) correction factor, defined as a function of AH by linearly interpolating HEGT for the measured AH in the AH-correction factor table. The correction is only weakly non-linear, therefore the remainder of this report assumes a linear HEGT-AH function. The correction factor ranges between 1 (i.e. 0%) at 0 g/kg and approximately 0.997 (i.e. 0.3%) at 30 g/kg, which constitutes a linear HEGT-AH gradient dHEGT/dAH of approximately 10×10^5 (i.e. 0.01%-p) per g/kg. Therefore if AH > 0, then HEGT > 1 and EGTK is increased. The latter coincides with expectations from the literature research, because the cooling effect of humidity needs to be compensated when correcting to dry conditions. The in-depth analysis of dHEGT/dAH is provided in Section 4.2.

CEGT The condensation or Relative Humidity (RH) correction factor, defined as a function of ideal inlet temperature rise ($\mathrm{T_{rise}}$) which itself is defined as a function of RH and TT2 by linearly interpolating for the measured RH and TT2 in the T_{rise} table. Similarly to HEGT, CN1 = 1 if RH = 0 but if RH > 0 than CEGT < 1 and EGTK is decreased. Given the heating effect of condensation discussed in literature, it makes sense that the correction achieves the opposite. Although the relation between CEGT and $\mathrm{T_{rise}}$ is linear, the underlying relation between $\mathrm{T_{rise}}$, RH and TT2 is a lot more complex. As will be substantiated in Subsections 4.3.1 and 5.4.5, OW condensation corrections are beyond the scope of this research.

EGTFM The EGT facility modifier, defined as a polynomial function of dry FN which serves as an proxy for test-cell mass flow. The coefficients of the polynomial function are determined empirically through the test-cell calibration, which was discussed in Subsection 2.3.3. That section in Chapter 2 also provided example figures from an outdated correlation report, where EGTFM varies only slightly between approximately 0.997 and 0.992. Although it has been observed that EGTFM < 1 for all engine types at KLM's facility, this cannot be extrapolated to other test-cells. Subsection 3.3.3 discussed potential physics-based explanations for the existence of EGTFM, including TT2 measurement effects and exhaust re-ingestion.

ΔEGT$_{\mathrm{cowl}}$ The test cowling adjustment, defined as a function of N1Kc by linearly interpolating $\Delta\mathrm{EGT}_{\mathrm{cowl}}$ for the actual N1Kc in the test cowling correction factor table. Note that N1Kc is defined in Subsection 4.1.3 but can be assumed roughly equal to N1K. While EGTFM corrects for facility-specific effects to enable comparability between indoor and outdoor testing, the test cowling correction corrects for test cowling and bell-mouth inlet effects to – in theory – enable comparison with OW operation. The magnitude of $\Delta\mathrm{EGT}_{\mathrm{cowl}}$ continuously increases N1Kc, with an approximate 5°C difference between 90% and 110% N1Kc.

$\Delta EGT_{\Delta N1K}$ The throttle push adjustment, defined as a function of ΔN1K by linearly interpolating values at $N1K_{rated}$ and actual N1Kc in the throttle push correction table and calculating the difference. In principle, the throttle push correction table defines the measured relation between EGT and N1Kc such that $\Delta EGT_{\Delta N1K}$ is the difference between the tabulated EGT at the desired $N1K_{rated}$ and at the actual N1Kc. The genericness of this method enables to use the same table for different engine ratings. Intuitively EGT increases with N1Kc according to the table, therefore if N1Kc < $N1K_{rated}$ then $\Delta EGT_{\Delta N1K} > 0$ and vice versa.

4.1.2. Hot Day EGT margin (EGTM)

As show in the previous subsection, most corrections are applied on EGTK. Subsequent derivation of the EGTKHD and EGTM is defined by Equations 4.5a and 4.5b. Although the equations include the additional *shunted* designation to stress the fact that these values are shunted or based on shunted values, the subscripts will be omitted for the remainder of this report. In other words, unlike EGTK, whenever values of EGTKHD and EGTM are given these will be shunted values.

$$EGTKHD_{shunted}\ [°C] = \left[EGTK\ [K] \cdot \left(\frac{1}{\Theta_{HD}}\right)^{XT_{HD}} - 273.15\right] \cdot SF \tag{4.5a}$$

$$EGTM_{shunted}\ [°C] = EGT_{TC\text{-}limit} - EGTKHD_{shunted} + \Delta EGTM_{N1MOD} \tag{4.5b}$$

Where:

XT_{HD} The Hot Day temperature correction exponent, defined by linearly interpolating XT for the *projected corner point* N1 in the temperature exponent table.

$EGT_{TC\text{-}limit}$ The shunted EGT limit for acceptance testing in °C. This value is different from the indicated shunted EGT redline ($EGT_{redline}$) used to determine OW EGT exceedance. The difference between the OW redline and performance testing limit is stated to account for operational differences, including: 1) the initial OW losses, probably referring to seal run-in; and 2) the difference between steady-state and transient EGT, as TC snapshots are taken after stabilisation while OW snapshots are allegedly recorded during peak EGT. Although $EGT_{redline}$ is fixed per engine type, the value of $EGT_{limit,TC}$ is defined separately per rating with 960°C for CF6-80E1A3 which is 15°C lower than $EGT_{redline}$.

$\Delta EGTM_{N1MOD}$ The fan speed modifier adjustment. If corrected thrust (FNK) deviates from the minimum rated thrust (FNK_{rated}) it is customary to apply a N1-modifier (N1MOD) which augments the physical N1 relative to indicated N1 (N1i) to prevent differential thrust. The discrete N1MOD level is defined as a function of FNK margin (FNM), and subsequently the corresponding $\Delta EGTM_{N1MOD}$ value is added to or subtracted from EGTM. Since $\Delta EGTM_{N1MOD}$ is applied to OW and TC EGTM, it should not be a potential cause for the OW-TC EGTM discrepancy. The reader is referred to Appendix A for the FNK calculations.

As will be revealed in Section 5.1, the OW EGTM calculations follow a procedure similar to TC EGTM. A few terms from the TC calculations are discarded because the underlying measurements are missing (e.g. HEGT) and a few terms are added to account for OW subsystems that affect performance (e.g. customer bleed).

4.1.3. Corrected fan speed (N1Kc)

In order to distinguish the different engine-level corrected fan speed definitions, two different symbols are used throughout this report: 1) N1K for the *basic corrected* or *power management* fan speed as defined by GE for OW operation and Equation 4.6a, which only accounts for TT2 through $\Theta_{2,SD}$ and a corresponding empirical exponent; and 2) N1Kc for the *fully corrected* or *certification* fan speed as defined by GE for TC operation and Equation 4.6b, which accounts for humidity and condensation gas

property changes as well.

$$\mathrm{N1K} = \mathrm{N1} \cdot \left(\frac{1}{\Theta_{2,\mathrm{SD}}} \right)^{\mathrm{XN1}} \tag{4.6a}$$

$$\mathrm{N1Kc} = \mathrm{N1} \cdot \left(\frac{1}{\Theta_{2,\mathrm{SD}}} \right)^{\mathrm{XN1}} \cdot \mathrm{HN1} \cdot \mathrm{CN1} \tag{4.6b}$$

Where:

XN1 The temperature correction exponent, defined as a function of N1 by linearly interpolating XN1 for the measured N1 in the temperature exponent table. For the CF6-80E1 the value of XT ranges from approximately 0.5 to 0.4 for the specified N1K range.

HN1 The Absolute Humidity (AH) correction factor, defined as a function of AH by linearly interpolating HN1 for the measured AH in the AH-correction factor table. Similarly to HEGT, HN1-AH is assumed linear and varies between 1 (i.e. 0%) at 0 g/kg and approximately 0.991 (i.e. -0.9%) at 30 g/kg, constituting a HN1-AH gradient (dHN1/dAH) of approximately -30×10^{-5} (i.e. -0.03%-p) per g/kg. Therefore if AH > 0, then HN1 < 1 and N1Kc is decreased with respect to N1K. The effect of HN1 on N1Kc also subsequently affects EGTK via the throttle push correction such that EGTK is further increased if AH > 0. In-depth analysis of the TC EGTM humidity correction is provided in Section 4.2.

CN1 The condensation correction factor, defined as a function of ideal inlet temperature rise ($\mathrm{T_{rise}}$) which is defined as a function of Relative Humidity (RH) and TT2 by linearly interpolating for the measured RH and TT2 in the $\mathrm{T_{rise}}$ table. Similarly to HN1, CN1 = 1 if RH = 0 and CN1 < 1 if RH > 0. In principle, CN1 corrects for the increased effective TT2 due to condensation by lowering N1Kc accordingly. Similar to CEGT, the relation between CN1 and $\mathrm{T_{rise}}$ is linear while the underlying relation between $\mathrm{T_{rise}}$, RH and TT2 is more complex and beyond the scope of this research.

The fully corrected fan speed (N1Kc) serves as an input for the EGTK throttle push correction, which depends on the difference between N1Kc and $\mathrm{N1K_{rated}}$ that is defined as ΔN1K.

4.2. Effects of humidity on EGT margin

The objective of the research presented in this section is to familiarise with humidity corrections for EGTM in preparation for the custom AH-corrections for OW EGTM in Chapter 5.

First, the underlying gas property changes due to humidity will be discussed in Subsection 4.2.1. Subsequently Subsection 4.2.2 discusses theoretical humidity corrections. Lastly, the influence of the official TC humidity corrections is visualised as well as compared with theory and simulations in Subsection 4.2.3.

4.2.1. Gas properties of humid air

The gas properties that are affected by humidity and relevant for corrected gas turbine analysis are the specific gas constant (R) and isentropic coefficient (γ), which is equivalent to ratio of the specific heats (C_p) and (C_v).

Specific gas constant

The specific gas constant is defined by Equation 4.7 with $\Re$ and M for the universal gas constant and average molar mass of the gas. The difference between the molar mass of water (18 g/mol) and dry air (29 mg/mol) affects the average molar mass and consequently R and density of a the gas if humidity is introduced. As given in Equation 4.8, the water-air mixture R can be derived using the water vapour ($w_{\mathrm{H_2O}}$) and dry air (w_{dry}) mass fractions or AH in g/kg. On a tropical day at 30°C with 100% RH, $R_{\mathrm{mix}} = 291.7\ \mathrm{J kg^{-1} K^{-1}}$ which is 1.61% higher than R_{dry}.

$$R = \frac{\Re}{M} \quad (4.7) \qquad R_{\text{mix}} = w_{\text{H}_2\text{O}} \cdot R_{\text{H}_2\text{O}} + w_{\text{dry}} \cdot R_{\text{dry}} = \frac{\text{AH} \cdot R_{\text{H}_2\text{O}} + 1000 \cdot R_{\text{dry}}}{\text{AH} + 1000} \quad (4.8)$$

The introduction of combustion products typically has a negligible influence on R, therefore the above mentioned increase of R_{mix} with respect to R_{dry} also holds for post-combustion stages in the gas turbine [46].

Isentropic exponent

Both the isobaric (C_p) and isochoric (C_v) heat capacities are affected by humidity. Similarly to evaluation of R_{mix}, a mass fractions based computation is typically used as shown in Equation 4.9 [50]. Higher accuracy can be achieved by taking into account real gas effects as is done in GSP [15] or correcting for real gas effects through an additional $\Delta C_{p,\text{mix}}$ term [78].

$$C_{p,\text{mix}} = w_{\text{H}_2\text{O}} \cdot C_{p,\text{H}_2\text{O}} + w_{\text{dry}} \cdot C_{p,\text{dry}} = \frac{\text{AH} \cdot C_{p,\text{H}_2\text{O}} + 1000 \cdot C_{p,\text{dry}}}{\text{AH} + 1000} \quad (4.9)$$

The humidity's effect on C_v can subsequently be derived using Equation 4.10. Although humidity affects both specific heats, the relative changes are not equal such that the isentropic exponent (γ_{mix}) defined in Equation 4.11 is also affected by humidity.

$$C_{v,\text{mix}} = C_{p,\text{mix}} - R_{\text{mix}} \quad (4.10) \qquad \gamma_{\text{mix}} = \frac{C_{p,\text{mix}}}{C_{v,\text{mix}}} \quad (4.11)$$

Considering 30°C conditions, the value of γ_{mix} can range from 1.4002 to 1.3966 between 0% and 100% RH, which constitutes a 0.255% decrease. Although γ is significantly affected combustion products, comparing the turbine inlet gas properties for dry and humid ambient conditions will reveal a similar decrease of γ due to the presence of water vapour.

4.2.2. Theoretical humidity corrections

Humidity effects on turbofan engine performance have received notable academic attention ever since the early days of the gas turbine. This subsection briefly discusses the most notable results with respect to humidity corrections, divided into component- and engine-level.

Component level

Section 3.1 laid the groundwork for corrected turbomachinery component parameters, by introducing the concept of flow similarity. The comprehensive 1995 AGARD report [46] on recommended practices for the assessment of humidity effects provided both a review and new proposals for humidity corrections. The stated requirements for full flow similarity of a compressible flow including humidity are [46]:

1. Geometrical similarity
2. Mach number similarity (i.e. constant axial (M_C) and circumferential (M_U) Mach number)
3. No Reynolds number effects (i.e. constant viscosity effects)
4. No Prandt number effects (i.e. constant heat transfer effects)
5. Constant isentropic exponent (i.e. constant γ)

Complete flow similarity cannot be achieved given the γ change. However, considerate assumptions can enable the derivation of meaningful equations to grasp the effect of humidity on corrected performance. The proposed assumptions in the AGARD report are:

1. Geometrical similarity, hence neglecting thermal expansion
2. Constant Prandtl and Reynolds effects
3. Constant inlet Mach numbers
4. Constant isentropic efficiency (η_{is}), irrespective of humidity
5. Constant stage work coefficient, which is a non-dimensional measure of the enthalpy change over that stage

Application of these assumptions enables the synthesis of a set of theoretical humidity correction factors on spool speed (N), mass flow ($\dot{m}$) and pressure ratio (PR). The factors for N and $\dot{m}$ are provided in Equations 4.12a and 4.12b. Note that $N_{c,\mathrm{dry}}$ – defined as $N/\sqrt{T_{t,\mathrm{in}}}$ – mirrors N1K as the component-level *basic* corrected speed, while $N_{c,\mathrm{mix}}$ mirrors N1Kc as the theoretical component-level *fully* corrected speed.

$$\frac{N_{c,\mathrm{dry}}}{N_{c,\mathrm{mix}}} = \frac{\left(\frac{N}{\sqrt{T_{t,\mathrm{in}}}}\right)_{\mathrm{dry}}}{\left(\frac{N}{\sqrt{T_{t,\mathrm{in}}}}\right)_{\mathrm{mix}}} = \sqrt{\frac{R_{\mathrm{dry}}}{R_{\mathrm{mix}}}} \cdot \sqrt{\frac{\gamma_{\mathrm{dry}}}{\gamma_{\mathrm{mix}}}} \cdot \sqrt{\frac{1 + \frac{\gamma_{\mathrm{mix}}-1}{2} \cdot M_{C,\mathrm{in}}^2}{1 + \frac{\gamma_{\mathrm{dry}}-1}{2} \cdot M_{C,\mathrm{in}}^2}} \tag{4.12a}$$

(4.12b)

$$\frac{\dot{m}_{c,\mathrm{dry}}}{\dot{m}_{c,\mathrm{mix}}} = \frac{\left(\frac{\dot{m}\sqrt{T_{t,\mathrm{in}}}}{P_{t,\mathrm{in}}}\right)_{\mathrm{dry}}}{\left(\frac{\dot{m}\sqrt{T_{t,\mathrm{in}}}}{P_{t,\mathrm{in}}}\right)_{\mathrm{mix}}} = \sqrt{\frac{R_{\mathrm{mix}}}{R_{\mathrm{dry}}}} \cdot \sqrt{\frac{\gamma_{\mathrm{dry}}}{\gamma_{\mathrm{mix}}}} \cdot \frac{\left(1 + \frac{\gamma_{\mathrm{mix}}-1}{2} \cdot M_{C,\mathrm{in}}^2\right)^{\frac{\gamma_{\mathrm{mix}}+1}{2(\gamma_{\mathrm{mix}}-1)}}}{\left(1 + \frac{\gamma_{\mathrm{dry}}-1}{2} \cdot M_{C,\mathrm{in}}^2\right)^{\frac{\gamma_{\mathrm{dry}}+1}{2(\gamma_{\mathrm{dry}}-1)}}} \tag{4.12c}$$

Regarding the corrections, it is observed that the effects of changing γ are dependent on $M_{C,\mathrm{in}}$ and small compared to the effects of changing R [46]. A common additional assumption is to set $M_{C,\mathrm{in}}$ to 0 for compressors and to 1 for turbines, although other *convenient* values have also been proposed [44, 50]. The theoretical humidity corrections are both plotted for 0% to 100% RH at 30°C in Figures 4.1 and 4.2 for different Mach numbers including the linear fit gradients, which reveals the small contribution of the Mach-related term. Although unobservable, the corrections are weakly non-linear. Furthermore, the correction factor values reconcile with the known effects of humidity.

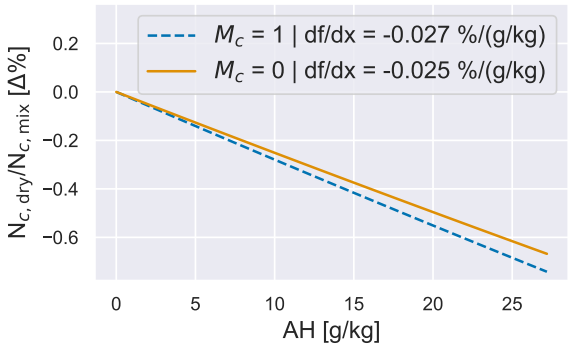

Figure 4.1: Theoretical component-level AH-correction for rotor speed (N_c)

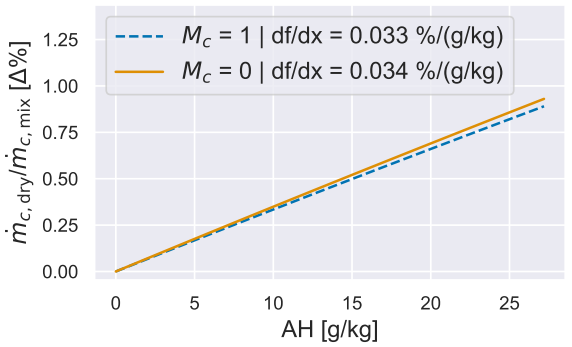

Figure 4.2: Theoretical component-level AH-correction for mass flow ($\dot{m}_c$)

Sticking to the assumptions used for derivation of the N_c and $\dot{m}_c$ corrections, an expression relating PR can be derived resulting in Equation 4.13a [46, 76]. Subsequently the temperature ratio correction can be deduced by putting the constant η_{is} as well as $\mathrm{PR}_{\mathrm{dry}}$ and $\mathrm{PR}_{\mathrm{mix}}$ in the isentropic relation.

$$\left(\frac{P_{t,\mathrm{out}}}{P_{t,\mathrm{in}}}\right)_{\mathrm{dry}} = \left[\left(\frac{\left(\frac{P_{t,\mathrm{out}}}{P_{t,\mathrm{in}}}\right)_{\mathrm{mix}}^{\frac{\gamma_{\mathrm{mix}}-1}{\gamma_{\mathrm{mix}}}} - 1}{\frac{R_{\mathrm{mix}} \cdot \gamma_{\mathrm{mix}} \cdot c_{p,\mathrm{dry}}}{R_{\mathrm{dry}} \cdot \gamma_{\mathrm{dry}} \cdot c_{p,\mathrm{mix}}}}\right) \frac{1 + \frac{\gamma_{\mathrm{mix}}-1}{2} M_{C,\mathrm{in}}^2}{1 + \frac{\gamma_{\mathrm{dry}}-1}{2} M_{C,\mathrm{in}}^2} + 1\right]^{\frac{\gamma_{\mathrm{dry}}}{\gamma_{\mathrm{dry}}-1}} \tag{4.13a}$$

(4.13b)

$$\frac{\left(\frac{T_{t,\mathrm{out}}}{T_{t,\mathrm{in}}}\right)_{\mathrm{dry}}}{\left(\frac{T_{t,\mathrm{out}}}{T_{t,\mathrm{in}}}\right)_{\mathrm{mix}}} = \frac{1 + \frac{1}{\eta_{\mathrm{is}}}\left[\left(\frac{P_{t,\mathrm{out}}}{P_{t,\mathrm{in}}}\right)_{\mathrm{dry}}^{\frac{\gamma_{\mathrm{dry}}}{\gamma_{\mathrm{dry}}-1}} - 1\right]}{1 + \frac{1}{\eta_{\mathrm{is}}}\left[\left(\frac{P_{t,\mathrm{out}}}{P_{t,\mathrm{in}}}\right)_{\mathrm{mix}}^{\frac{\gamma_{\mathrm{mix}}}{\gamma_{\mathrm{mix}}-1}} - 1\right]} \tag{4.13c}$$

Engine level
Although engine parameter corrections for humidity – including EGT – were proposed as early as 1950 by Samuels and Gale [50], the extensive algebraic expressions and long list of underlying assumptions – some of which have been invalidated [44] – severely limit the practical application [46]. Later Fishbeyn and Pervyshin [49] constructed weakly quadratic correction equations using basic engine simulations based on coupling of algebraic component models.

Current practice is to empirically determine the required humidity corrections, similarly to the temperature and pressure correction exponents discussed in Section 3.1.

4.2.3. Official test-cell humidity corrections

As has been shown in Section 4.1, the cooling effect of humidity on EGT is accounted for in two ways considering TC EGTM calculations: 1) explicitly through the EGT-AH correction factor (HEGT), which increases EGTK directly; and 2) implicitly through the throttle push adjustment ($\Delta\mathrm{EGT}_{\Delta\mathrm{N1K}}$), since the decrease of N1Kc due to the N1K-AH correction factor (HN1) results in an increase of $\Delta\mathrm{EGT}_{\Delta\mathrm{N1K}}$.

In preparation for proposing custom AH-corrections for OW EGTM, an effort was made to expose the physical origin of the HN1-AH and HEGT-AH relations – summarised by dHN1/dAH and dHEGT/dAH – in the Engine Shop Manuals [10, 11] on the basis of simulations in GSP and the theory from the previous subsection.

Afterwards, the combined effect of the implicit and explicit humidity corrections for TC EGTM are studied. The following is all based on the CF6-80E1 manual, nevertheless comparison with GSP is justified given the geometrical similarity of the types and almost identical TC humidity corrections.

Comparison with theory
The starting point for this analysis is the comparison of the theoretical AH-correction for N_c in Equation 4.12a with the tabulated HN1-AH relation. If GE's HN1-AH relation is based solely on correcting for the flow effects in the fan, one would expect the component-level theoretical corrections to reconcile with the empirical corrections.

The linear gradient dHN1/dAH of GE's correction equals approximately -30×10^{-5} or -0.03% per g/kg, which can only be achieved with the theoretical correction with a non-physical values of $M_{C,\mathrm{in}} \approx 1.6$. Simulations with the CF6-80C2 GSP model predict $M_{C,\mathrm{in}}$ between 0.5 and 0.65, corresponding to a theoretical dHN1/dAH of approximately -25.5×10^{-5} or -0.0255% per g/kg.

Considering the direct AH-correction for EGTK using HEGT, there is no meaningful theoretical equivalent.

Comparison with simulations
As Section 3.1 already explained, maintaining – or in the case of humidity staying close to – flow similarity cannot be achieved for a complete turbofan. Concerning engine-level corrections, the common practice is to use empirical corrections to maintain engine-level similarity rather than component-level flow similarity. Based on the following analysis, it is concluded that GE used FNK as engine-level *similarity parameter* for the empirical HN1-AH relation.

Figures 4.3 and 4.4 give empirical HN1-AH and HEGT-AH relations based on simulation with the CF6-80C2 GSP model. These relations were obtained by simulating steady-state series with increasing RH at ISA + 15°C, while controlling the simulated FN to equal the CF6-80C2B1F rated thrust of 250 kN. Furthermore simulations were also performed with positive condition deltas ($\Delta\eta_{\mathrm{is}}$) between 1.5% and 3.0%, which should be closer to a factory-new engine.

The simulated HN1 is defined as the ratio between N1K at AH = 0 g/kg ($\mathrm{N1K}_{\mathrm{dry}}$) and the humid N1K, which reflects the correction on N1K required to maintain FN. The simulated HEGT is defined similarly by the ratio of the dry EGT and humid EGT, therefore HEGT corrects for the decrease of EGT due to humidity even if FNK (and N1Kc) is maintained.

The simulated HN1-AH gradients are -27.1×10^{-5} or -0.0271% and -29.1×10^{-5} or -0.0291% per g/kg for baseline model and the improved efficiency model respectively. Both are higher than the aforementioned theoretical gradient of -25.5×10^{-5} or -0.0255% per g/kg. The improved efficiency simulation almost reconciles with GE's value for dHN1/dAH of -30×10^{-5} or -0.03% per g/kg.

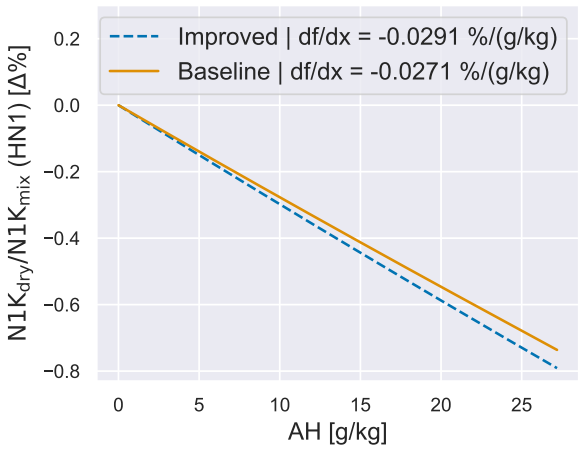

Figure 4.3: Simulated AH-correction for N1K (HN1) using GSP CF6-80C2 model

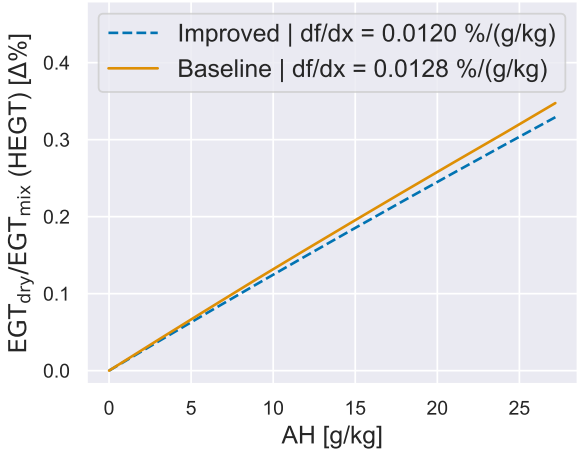

Figure 4.4: Simulated AH-correction for EGT (HEGT) using GSP CF6-80C2 model

Regarding the EGT-AH correction, the simulated values for dHEGT/dAH are 12.0×10^{-5} or 0.012% and 12.8×10^{-5} or 0.0128% per g/kg. Both are in the same order of magnitude as GE's gradient of 10×10^{-5} or 0.01% per g/kg AH. Furthermore, similarly to HN1, the improved efficiency model results are the closest to the official ESM value.

The above analysis demonstrates how engine-level humidity corrections based on *thrust similarity* can be empirically determined. The residual discrepancy can be contributed to the limitations of the GSP model and the unknown condition of the engine used by GE.

Furthermore, the hypothesis that FN is used as engine-level performance similarity indicator is backed by the values of GE's FN-AH correction factor (HFN) in Appendix A, which has a negligible effect on FNK such that all humidity-related effects on FN are accounted for by the thrust throttle push adjustment ($\Delta\mathrm{FNK}_{\Delta\mathrm{N1K}}$).

Effect on Standard Day EGT (EGTK)

Apart from humidity itself, the effect of AH-corrections on TC EGTK is related to N1K and EGT as well. Figure 4.5 confirms this by visualising the net effect ($\Delta\mathrm{EGTK}_{\mathrm{AH}}$) and the individual HN1-related and HEGT-related contributions for a range of AH values. The assumed measured combinations of EGT and N1K are based on the throttle push correction table in the manual.

Additionally Figure 4.6 plots $\Delta\mathrm{EGTK}_{\mathrm{AH}}$ and its contributors with respect to N1K for AH = 27.2 g/kg. Although HEGT is constant for a given AH, the absolute HEGT-related contribution increases with N1K because the measured EGT is assumed to increase. The indirect effect of HN1 on $\Delta\mathrm{EGTK}_{\mathrm{AH}}$, which is maximum at approximately 102% N1K, is the main contributor over the full operating range. The variation of this contribution can be explained by the EGT-N1K data in the throttle push correction table, whose gradient initially is almost constant at 10°C EGT per %-N1K but decreases beyond 100% N1K to 7.5°C/% at 110% N1K.

The average combined correction $\Delta\mathrm{EGTK}_{\mathrm{AH}}$ at AH = 27.2 g/kg over the plotted operating range is 0.874% of the humid EGTK, which corresponds to approximately 0.0321%-p per g/kg humidity. These values will be compared to the EGTM-AH correlations in the OW data in Chapter 5.

4.3. Effects of condensation on EGT margin

The objective of the research presented in this section is to familiarise with inlet condensation and assess the TC condensation corrections. First, Subsection 4.3.1 discusses theoretical corrections and the corresponding challenges. Afterwards, Subsection 4.3.2 assesses the official TC condensation corrections.

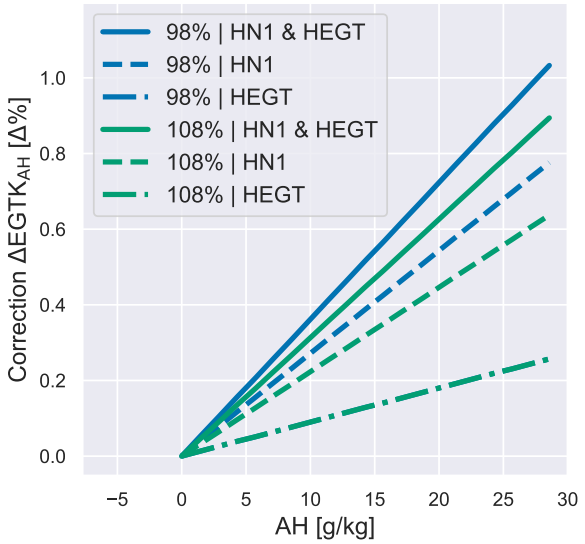

Figure 4.5: Effect of official CF6-80E1 TC humidity correction on EGTK ($\Delta EGTK_{AH}$) as function of AH

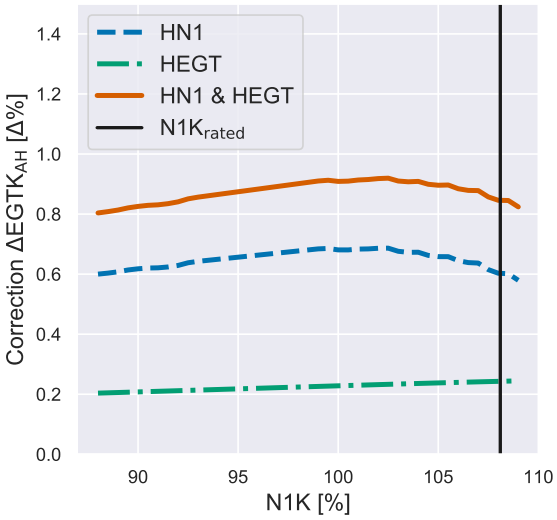

Figure 4.6: Effect of official CF6-80E1 TC humidity correction on EGTK ($\Delta EGTK_{AH}$) for AH = 27.2 g/kg as function of power setting for CF6-80E1

4.3.1. Theoretical condensation corrections

Inlet condensation can occur when flow is accelerated in the inlet, typically at low speed or stationary operation. The acceleration decreases static temperature and pressure, which effectively increases Relative Humidity (RH). In combination with high ambient humidity the flow might locally become supersaturated (i.e. RH>100%) such that potentially part of the water-vapour condensates.

The primary challenge with condensation corrections is the complexity and unpredictability of the condensation phenomena [23, 45, 46]. Spontaneous condensation due to supersaturation typically only occurs in significant quantities beyond RH > 400%, which is therefore only significant for supersonic inlet conditions [46].

The alternative method of condensation that can occur if RH > 100% is heterogeneous condensation, however this method of condensation is very sensitive to the often unmeasurable characteristics of particulate matter that can act as condensing nuclei [46].

The full list of parameters that affect *if* and *how much* condensation occurs is much longer and also includes among others: 1) ambient and inlet Mach numbers; 2) ambient pressure and temperature; 3) relative humidity; and 4) inlet pressure recovery.

Furthermore, quantification of the effect of the condensation on the engine is also non-trivial because it depends among others on the residence time in the inlet at supersaturated conditions and the location where the condensate evaporates again [46]. If re-evaporation occurs in front of the fan, the effect of condensation is only an undetected increase of effective TT2. In case of later re-evaporation the effective humidity experienced by the fan and booster is lower, but nevertheless higher temperatures are measured at stations after re-evaporation in the compression system.

A common approach for condensation corrections, as is performed with the TC EGTM calculations, is to empirically determine a correction factor as function of the theoretical temperature rise (T_{rise}). The latter equals the theoretical temperature increase observed when the supersaturated flow is let to fully condensate towards 100% RH in a 1D-duct. Figure 4.7 provides some insights into the relation between T_{rise}, TT2 and RH based on the T_{rise}-table for official TC condensation corrections.

Given that the relation between T_{rise} and the required corrections depends on the condensing nuclei concentration, the related condensation correction inherently assumes a particle concentration. Therefore the accuracy of T_{rise}-based corrections is not guaranteed [46].

4.3.2. Official test-cell condensation corrections

No custom OW condensation corrections will be proposed for OW EGTM due to the challenges presented in the previous subsection. Furthermore given that actual condensation effects depend heavily

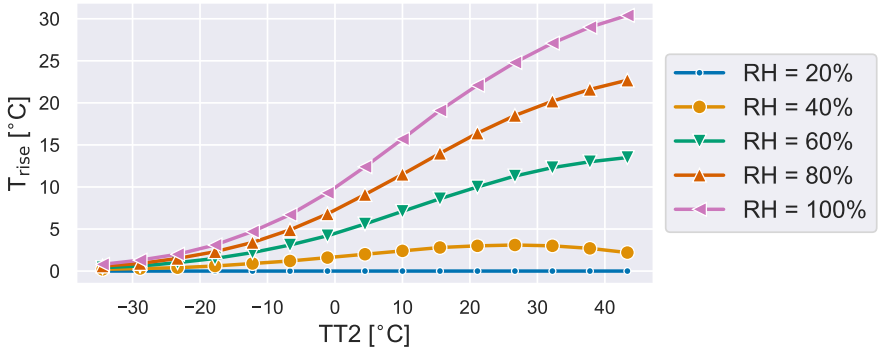

Figure 4.7: Official CF6-80E1 TC T_{rise} as function of RH and TT2 [11]

on unknown quantities like condensing nuclei density, there is a risk that the T_{rise}-based correction method used for TC EGTM is over- or under-compensating.

As has been shown in Section 4.1, the effects of condensation on EGT are accounted for in two opposing ways concerning TC EGTM calculations: 1) explicitly through the EGT-RH correction factor (CEGT), which decreases EGTK directly; and 2) implicitly through the throttle push adjustment ($\Delta EGT_{\Delta N1K}$), since the decrease of N1Kc due to the N1K-RH correction factor (CN1) results in an increase of $\Delta EGT_{\Delta N1K}$. The relative effect of the official TC correction on EGTK at $N1K_{rated}$ (i.e. 108.1%) is plotted in Figure 4.8 as function of TT2 and RH. In contrast to the AH-corrections, the condensation correction is highly non-linear.

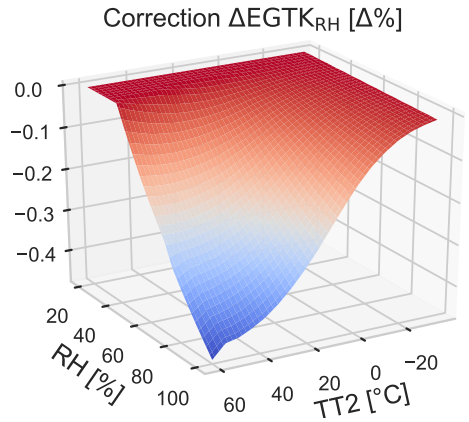

Figure 4.8: Effect of official CF6-80E1 TC condensation correction on EGTK ($\Delta EGTK_{RH}$) as function of RH and TT2 at N1K = $N1K_{rated}$

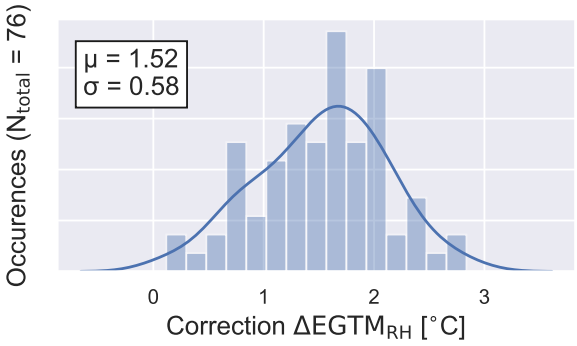

Figure 4.9: Distribution of official condensation correction contribution to reported TC EGTM for CF6-80E1 acceptance tests

The distribution of the condensation correction's contribution to the reported EGTM values for all CF6-80E1 acceptance tests is provided in Figure 4.9. An actual assessment of the accuracy of the condensation corrections is left for the recommendations given the present lack of data to support such analysis. Nevertheless based on Figure 4.9 it is concluded that in the extreme case without actual condensation the impact on $\mu(\Delta EGTM_{OW-TC})^{(1)}$ and $\sigma(\Delta EGTM_{OW-TC})^{(2)}$ is −1.5°C and 0.58°C.

4.4. Effects of facility modifier & cowling correction on EGT margin

The process of test-cell correlation is used to determine specific aerodynamic- and sensor-related effects compared to GE's outdoor facility. The results are summarised by correction factors, called Facility Modifiers (FMs), for the key performance indicators such as FNK (FNFM), WFK (WFFM) and EGTK

(1) $\mu(\Delta EGTM_{OW-TC})$: the mean of the $\Delta EGTM_{OW-TC}$ distribution
(2) $\sigma(\Delta EGTM_{OW-TC})$: the standard deviation of the $\Delta EGTM_{OW-TC}$ distribution

(EGTFM). The modifiers are defined by the four coefficients that describe a cubic polynomial as function of FNK.

Furthermore an adjustment ($\Delta\mathrm{EGT}_{\mathrm{cowl}}$) is applied to EGTK to account for the difference between the TC and OW cowling. This section briefly addresses the net effect of EGTFM and $\Delta\mathrm{EGT}_{\mathrm{cowl}}$ on the EGTK to evaluate the potential contribution to the OW-TC EGTM discrepancy.

The official EGTFM polynomial coefficients for KLM's facility are considered confidential and are therefore not disclosed in this report. The magnitude of the FM-correction on EGTM ($\Delta\mathrm{EGTM}_{\mathrm{FM}}$) can be evaluated for measured combinations of EGTK and FNK – both before FM and cowling adjustments – using the official EGTFM-FNK curve. The contribution of $\Delta\mathrm{EGT}_{\mathrm{cowl}}$ to the official EGTM can simply be determined by interpolating its value for the measured N1K in the cowling adjustment table.

The combined net effect of EGTFM and $\Delta\mathrm{EGT}_{\mathrm{cowl}}$ on the reported EGTM is plotted in Figure 4.10 for all CF6-80E1 acceptance tests since 2013, where the scatter-plot colours represent EGTK values – before EGTFM and $\Delta\mathrm{EGT}_{\mathrm{cowl}}$ – via the colour-map.

Based on the narrow range of $\Delta\mathrm{EGTM}_{\mathrm{FM\&cowl}}$ values, it is concluded that TC-related effects do not vary significantly within the FNK range typical for TO performance snapshots. Therefore potential inaccuracy in EGTFM or $\Delta\mathrm{EGT}_{\mathrm{cowl}}$ is unlikely to contribute significantly to the observed scatter of the OW-TC EGTM discrepancy. Relating $\Delta\mathrm{EGTM}_{\mathrm{OW-TC}}$ with FNK also produced negligible correlation coefficients, further substantiating that EGTFM and $\Delta\mathrm{EGT}_{\mathrm{cowl}}$ do not contribute to the $\sigma(\Delta\mathrm{EGTM}_{\mathrm{OW-TC}})$.

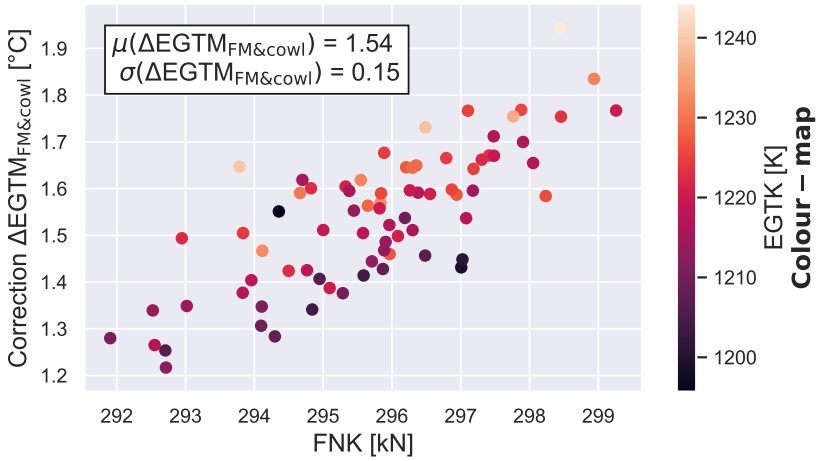

Figure 4.10: FM and $\Delta\mathrm{EGT}_{\mathrm{cowl}}$ contribution to reported TC EGTM ($\Delta\mathrm{EGTM}_{\mathrm{FM\&cowl}}$) as function of FNK and EGTK (excluding FM and cowling adjustment) for CF6-80E1 acceptance tests

The isolated effect of EGTFM and $\Delta\mathrm{EGT}_{\mathrm{cowl}}$ on the negative mean of the $\Delta\mathrm{EGTM}_{\mathrm{OW-TC}}$ distribution cannot be quantified based on the currently available data. In case all other potential causes have been accounted for, the unexplained residual $\mu(\Delta\mathrm{EGTM}_{\mathrm{OW-TC}})$ can be used as an indicator of the inaccuracy of EGTFM and $\Delta\mathrm{EGT}_{\mathrm{cowl}}$.

Quantifying the accuracy of EGTFM individually requires re-correlation or in-depth analysis of the back-to-back testing results and performance trending parameters from KLM's test-cell facility which is left as an recommendation. Assessing the accuracy of $\Delta\mathrm{EGT}_{\mathrm{cowl}}$ requires in-depth comparison of OW data with test data from GE's outdoor test-cell facility.

5

On-wing engine performance monitoring

The observed discrepancy between on-wing and test-cell performance can originate from either test-cell (TC) or on-wing (OW) causes and either physical or numerical causes. Therefore a thorough understanding of corrected on-wing engine performance is required, both in terms of the official correction equations and models as well as any inaccuracies or limitations inhibited by those equations and models. This chapter will first of all address those official EGTM calculations in Section 5.1.

Given that many of the potential causes discussed in Section 3.3 contribute to the OW-TC differences through OW EGTM, identification or elimination of OW EGTM related potential causes was prioritised during the research. The ample availability of OW data also contributed the chosen prioritisation.

To this end, the data was first adjusted for faults as is discussed in Section 5.2. Then Section 5.3 assesses the effect of throttle setting and the accuracy of the throttle push correction. Subsequently, similar analyses are addressed for absolute humidity and inlet temperature in Section 5.4. Sections 5.5 and 5.6 then conclude the N1K, AH and TT2 effect studies by providing the method and results belonging to proposed improvements to the OW EGTM calculations. Lastly, the impact of customer bleed and power off-take are briefly studied in Section 5.7

5.1. EGT margin calculations

Analogous to Section 4.1 for TC EGTM, this section elaborately discusses the OW EGTM calculations used to convert measured performance into corrected performance. Given that the correction equations and tables for OW EGTM calculations are considered confidential by GE and not disclosed to their clients, considerable efforts were made to reverse-engineer the unknown equations and tables based on the data. The general methodology of that reverse-engineering process is discussed in Appendix B.

The resulting EGTK and EGTM definitions are provided in Sections 5.1.1 and 5.1.2. Additionally, Subsection 5.1.3 defines the additional parameter called EGTM deviation (EGTMDEV) that will be used extensively throughout this chapter.

5.1.1. Standard Day EGT (EGTK)

Just like the TC EGTM calculations, first of all measured performance is corrected to Standard Day EGT (EGTK) as defined by Equation 5.1. It should be noted that it is not guaranteed that GE's definition has the exact same formulation, only that it is mathematically equivalent given that the reverse-engineering achieved root mean square errors in the order of 1×10^{-5}. Some of the adjustments can be applied either in the EGKT, EGTKHD or EGTM equation, which results in slightly different values in the underlying tables, among others due to application of the SF on EGTKHD and EGTM.

It was decided to include all corrections and adjustments for physical effects, which depend on engine parameters, in the calculations of EGTK to improve comparability of EGTK with simulated results. Purely numerical factors and adjustments such as the shunt factor were put in the EGTKHD and EGTM calculations, as is discussed in Subsection 5.1.2.

Most contributing factors and adjustments in Equation 5.1 are only discussed briefly, assuming the reader is familiar with the content of Section 4.1 on the TC EGTM calculations and conventions.

Regarding the bleed-related adjustments, it was revealed that EGTK is corrected to inactive bleed systems operation. Lastly, although the equations and tables were reverse-engineered, it was decided in consultation with KLM ES to not disclose all the exact values in the underlying tables.

$$\mathrm{EGTK[K]} = \mathrm{EGT} \cdot \left(\frac{1}{\Theta_{2,\mathrm{SD}}}\right)^{\mathrm{XT}} + \Delta\mathrm{EGT}_{\Delta\mathrm{N1K}} + \Delta\mathrm{EGT}_{\mathrm{NAI}} + \Delta\mathrm{EGT}_{\mathrm{WAI}} + \Delta\mathrm{EGT}_{\mathrm{WB}} \tag{5.1}$$

Where:

EGT The unshunted or physical EGT in K.

XT The temperature correction exponent, which is constant for the full operating range with a value of approximately 0.87 for the CF6-80E1.

ΔEGT$_{\Delta$N1K$}$ The throttle push adjustment, defined by linearly interpolating its value for actual N1K in the throttle push correction table. The corresponding tables are rating-specific, for this research the tables were reverse-engineered for the CF6-80E1A3 and CF6-80C2B1F only. The previously established distinction between the basic (N1K) and fully (N1Kc) corrected speeds is superfluous concerning OW EGTM due to the (current) lack of humidity corrections. The temperature correction exponent (XN1) used for N1K is the same for OW and TC calculations.

ΔEGT$_{\mathrm{NAI}}$ The Nacelle Anti-Ice (NAI) adjustment, which is used to account for the adverse effects of NAI bleed extraction by decreasing EGTK with a few °C if the NAI-system is active. Since the actual bleed mass flow for NAI is not measured, the correction is discrete with a single value for $\Delta\mathrm{EGT}_{\mathrm{NAI}}$ per engine type.

ΔEGT$_{\mathrm{WAI}}$ The Wing Anti-Ice (WAI) adjustment, which is used to account for the adverse effects of WAI bleed extraction on EGTK similarly to the NAI adjustment mentioned above. Values are similar but not equal to the values for $\Delta\mathrm{EGT}_{\mathrm{NAI}}$.

ΔEGT$_{\mathrm{WB}}$ The customer bleed flow (WB) adjustment, which is used to account for the adverse effects of customer bleed extraction on EGTK. In case of the CF6-80E1, the magnitude of the adjustment ranges between approximately 0°C and -6°C and is evaluated by linearly interpolating its value for measured WB in the bleed correction table.

5.1.2. Hot Day EGT margin (EGTM)

The conversion of unshunted EGTK in K to shunted Hot Day EGTK (EGTKHD) in °C and shunted Hot Day EGT margin (EGTM) is described by Equations 5.2 and 5.3. The equations are similar to the TC EGTM calculations except for an additional factor (F_{EGTM}) and constant adjustment (C_{EGTM}).

$$\mathrm{EGTKHD\ [°C]} = \left[\mathrm{EGTK\ [K]} \cdot \left(\frac{1}{\Theta_{\mathrm{HD}}}\right)^{\mathrm{XT_{HD}}} - 273.15\right] \cdot \mathrm{SF} \tag{5.2}$$

$$\mathrm{EGTM\ [°C]} = \mathrm{EGT_{redline}} - F_{\mathrm{EGTM}} \cdot \mathrm{EGTKHD} + \Delta\mathrm{EGTM_{N1MOD}} + C_{\mathrm{EGTM}} \tag{5.3}$$

Where:

XT$_{\mathrm{HD}}$ The Hot Day temperature correction exponent, equal to the constant overall XT for OW calculations.

EGT$_{\mathrm{redline}}$ The indicated shunted EGT redline, which is 975°C for the CF6-80E1. Therefore the physical EGT limit is 1060°C with a 85°C shunt.

F_{EGTM} A constant numerical correction factor with unknown physical meaning. During the reverse-engineering process a residual linear correlation between the error and GE's EGTM was observed, which could be eliminated only by including F_{EGTM} in the formulation. Given that for both engine types F_{EGTM} is just above 1 and no analogous factor is included in the TC EGTM calculation, it serves as a safety factor to make EGTM more conservative.

C_{EGTM} A constant numerical adjustment with unknown physical meaning which is -2°C for the CF6-80E1. Similarly to F_{EGTM}, this constant adjustment was required to achieve RMSE ≈ 0. In case OW EGTM is not calculated using the actual peak EGT limit, this constant adjustment could be the difference between the assumed and actual $\mathrm{EGT}_{\mathrm{redline}}$.

5.1.3. Hot Day EGT margin deviation (EGTMDEV)

The EGTM deviation (EGTMDEV) is a parameter that will be used extensively in the process of improving OW EGTM accuracy in order to reduce OW-TC EGTM discrepancy, which will be discussed for the remainder of this chapter. The definition of EGTMDEV used in this research is provided in Equation 5.4, where i is the chronological cycle number and $\mathrm{SMA}_{\mathrm{EGTM},i}$ is the current centred, 21-cycle Simple Moving Average (SMA).

$$\mathrm{EGTMDEV}_i = \mathrm{EGTM}_i - \frac{1}{21}\sum_{j=i-10}^{i+10} \mathrm{EGTM}_j = \mathrm{EGTM}_i - \mathrm{SMA}_{\mathrm{EGTM},i} \tag{5.4}$$

As its name suggests, EGTMDEV quantifies how far the current EGTM *deviates* from the current expected EGTM. The primary purpose of EGTMDEV is to eliminate the EGTM variation caused by engine condition variation, both gradual deterioration as well as sudden improvements due to water-washes[(1)] and on-wing maintenance. This is visually demonstrated by Figure 5.1a which compares EGTM degradation and EGTMDEV variation as function of cycle number for a single CF6-80C2 installation period. The use of EGTMDEV instead of EGTM enables:

- ***Outlier removal:*** Other than EGTM itself, EGTMDEV in normally distributed as shown in Figure 5.1b, therefore enabling standard deviation (σ) based outlier removal. In case of this research, initial filtering was performed per engine installation to remove faulty EGTM values based on a 4-σ bandwidth, without discarding the complete snapshot.
- ***Scatter quantification:*** EGTMDEV is a direct measure of EGTM scatter. Therefore EGTMDEV-based objective functions can be used for scatter minimisation and hence EGTM accuracy optimisation. Additionally, by eliminating engine condition-based variation of EGTM, EGTMDEV can be used effectively to identify correlations with input parameters that originate from inaccurate corrections.

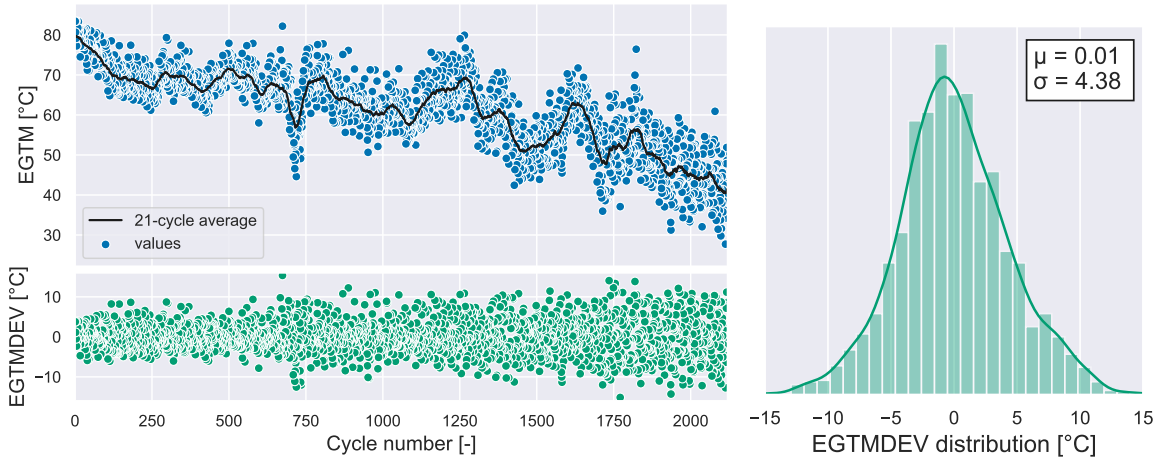

(a) Comparison of time-dependent EGTM degradation (top) and EGTMDEV variation (bottom)

(b) EGTMDEV distribution

Figure 5.1: Comparison of EGTM and EGTMDEV from a single CF6-80C2 installation period

Choosing the exact definition of EGTMDEV, or more specifically the underlying rolling averaging method, is non-trivial. Considering the averaging window, a small width has the advantage that a sudden EGTM

(1) *Water-wash:* a performance enhancement procedure, that can be performed without engine removal, using high pressure water and detergent spray to clean the core components by removing fouling

shift (e.g. water-wash) only affects a small number of EGTMDEV values. On the other hand, the effects of short- to midterm shifts of operating conditions (e.g. heat wave in Amsterdam) might also be unintentionally filtered from EGTMDEV.

The final decision for this thesis was to use a centred, 21-cycle SMA, therefore making the underlying assumption that the average of the previous 10 and subsequent 10 cycles are a good indicator of current engine condition. Given the snapshots with empty EGTM value, the SMA was configured to not return a value if it was based on less than 10 EGTM values. The limit of 10 values was chosen such that initial EGTMDEV values could still be calculated (e.g. $\mathrm{EGTMDEV}_1$ uses the average of cycle 1-11 for $\mathrm{SMA}_{\mathrm{EGTM},1}$).

More elaborate smoothing methods such as exponential moving averaging or even Kalman filters were considered beyond the scope of this research. Nevertheless using these in combination of with the customised corrections from Section 5.5 is left as a recommendation.

5.2. Data corruption & faults

Familiarisation with the OW data revealed unexplainable temporary fleet-wide shifts of EGTM and other engine parameters in the GE data. Understandably, non-physical temporary trend shifts are a potential cause for the OW-TC EGTM discrepancy, therefore justifying the extensive efforts to *fix* GE's data before commencing further research that are discussed briefly in this section.

Given that KLM's OW data and its shortcomings are understandably confidential, the content of this section does not reflect the amount of related work. Although it was found that multiple engine parameters contributed to various temporary shifts of fleet-average OW EGTM, this section discusses the data fixing process with Nacelle Anti-Ice (NAI) on the CF6-80E1 as example. An overview of the results of adjusting for all identified faults is also included at the end.

Identification of faults

Figure 5.2 provides the fleet-wide rolling average of NAI (top) and EGTM (bottom) for the Airfrance (AFR) and KLM fleet separately. Note that all values have been removed from the axes for confidentiality, but the total covered time period is approximately six years.

Considering the fleet-averaged EGTM, a clearly distinguishable upward trend shift without underlying physical cause is observed for KLM's fleet. An in-depth analysis of the other engine parameters revealed that – among others – NAI contributes to the shift, as NAI shows an equally timed trend shift.

Given that the seasonal trend of fleet-averaged NAI is still observable, it was concluded that a full reversal of NAI definition was in effect during the trend shift. It was later confirmed that a mismatch between engine-level and aircraft-level software definitions was to blame.

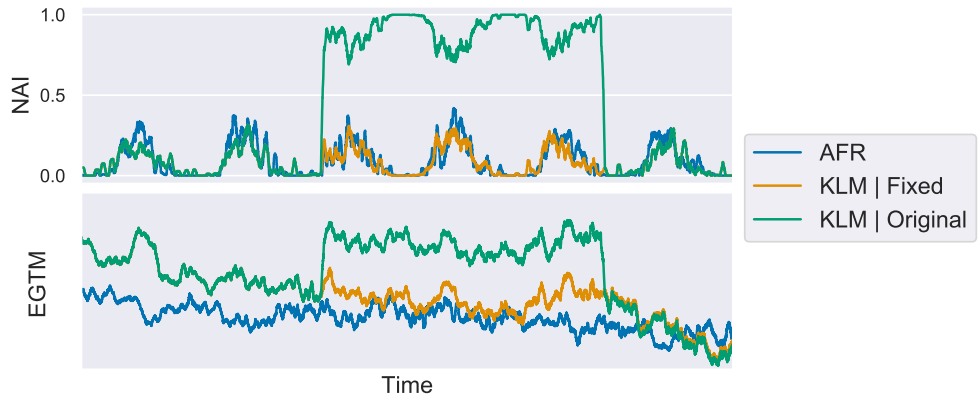

Figure 5.2: Comparison of Air France (AFR) and KLM CF6-80E1 fleet-average Nacelle Anti-Ice (NAI) (top) and EGTM (bottom) over period of six years (NB: axes values intentionally left out for confidentiality)

Adjusting faults

Continuing with the fleet-wide NAI shift as example, first of all the start and end timestamp of the NAI shift were accurately determined and subsequently all NAI values for KLM CF6-80E1 snapshots

between those timestamps were *flipped* (i.e. 1 changed to 0 and vice versa). The adjusted KLM NAI trend reconciles with AFR values.

Following the adjustment of NAI, the benefit of the reverse-engineered EGTM calculations was demonstrated by adjusting EGTM accordingly using the known value of $\Delta\mathrm{EGT}_{\mathrm{NAI}}$. The resulting *fixed* fleet-averaged EGTM for KLM clearly demonstrates successful elimination of the non-physical shift.

Fixing the data for the NAI shift as well as other unmentioned faults was enthusiastically received by KLM engineers and its results are used on daily basis in an engine fleet performance dashboard. Furthermore all subsequent research in this report is based on the fixed data unless specifically stated otherwise.

Overview of results

After the OW data was *fixed* for the identified faults, including the NAI-related EGTM shift, the predicted effect of that adjustment on the OW-TC EGTM discrepancy distribution was evaluated. The results hereof are provided in Figure 5.3, which gives the distribution of the installation-specific change of cycle 11-20 EGTM from the CF6-80E1 fleet.

Most installations are unaffected by the process of fixing data faults, however for some of the installation periods cycle 11-20 mean EGTM is decreased by more than 6°C such that fleet-average shift of $\mu(\Delta\mathrm{EGTM}_{\mathrm{OW-TC}})$ is −2.0°C. In other words, the original $\mu(\Delta\mathrm{EGTM}_{\mathrm{OW-TC}})$ was 2.0°C too high due to the faults in GE OW data.

It is expected that the faults also contributed to $\sigma(\Delta\mathrm{EGTM}_{\mathrm{OW-TC}})$. The adjusted $\Delta\mathrm{EGTM}_{\mathrm{OW-TC}}$ distributions, including the adjustments from the application of customised installation-specific N1K-, AH- and TT2-corrections that will be discussed in Sections 5.5 and 5.6, will be provided in Section 6.1 in Chapter 6.

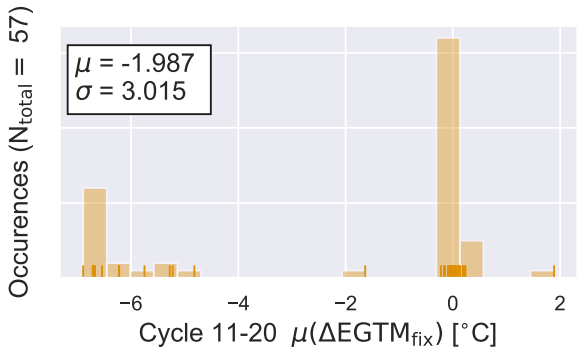

Figure 5.3: Distribution of installation-specific effect of fixing data for faults on cycle 11-20 average EGTM from the CF6-80E1 fleet

5.3. Effects of throttle setting on EGT margin

The OW throttle push correction is used to account for the discrepancy between actual (N1K) and rated ($\mathrm{N1K}_{\mathrm{rated}}$) corrected fan speed resulting among others from de-rated or high-altitude takeoffs. As has been discussed in Subsection 4.1.1 and Subsection 5.1.1, the throttle push correction makes an adjustment ($\Delta\mathrm{EGT}_{\Delta\mathrm{N1K}}$) which can be interpolated from the reverse-engineered throttle push table for the measured N1K.

Nevertheless, significant non-linear correlations between EGTMDEV and N1K were observed in the OW data. Given that average OW N1K is significantly lower than $\mathrm{N1K}_{\mathrm{rated}}$ and TC N1Kc, inaccuracies in the throttle push correction potentially contribute to OW-TC EGTM discrepancy.

This section first of all provides a data-driven analysis of the EGTMDEV-N1K correlations in Subsection 5.3.1 followed with a theoretical analysis to expose the underlying physical explanation for those correlations in Subsection 5.3.2.

Furthermore, Section 5.5 addresses the proposed methodology to customise OW corrections – including customised N1K-, AH- and TT2-corrections – per engine installation in order to eliminate the contributions of those parameters to the OW-TC EGTM discrepancy towards achieving the secondary research objective. The results of that method are provided in Section 5.6.

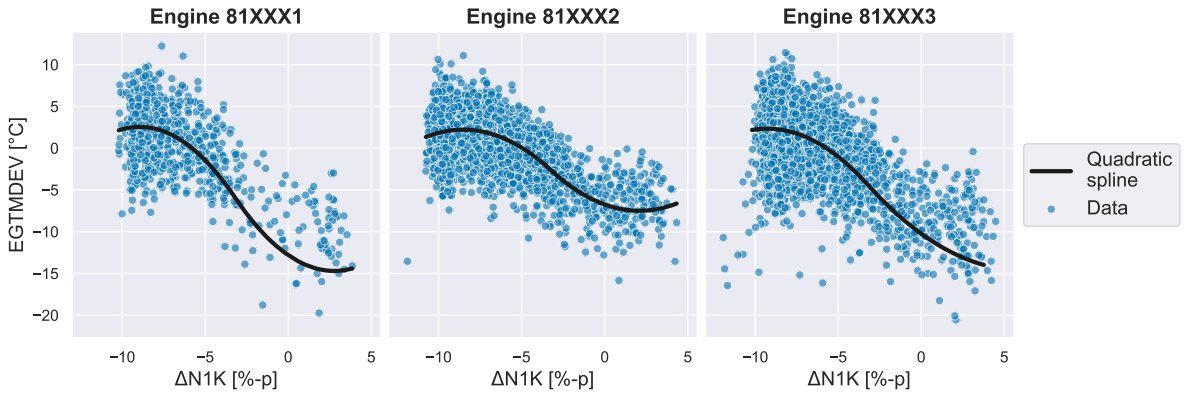

Figure 5.4: Observed EGTMDEV - ΔN1K correlation in original data from 3 CF6-80E1 installation periods

5.3.1. Data analysis

Figure 5.4 renders the observed EGTMDEV-N1K correlation from three example CF6-80E1 installation periods, where ΔN1K on the x-axis is defined as the difference between actual and rated corrected fan speed.

The scatter-plots also include a quadratic spline function that describes the correlation between EGTMDEV and ΔN1K that was found with the combined custom correction optimisation in Section 5.5. Hence, the corresponding definitions and the fact that they are not an exact least-square fit to the EGTMDEV-N1K are addressed in that section. Irrespective of the fitted function, there is a distinct non-linear correlation between EGTMDEV and N1K observed for all examples in Figure 5.4.

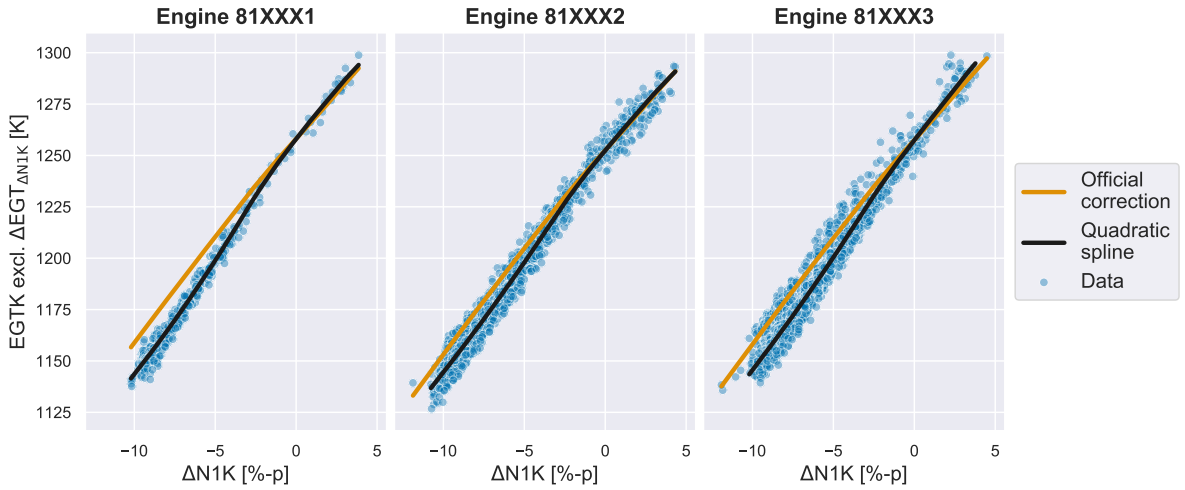

Figure 5.5: Observed EGTK (excluding $\Delta\mathrm{EGT}_{\Delta\mathrm{N1K}}$) - ΔN1K correlation in original data from 3 CF6-80E1 installation periods

Given that the correlations look non-physical in the EGTMDEV domain, Figure 5.5 also shows same correlation translated to the EGTK – excluding the contribution of $\Delta\mathrm{EGT}_{\Delta\mathrm{N1K}}$ – domain which makes understanding the physical meaning of the EGTMDEV-N1K correlations more accessible. The actual fits are hence also an exact representation of the splines in Figure 5.4.

Additionally, the official linear-splines based on the official reverse-engineered throttle push table have been included, which are translated such that the official EGTK at ΔN1K = 0 corresponds with the data's value at ΔN1K = 0 as is inherently also assumed when the throttle push correction is applied.

The primary conclusion to be drawn from Figure 5.5 is that the relation between EGT and N1K – i.e. how the engine heats up if throttle setting is increased – described by the data is not equal to the assumed relation used to corrected de-rated TO data to $\mathrm{N1K}_{\mathrm{rated}}$, which expresses itself as an undesired correlation between EGTM and N1K.

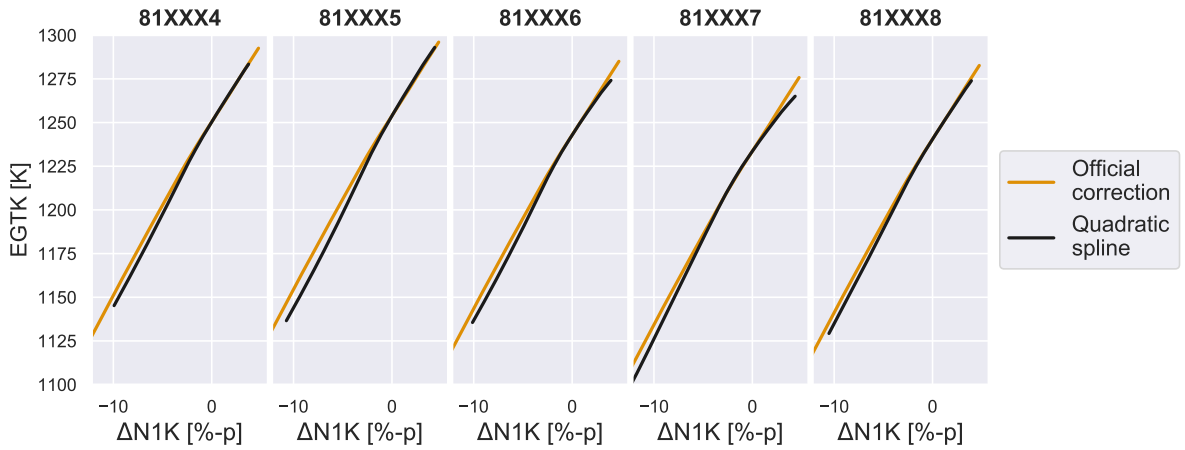

Figure 5.6: Comparison of observed EGTK (excluding $\Delta\mathrm{EGT}_{\Delta\mathrm{N1K}}$) - ΔN1K correlations with official relationship from GE's throttle push table in original data from 5 CF6-80E1 installation periods

Also, it is observed that the discrepancy between the official and actual EGT-N1K relationship differs for each of the three engine installation period examples. This is substantiated by the additional 5 examples in Figure 5.6 as well as the overall analysis of over 150 CF6-80C2 and CF6-80E1 installation periods. It is concluded that each installation period has its own, distinctive EGTK-N1K and hence EGTMDEV-N1K signature. The physical explanation for these data-driven observations is discussed in the subsequent subsection.

Furthermore the results of the combined custom correction optimisation that will be discussed in Section 5.6 will be used to assess the contribution of inaccurate throttle push corrections on the observed non-zero mean and scatter of $\Delta\mathrm{EGTM}_{\mathrm{OW-TC}}$.

5.3.2. Theoretical analysis

The goal of this section is to expose the theoretical and physical grounds for the EGTMDEV-ΔN1K correlations discussed in the previous subsection. First, a simple schematic example will demonstrate how a discrepancy between the official throttle push correction and actual ΔEGT-ΔN1K relationship can produce inaccurate and non-conservative EGTM values. Afterwards, a GSP-based analysis is used to validate how the known trend discrepancy can develop in the first place.

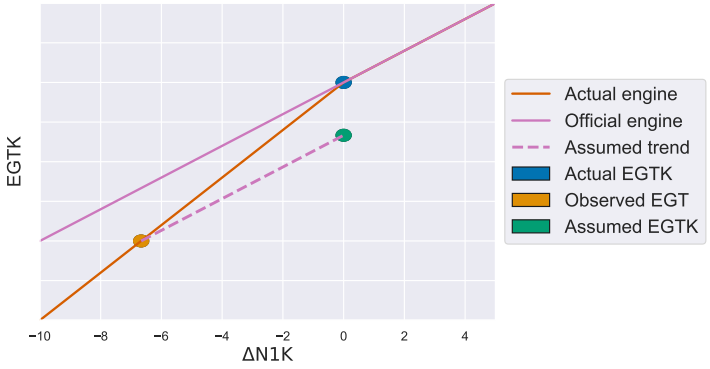

Figure 5.7: Schematic explanation for inaccurate EGTK as result of inaccurate official throttle push ΔEGT-ΔN1K relationship

Origin of EGTMDEV-N1K correlation

Figure 5.7 schematically explains how a discrepancy between the assumed and actual ΔEGT-ΔN1K trend can result in inaccurate EGTK values. The observed EGT will per definition always be on the trend-line of the actual engine, which in most cases – based on fleet-wide analysis – has a steeper gradient than the official engine trend-line below $\mathrm{N1K}_{\mathrm{rated}}$ or ΔN1K = 0. If the official gradient is used to translate observed EGT to ΔN1K = 0, the assumed EGTK is lower than the EGTK based on the

actual engine ΔEGT-ΔN1K gradient. Hence, if the actual gradient is larger than the official gradient or alternatively if the actual engine heats up faster with N1K, the calculated EGTM values of snapshots with ΔN1K < 0 are non-conservative.

Origin of engine-to-engine differences

Engine-to-engine differences are unavoidable, since even among factory new engines a spread of delivery EGTM of several °C is very common. Furthermore, the CF6-80E1 engines from AF-KLM engine pool are all within their second or higher installation period. Therefore the combination of engine-specific deterioration and maintenance will have increased the spread of engine-to-engine variation in terms of component efficiencies, pressure ratios and corrected mass flows.

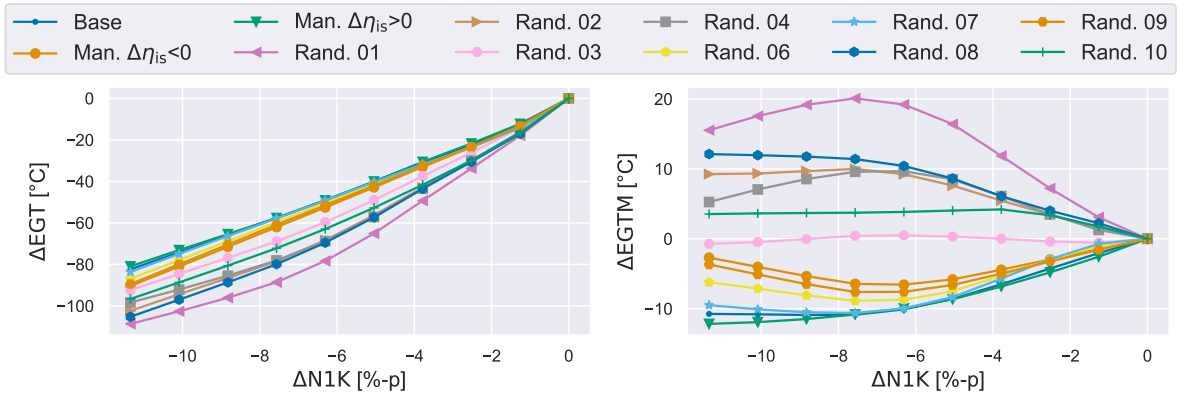

Figure 5.8: Simulated engine-specific ΔEGT-ΔN1K (left) and ΔEGTM-ΔN1K (right) correlations based on CF6-80C2 GSP model and deterioration cases from Appendix C

The hypothesis here is that those engine-to-engine variations also affect the accuracy of the official, generic throttle push correction. This hypothesis was validated using simulations with the CF6-80C2 GSP model

First, 13 distinct cases of component deterioration where defined: 1) 10 random (e.g. *Rand. 1*) cases with randomly assigned $\Delta\eta_{is}$ and $\Delta\dot{m}_c$ values for each component[(2)]; 2) 2 manually defined cases with either $\Delta\eta_{is} > 0$ or $\Delta\eta_{is} < 0$ for all components (e.g. *Man.* $\Delta\eta_{is} > 0$); and 2) the baseline model. The exact values of $\Delta\eta_{is}$ and $\Delta\dot{m}_c$ per case are defined in Appendix C. The component-level deterioration profiles are based on values encountered in previous research [2, 19]. Nevertheless some *questionable* engine-level combinations of good and bad components might be included.

For each case, a steady-state series simulation was performed between 90% and 103.5% N1K (i.e. $N1K_{rated}$ for the CF6-80C2B1F), specifically avoiding higher N1K values given the model's limitations mentioned in Subsection 3.4.4. The simulated EGT-N1K relationships were also converted into the EGTM domain by assuming the average EGT-N1K trend of the simulated cases as throttle push correction.

Concerning the results of the simulated analysis in Figure 5.8, which were normalised with respect to N1K = 103.5% , notable differences between the EGT-N1K relationships are observed which are also expressed in the EGTM domain. Although the actual magnitudes of the EGTM-N1K trends are not to be taken for granted, the analysis does support the hypothesis that engine-to-engine variations results in distinct EGTM-N1K correlation signatures due to incorrect throttle push corrections.

Furthermore, based on the manually set cases, the expected observation is made that an efficient engine heats up slower with N1K than an inefficient engine. The latter also explains why for most of the analysed CF6-80E1 engines, the actual EGTK-N1K trend is steeper than the official trend.

5.4. Effects of humidity & temperature on EGT margin

Engine inlet conditions affect turbofan performance and hence should be accounted for when calculating corrected performance parameters such as EGTM. However, due to the lack of a humidity sensor on

[(2)] *Rand. 5:* This case encountered convergence issues as was therefore discarded from the results

aircraft, current practice for the CF6-80C2 and CF6-80E1 types is to assume dry conditions irrespective of the actual humidity level for all on-wing EGTM calculations.

Given that TC EGTM is corrected for the measured humidity, the influence of humidity on the OW EGTM values is a potential cause for OW-TC EGTM discrepancy, and should be analysed and preferably eliminated.

This section addresses an in-depth analysis of AH on OW EGTM, whereas fan inlet temperature (TT2) is also included for reasons that will be discussed shortly. First, the steps taken to merge humidity data into the OW dataset is discussed in Subsection 5.4.1. Subsequently separate data-driven and theoretical analyses are provided in Subsection 5.4.2 and 5.4.3. Additionally, Subsections 5.4.4 and 5.4.5 briefly discuss the effects of non-gaseous water ingestion and condensation.

Finally, Section 5.5 addresses the combined optimisation of engine-specific custom N1K-, AH- and TT2-corrections, which builds on the analyses in this and the previous section.

5.4.1. Humidity data collection and processing

Although most modern aircraft do not measure humidity, airports broadcast an hourly Meteorological Aerodrome Report (METAR) code that includes essential measured and predicted weather information for the pilots. These reports have been ingested into a database at KLM for all its destinations since 2000.

These METAR codes were extracted and parsed into airport temperature ($TS_{airport}$), altimeter setting[(3)] (PS_{SL}) and dew point temperature (TDEW) and converted into AH in g/kg and RH in % using Buck's equations [79].

Subsequently, the airport and humidity data was merged with the OW data by matching the airport and choosing the nearest METAR timestamp. Due to missing departure station data, insufficient METAR data could be merged with CF6-80C2 snapshots. The fact that other columns in the CF6-80C2 data were also insufficiently filled, substantiates the decision to mostly discard the CF6-80C2 results from this report.

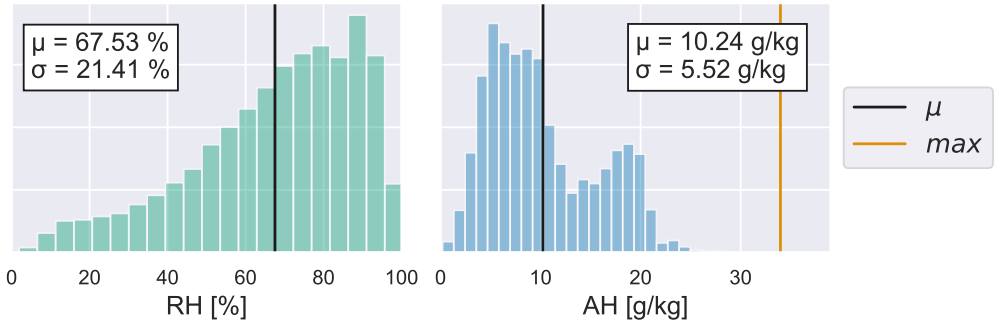

Figure 5.9: Distribution of absolute (AH) and relative (RH) humidity from CF6-80E1 fleet snapshots

Figure 5.9 provides the distributions of AH and RH experienced by the CF6-80E1 fleet, which is also representative for a single engine installation period.

Additionally, Figure 5.10 depicts the relationships between AH, RH and TT2 based on a single, representative CF6-80E1 installation period. Given that TT2 and $TS_{airport}$ are logically strongly correlated, an engine intuitively experiences the highest humidity in combination with high TT2. The high TT2, low AH combinations in the lower right corner correspond to dessert airports such as Riyadh, Saudi-Arabia. The significance of the AH-TT2 correlation will come to light in subsequent subsections.

The described merging procedure inherently assumes: 1) constant humidity between airport and aircraft altitude (i.e. dAH/dh = 0); and 2) constant humidity between the METAR and TO timestamp (i.e. dAH/dt = 0).

It was found that humidity-altitude gradients are very unpredictable which impedes generic adjustment [80, 81]. Furthermore fellow graduate intern at KLM ES [76] predicted an AH-h gradient of approx-

(3) *Altimeter setting:* this value corresponds to the measured airport pressure converted to sea-level on basis of ISA relations. It is used by pilots to determine accurate pressure-based aircraft altitude (w.r.t. sea-level)

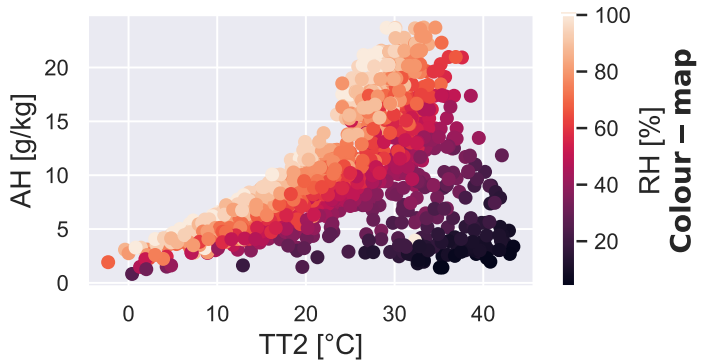

Figure 5.10: Observed correlation between absolute humidity (AH), relative humidity (RH) and inlet temperature (TT2) from a single, representative CF6-80E1 installation

imately 0.001 g/kg/ft based on [82]. Given that TO snapshots are on average measured 400 ft above the runway with maxima at 2000 ft, the average and maximum airport-to-aircraft humidity discrepancy is predicted to be 0.4 g/kg and 2 g/kg, both small compared to the values of AH.

The second assumption could be avoided with time-dependent interpolation of the airport humidity with a linear or more complex spline, but was avoided because hour-to-hour variations of AH were found to be small [76].

5.4.2. Data analysis

Figure 5.11 gives the correlation between EGTMDEV and AH for a single, representative CF6-80E1 installation period. Assuming linear AH effects, similar to the TC EGTM-AH corrections in Section 4.2, the corresponding dEGTM/dAH gradient is 0.2°C per g/kg. Assuming an EGTK in the order of 1000 K, this corresponds to dEGT/dAH gradient of -0.02%-p per g/kg.

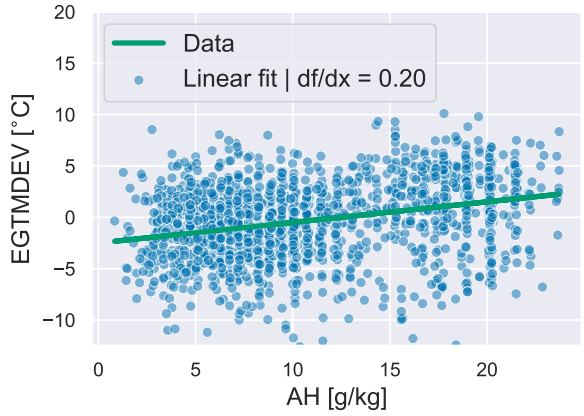

Figure 5.11: Data and linear fit of EGTMDEV-AH correlation from a single, representative CF6-80E1 installation

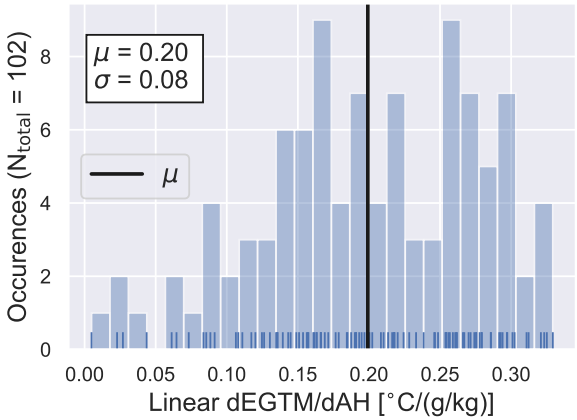

Figure 5.12: Distribution of observed installation-specific linear dEGTM/dAH values from the CF6-80E1 fleet

Similar linear fit gradients were determined for the all individual CF6-80E1 installations, whereof the distribution is visualised by the histogram in Figure 5.12. Two notable observations are:

- The average observed dEGTM/dAH is 0.2°C per g/kg and corresponding approximate dEGT/dAH is -0.02%-p per g/kg, which is considerably lower than the expected -0.0325%-p per g/kg based on the TC and theoretical AH-corrections from Section 4.2.
- The dEGTM/dAH values are significantly scattered between approximately 0.0°C and 0.4°C per g/kg humidity, therefore some engine installations are even seemingly unaffected by AH.

The theoretical analysis in Section 4.2 confirmed that empirical AH-corrections dependent on engine condition. Nevertheless the observed scatter of dEGTM/dAH within the CF6-80E1 fleet data is beyond

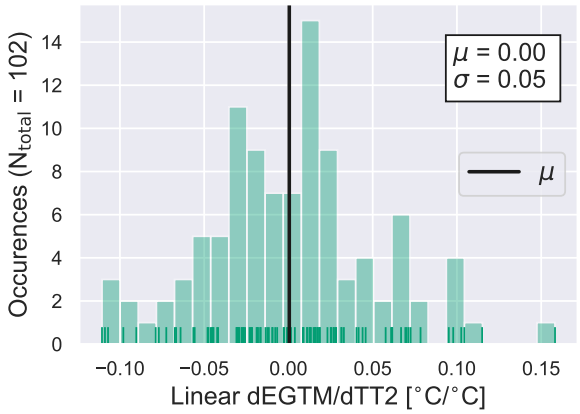

Figure 5.13: Distribution of observed installation-specific linear dEGTM/dTT2 values from the CF6-80E1 fleet

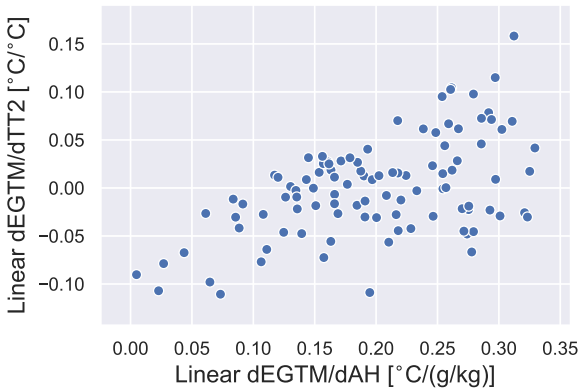

Figure 5.14: Observed correlation between installation-specific linear EGTMDEV-AH and EGTMDEV-TT2 gradients from the CF6-80E1 fleet

expectations. Given the correlation between AH and TT2 shown previously in Figure 5.10, it was hypothesised that inaccurate TT2-corrections mask the effect of AH on EGTM.

Figure 5.13 provides the distribution of the linearised EGTMDEV-TT2 gradients from the same CF6-80E1 installations. Similar to dEGTM/dAH, there is significant scatter with typical values ranging between −0.1°C and 0.1°C per °C which does support the hypothesis of inaccurate TT2-corrections.

Furthermore, plotting dEGTM/dTT2 with respect to dEGTM/dAH as in Figure 5.14 reveals a slight correlation between both gradients. For example, the installation with dEGTM/dAH ≈ 0 can be explained by the corresponding negative dEGTM/dTT2 because the AH-related EGTM increase is masked by the TT2-related EGTM decrease.

The results of the combined custom correction optimisation that will be discussed in Section 5.6 will be used to assess the contribution of inaccurate TT2-corrections and lack of AH-corrections on the observed non-zero mean and scatter of $\Delta\mathrm{EGTM}_{\mathrm{OW-TC}}$.

5.4.3. Theoretical analysis

This subsection addresses the physical and theoretical grounds for the observed average value and scatter of dEGTM/dAH and dEGTM/dTT2 in the previous subsection, while building on the content of Section 4.2 on the TC humidity corrections. The analysis's results serve as justification for the customised AH- and TT2-correction optimisation that is proposed in Section 5.5.

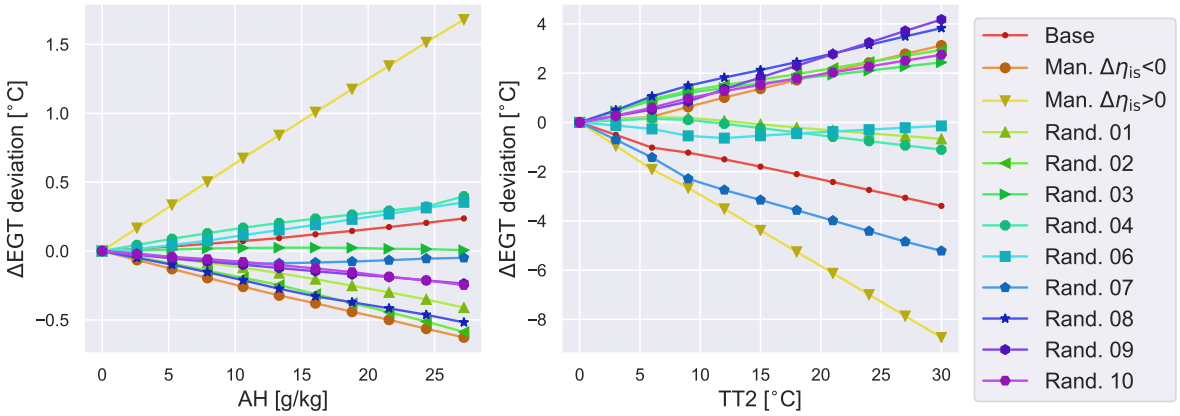

Figure 5.15: Simulated engine-specific ΔEGT-AH (left) and ΔEGTM-TT2 (right) correlations based on CF6-80C2 GSP model and deterioration cases from Appendix C, where ΔEGT is normalised w.r.t. average relation per plot

First of all consider Figure 5.15, which provides insights on the effect of overall engine condition on EGT-AH and EGT-TT2 relationships based on GSP simulations with the previously discussed deterioration cases from Appendix C.

The AH-effect analysis on the left is based on steady-state series simulations at constant 100% N1K – according to GE's OW N1K definition – and ISA+15°C conditions with 0% to 100% RH. The TT2-effect analysis on the right is based on simulations at constant 100% N1K and ISA-15°C to ISA+15°C conditions with 0% RH.

In order to visualise the differences, the simulated EGT-AH and -TT2 results are normalised: 1) with respect to the baseline (i.e. AH = 0 g/kg or TT2 = 0°C) of the current case; and 2) with respect to the average ΔEGT-AH and -TT2 relation of all cases. The result is referred to as the ΔEGT deviation.

The primary conclusion to draw from Figure 5.15 is that the effect of AH and TT2 on EGT depends on engine condition. Therefore engine-to-engine differences originate the scattered dEGTM/dTT2 distribution in Figure 5.13. Additionally, minor aircraft-to-aircraft differences of TT0-sensor characteristics are also a potential contributor to the scatter of dEGTM/dTT2 because the OW temperature correction is based on TT0. That potential cause for $\Delta\mathrm{EGTM}_{\mathrm{OW-TC}}$ is not investigated in this research, as is substantiated in Section 6.4.

The scattered dEGTM/dAH distribution in Figure 5.12 originates from engine-to-engine variations in two ways: 1) directly because the physical EGT-AH relation is engine-specific as shown in the left of Figure 5.15; and 2) indirectly because the non-zero dEGTM/dTT2 relations mask the effects of AH.

Further analysis of the simulated results also revealed that engine with higher thermal efficiency are less sensitive to humidity and temperature related effects. This conclusion reconciles with the similar conclusion drawn from the simulated throttle effects study.

5.4.4. Non-gaseous water ingestion

The METAR code also includes a precipitation report. In order to assess the contribution of non-gaseous water ingestion to OW-TC EGTM discrepancy, the METAR code was parsed into meaningful precipitation categories to study the effects based on the data.

Based on the fact that only 6.5% of the snapshots are *potentially* affected, it can already be concluded that non-gaseous water ingestion does not systematically contribute to OW-TC EGTM differences. Note the use of *potentially* because more than half of those 6.5% corresponds to *shower* conditions instead of continuous precipitation.

Furthermore, data-driven analysis of the effects of non-gaseous water ingestion on EGTMDEV revealed small and inconsistent dependencies. This is summarised by Figure 5.16, which gives the distribution of the difference between average EGTMDEV with precipitation ($\mu(\mathrm{EGTMDEV}_{\mathrm{wet}})$) and without precipitation ($\mu(\mathrm{EGTMDEV}_{\mathrm{dry}})$) per installation from the CF6-80E1 fleet.

Given that reliable and generic corrections for water ingestion are unrealistic due to the high complexity and poor scalability [46, 52, 53], it was therefore decided to not do further research and conclude that non-gaseous water ingestion has a negligible contribution to the OW-TC EGTM discrepancy.

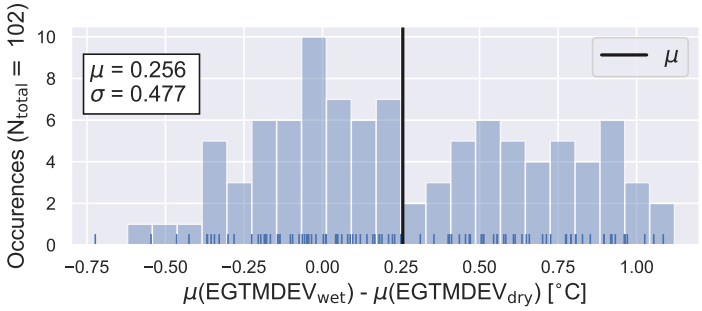

Figure 5.16: Distribution of installation-specific difference between precipitating and non-precipitating conditions mean EGTM values from the CF6-80E1 fleet

5.4.5. Condensation effects

Although condensation will not be included in the customised correction that will be discussed in Section 5.5, it is not said that condensation has no contribution to OW EGTM scatter or OW-TC EGTM

discrepancy. Therefore this section briefly assesses the effect of condensation on OW EGTM. It is assumed that the reader is familiar with Section 4.3 on the official TC and theoretical condensation corrections. Apart from the aforementioned theoretical limitations, analysis of CF6-80E1 OW data also substantiates the decision to not include a condensation correction in the proposed improvements.

A prerequisite for inlet condensation is a local decrease of static temperature or pressure such that RH increases beyond 100%. Hence condensation primarily affects turbofan performance during spool-up and the ground-run when TS1/TS0[(4)] and PS1/PS0 are lowest due to the combination of low aircraft and high inlet throat Mach number. A simulated study was conducted with the CF6-80C2 GSP model to assess those ratios for the M0, TS0 (or ΔT_{ISA}) and PS0 (or h_{ISA}) envelope experienced during TO snapshots at 105% N1.

The results hereof for the envelope edges are provided in Figure 5.17. Both PS1/PS0 < 1 and TS1/TS0 < 1 hold for the complete envelope, therefore theoretically condensation is possible over the complete envelope as well.

The plot on the right also predicts humidity in the inlet throat (RH1) assuming 100% free-stream humidity (RH0). Based on the range of predicted RH1 values, homogeneous condensation is unlikely to occur. Hence the level of condensation in those operating conditions will depend on the other pre-requisite that is sufficient condensing nuclei density.

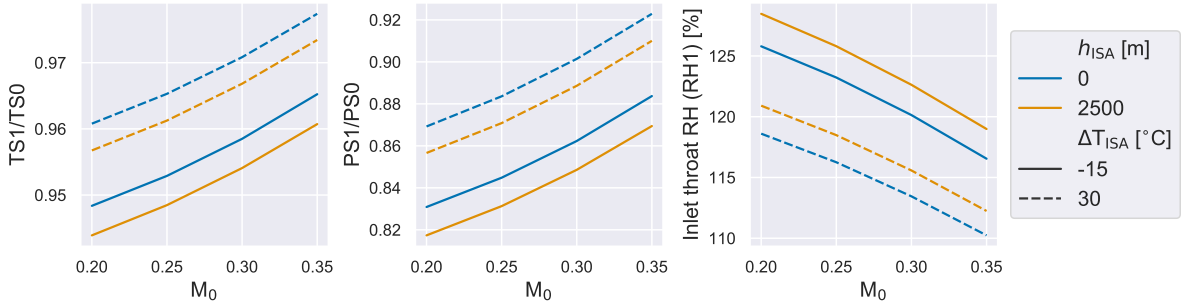

Figure 5.17: Simulated PS1/PS0 (left), TS1/TS0 (middle) and inlet throat humidity (RH1) (right) for typical takeoff M0, TS0 and PS0 envelope at 100% ambient RH based on CF6-80C2 GSP model

Subsequent data-driven analyses revealed that the original EGTMDEV is positively correlated to RH with a fleet average linear dEGTM/dRH of 0.04°C per % RH, which contradicts theoretical condensation effects because of the correlation between RH and AH. If the adjusted EGTMDEV data – corrected with the customised N1K-, AH- and TT2-corrections as will be discussed in Section 5.5 – is consulted, the fleet average dEGTM/dRH is 0.0°C per % RH with only negligible differences if individual engine installations are considered. Figure 5.18 presents the original and adjusted EGTMDEV-RH correlation for a single, representative CF6-80E1 installation period.

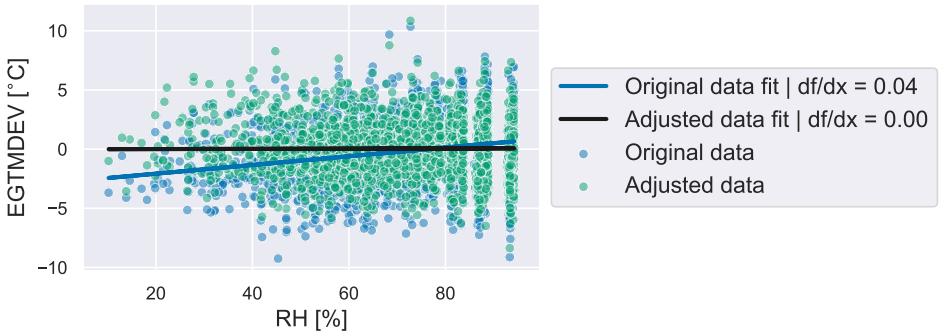

Figure 5.18: Comparison of data and fit of EGTMDEV - RH correlation from a single, representative CF6-80E1 installation

(4) *Station 1:* inlet throat

To conclude, it is expected that occasionally TO snapshots will be affected by condensation given the flow acceleration into the inlet. Nevertheless no correlation between on EGTM and RH was detected in the data, hence the influence of condensation on the OW-TC EGTM discrepancy is expected to be insignificant with regards to the non-zero average and scatter of $\Delta\mathrm{EGTM}_{\mathrm{OW-TC}}$.

Additional research on condensation effects is left for the recommendations. Given the high sensitivity of condensation to its prerequisites, it is first of all recommended to improve RH data accuracy. For example by time-wise interpolating its value when merging weather and engine data. It is also proposed to study if the difference between TT0 and TT12 can be used to assess if a snapshot is affected by condensation.

5.5. Methodology for customised corrections for EGT margin

Given the observed engine-specific correlations between EGTMDEV and N1K, AH and TT2 – all of which potentially contribute to OW-TC EGTM discrepancy – this section continues by addressing the proposed methodology to simultaneously optimise custom throttle push, absolute humidity and inlet temperature corrections per engine installation period.

The objective of the customised corrections is twofold. Firstly, a proof of concept for the application of customised engine-specific corrections for N1K, TT2 and AH to enhance OW EGTM accuracy which should also contribute to elimination of potential causes for the OW-TC EGTM discrepancy. Secondly, the results enable to quantify the influence of inaccurate N1K-, AH- and TT2-corrections on the original $\Delta\mathrm{EGTM}_{\mathrm{OW-TC}}$.

First the optimisation problem – that is solved for each individual installation period – is defined in Subsection 5.5.1, followed by the implementation in Subsection 5.5.2. The primary underlying assumptions are addressed in Subsection 5.5.3. The fitting analysis that was performed to prevent under- or overfitting is discussed in Subsection 5.5.4.

5.5.1. Optimisation problem

The customisation of N1K-, AH- and TT2-corrections was treated by defining and solving the same optimisation problem for each individual engine installation period. The essential components of such problem are the objective function, design vector, bounds and constraints.

Objective function

The primary goal of optimising the corrections is to eliminate residual EGTMDEV correlations with ΔN1K, AH and TT2 such that OW EGTM scatter is reduced. Therefore the standard deviation of EGTMDEV ($\sigma(\mathrm{EGTMDEV})$) was used as the to-be minimised objective function. Given that $\mu(\mathrm{EGTMDEV})$ is approximately 0°C, the RMS and σ of EGTMDEV are essentially interchangeable.

customised throttle push correction

The official OW throttle push correction is based on a table that describes the empirical relation between ΔN1K and $\Delta\mathrm{EGT}_{\Delta\mathrm{N1K,official}}$ for a discrete number of ΔN1K values, whereas linear interpolation is to be used when the correction for an non-tabulated ΔN1K value is required.

The design variables related to the customised N1K-correction should therefore enable the optimiser to change the ΔEGT-ΔN1K relationship until the actual trend is captured. Instead of completely redefining the throttle push tables, a second customisable throttle push table is formulated for each installation that augments the official throttle push correction according to Equation 5.5.

$$\Delta\mathrm{EGT}_{\Delta\mathrm{N1K}} = \Delta\mathrm{EGT}_{\Delta\mathrm{N1K,official}} + \Delta\mathrm{EGT}_{\Delta\mathrm{N1K,custom}} \tag{5.5}$$

The degrees of freedom concerning the optimisation of the customisable throttle push table that describes $\Delta\mathrm{EGT}_{\Delta\mathrm{N1K,custom}}$ are: 1) the custom throttle push table formulation, i.e. the number of rows and corresponding ΔN1K values; and 2) the ΔEGT values.

Regarding the optimisation, the ΔEGT values are included in the to-be optimised design vector while the table formulation was chosen beforehand based on the fitting analysis that will be discussed in Subsection 5.5.4. No constraints or bounds on the design variables were formulated.

customised temperature correction
Current EGTM calculations already include a TT2-correction, hence the logical design variable to associate with optimising the custom temperature correction is the corresponding exponent (XT). The final results were obtained without the need for bounds or constraints to guarantee physical solutions. The initial value of XT was set to GE's official value of approximately 0.87.

customised humidity correction
Other than the N1K- and TT2-corrections, current OW EGTM calculations do not include a AH-related correction such that defining related design variables is less trivial. The TC humidity corrections that received ample attention in Section 4.2 influence the final EGTK and EGTM value: 1) explicitly through the HEGT correction factor on EGTK; and 2) implicitly through the HN1 correction factor on N1K and subsequent related EGTK adjustment ($\Delta\mathrm{EGT}_{\Delta\mathrm{N1K}}$). Both HEGT and HN1 can be represented by linear functions with value 1 at AH = 0, where dHEGT/dAH equals 10×10^{-5} per g/kg and dHN1/dAH equals -30×10^{-5} per g/kg.

Furthermore it was concluded in Section 4.2 that the variation of HN1 is based on correcting for the loss of thrust due to humidity, while HEGT is based on correcting for the cooling effect of humidity if the engine was thrust-controlled. Since FNK is not measured on-wing, the optimised custom AH-correction can only be based on AH and EGT.

Interim correction optimisations were performed with both dHEGT/dAH and dHN1/dAH included as design variables, but it was concluded that the contributions of HN1 and HEGT to the overall humidity correction were interchangeable given the lack of an FNK-based constraint for HN1. Although the combined influence of the optimised AH-corrections was reconcilable with TC and theoretical corrections, the underlying combinations of dHEGT/dAH and dHN1/dAH were inconsistent and non-physical.

Therefore the final custom corrections optimisation only incorporates dHEGT/dAH as design variable related to the AH-correction, without any bounds or constraints and with an initial value of 0 (i.e. HEGT = 1 ∀ AH). As will be demonstrated by the fitting analysis in Subsection 5.5.4, it was found that discarding dHN1/dAH as design variable had negligible effect on the achieved EGTMDEV scatter reduction (σ/σ_0).

Complete problem statement
Based on the above defined objective function and design variables, the full optimisation problem can be summarised as shown below. Here $\mathrm{N}_{\Delta\mathrm{N1K}}$ represent the number of rows in the to-be-customised throttle push correction table.

$$\min_{x} \quad J = \sigma(\mathrm{EGTMDEV})$$
$$\text{where:} \quad x = \left[\mathrm{XT}, \frac{\mathrm{dHEGT}}{\mathrm{dAH}}, \Delta\mathrm{EGT}_i\right] \quad \forall i = 1, \mathrm{N}_{\Delta\mathrm{N1K}}$$

5.5.2. Implementation

The above defined optimisation problem was implemented in Python and iteratively solved for each engine installation period. The overall workflow is as follows:

1. ***Filters:***

   (a) *Incomplete snapshots:* When all EGTM, Simple Moving Average (SMA) and EGTMDEV values are iteratively re-calculated, some EGTM data is *lost* by incomplete snapshots. For accurate quantification of the scatter reduction, incomplete snapshots are discarded beforehand. Also, it was decided to fix the cycle numbers corresponding to each $\mathrm{SMA}_{\mathrm{EGTM}}$ value (i.e. given 2 incomplete snapshots within cycle i-10 through i+10, $\mathrm{SMA}_{\mathrm{EGTM},i}$ is evaluated with the remaining 18 cycles instead of including 2 additional cycles).

   (b) *N1K outliers:* Since the throttle push table is formulated per installation based on the N1K domain spanned by the data, an additional filter was used to identify and discard data clusters with exceptional N1K values depending on a data density threshold. The filtering was based the Density-

Based Spatial Clustering of Applications with Noise (DBSCAN) algorithm from the Scikit-Learn package[5] with the goal of preventing over-fitting.

2. ***Initialisation:*** The throttle push table is formulated with equispaced ΔN1K values, based on the N1K range spanned by the filtered data and the pre-determined maximum permissible N1K step size ($\max(\Delta\Delta\mathrm{N1K})$), which will be discussed in Subsection 5.5.4 on the fitting analysis. The initial design vector contains 0°C for all $\Delta\mathrm{EGT}_i$, GE's OW value for XT and 0 for dHEGT/dAH.

3. ***Optimisation:*** Given the convex and continuous nature of the objective function, minimisation is performed by the gradient-based SLSQP algorithm from the SciPy-package[6]. The optimiser iteratively evaluates $\sigma(\mathrm{EGTMDEV})$ by re-calculating all EGTM and EGTMDEV for varying N1K-, AH- and TT2-corrections. Alternative to $\Delta\mathrm{EGT}_{\Delta\mathrm{N1K,official}}$, quadratic interpolation is used to derive $\Delta\mathrm{EGT}_{\Delta\mathrm{N1K,custom}}$ from the customised table, which improved the ability to capture the physical EGT-N1K relationship with a minimal number of ΔN1K values ($\mathrm{N}_{\Delta\mathrm{N1K}}$). Convergence is achieved when subsequent $\sigma(\mathrm{EGTMDEV})$ improvements or the Jacobian are within set tolerances.

4. ***Post-processing:*** The resulting design vector and other related parameters are saved to a *customised corrections database*. Separate Python functions were written to apply the optimised custom corrections to the original data to re-evaluate EGTM and EGTMDEV, including the possibility to apply the corrections consecutively to isolate the contribution of each individual customised correction.

5.5.3. Assumptions

Below the most noteworthy assumptions related to the methodology from the previous subsection are discussed.

Constant signature assumption

The most notable assumption at the basis of the above mentioned approach for data-driven optimisation of engine-specific N1K-, AH- and TT2-corrections is that the underlying physical EGT-N1K, -AH and -TT2 relationships are assumed to be constant over the time-period spanned by the data. At glance this *constant signature assumption* seems inexplicable given the fact that customised corrections stem from deterioration and the resulting engine-to-engine variations.

Despite the fact that OW EGTM degradation originates from gradual deterioration of a turbofan's components, it was unveiled that the overall shapes of the underlying EGT-N1K, -AH and -TT2 relations are in most cases preserved during installation periods. That is, OW deterioration appears to mostly translate rather than transform how EGT changes with N1K, AH and TT2.

Figure 5.19 illustrates that preservation of signatures based on correction optimisation results from three separate cycle number ranges from a long CF6-80E1 installation period. The optimised XT and dHEGT/dAH results are very comparable for all three cycle number ranges. For ΔN1K > 1%-p considerable differences are observed, which can be contributed to over-fitting as will be discussed in Section 5.6.3. Given that the vast majority of recorded ΔN1K values fall between -8°C and 0°C, it can be expected that considerable OW EGTM scatter reduction will be achieved even if full installation periods are used for the customisation.

Additionally, if the constant signature assumption would be completely invalid, smaller relative EGTMDEV scatter reductions (σ/σ_0) would be expected for longer installation periods because the customisation will be unable to account for the changing signatures. However, no such correlation was found.

Nevertheless, it was decided to optimise the corrections based on the first 500 cycles for this thesis given that OW-TC EGTM discrepancy research primarily requires accurate EGTM values for the initial cycles. Using fewer cycles was also tested, but interim results indicated an increased risk of over-fitting and an insufficient amount of data around $\mathrm{N1K}_{\mathrm{rated}}$. In order to adjust the discrepancy definition that uses the OW-method-based TC EGTM ($\Delta\mathrm{ETGM}^{\mathrm{ow}}_{\mathrm{OW-TC}}$), the customised N1K-corrections need to be accurate at $\mathrm{N1K}_{\mathrm{rated}}$ given that TC EGTM is recorded at $\mathrm{N1K}_{\mathrm{rated}}$ as well.

The current approach is deemed sufficiently accurate within the scope of this research effort where OW EGTM accuracy is not the primary objective. For accurate OW monitoring purposes, it is recommended

[5]URL: https://scikit-learn.org/stable/modules/generated/sklearn.cluster.DBSCAN.html
[6]URL: https://docs.scipy.org/doc/scipy/reference/generated/scipy.optimize.minimize.html

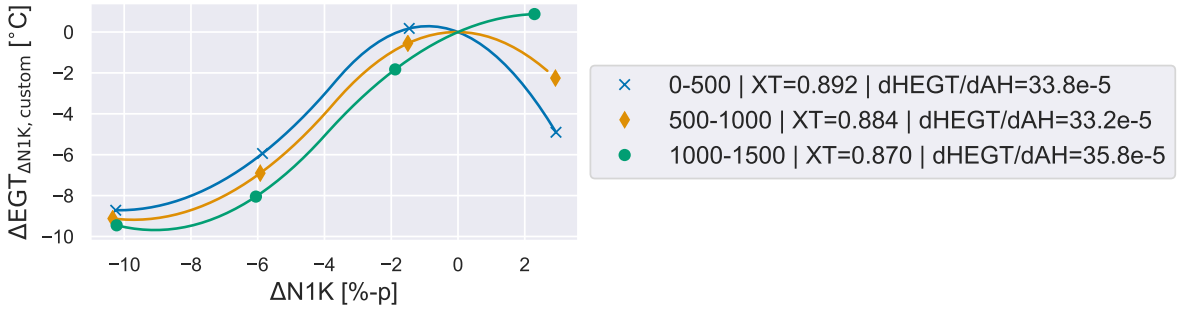

Figure 5.19: Optimised N1K-, AH- and TT2-correction results per cycle number range from a single CF6-80E1 installation

to develop adaptive customised corrections that are iteratively re-evaluated based on the last 100 to 200 cycles. As mentioned before, using more complex definitions of EGTMDEV for the objective function, such as using a Kalman filter or weighted moving averages, is also recommended to improve the physical accuracy.

Constant XT assumption

Additionally, it is assumed that a constant XT over the complete operating range is able to capture the EGT-TT2 relation. This assumption is primarily substantiated by the fact that the same holds for the official OW EGTM calculations.

Alternatively the official TC EGTM calculations include a TT2-correction exponent table which describes XT as a function of N1. Interim correction customisation results using a similar approach were unsatisfactory because the resulting XT-N1 relationship was clearly non-physical due to over-fitting to the data.

Humidity correction assumptions

Other than the previously mentioned assumptions on the accuracy of the merged AH data, the notable assumptions concerning the new, customised AH-correction for OW EGTM are: 1) only direct EGTK correction with HEGT; and 2) linearisation of HEGT-AH.

The former stems from the fact that insufficient parameters are available to *help* the optimiser balance the indirect (with HN1) and direct (with HEGT) correction contributions. Hence HN1 was discarded to prevent over-fitted, non-physical relationships. Based on the analysis of TC AH-corrections in Section 4.2, it can be concluded that the net effect of both correction terms is only weakly dependent on N1K. Furthermore the thesis specifically on humidity effects by Van Vuuren conducted at KLM ES [76] applies the same assumption.

Finally, the assumed linearity of HEGT-AH stems from the fact that both the theoretical and TC corrections are only very weakly non-linear. Comparison of the official and linearised corrections revealed no noticeable difference between both calculated EGTM values.

5.5.4. Fitting analysis

Despite the physics-based foundation in Sections 5.3 and 5.4 for customised engine installation-specific corrections, the data-driven nature of the combined N1K-, AH- and TT2-correction optimisation inhibits the risk of under- or over-fitting. Whenever data-driven models are used, model complexity should be tuned such that the model captures the underlying (physical) patterns without just memorising the (noisy) data.

Concerning the data-driven customisation of N1K-, AH- and TT2-corrections the only tunable parameter is the aforementioned maximum permissible ΔN1K step size ($\max(\Delta\Delta\mathrm{N1K})$) in the throttle push table. That parameter dictates the number of $\Delta\mathrm{EGT}_{\Delta\mathrm{N1K,custom}}$-$\Delta\mathrm{N1K}$ pairs in the table, and is therefore roughly equivalent to choosing the degree of the fitted polynomial. Figure 5.20 visualises the concept of under- and over-fitting concerning the customised throttle push correction based on fitting a 1st-, 4th- and 25th-order polynomial to the EGTMDEV-N1K correlation of a single CF6-80E1 install.

Deciding on a $\max(\Delta\Delta\mathrm{N1K})$ value was performed on the basis of a comprehensive cross-validation approach. For each engine installation and for a range of $\max(\Delta\Delta\mathrm{N1K})$ values, a 5-fold cross-validation

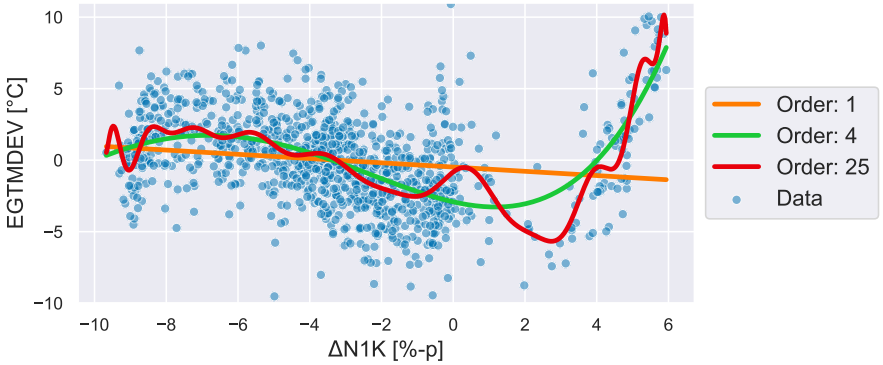

Figure 5.20: Example of under- and over-fitted polynomial fit with EGTMDEV-N1K data from single CF6-80E1 installation

was performed using the KFold function from the Scikit-Learn package[7] to randomly generating the five *data folds*.

The 5-fold cross validation consists of iteratively optimising the corrections based on 4-out-of-5 folds as *training set* and subsequently evaluating the fit quality (i.e. EGTMDEV σ/σ_0) of the training set and 5th-fold as *validation* set. The average fit quality values for the training and validation set over the five iterations are then saved for further analysis.

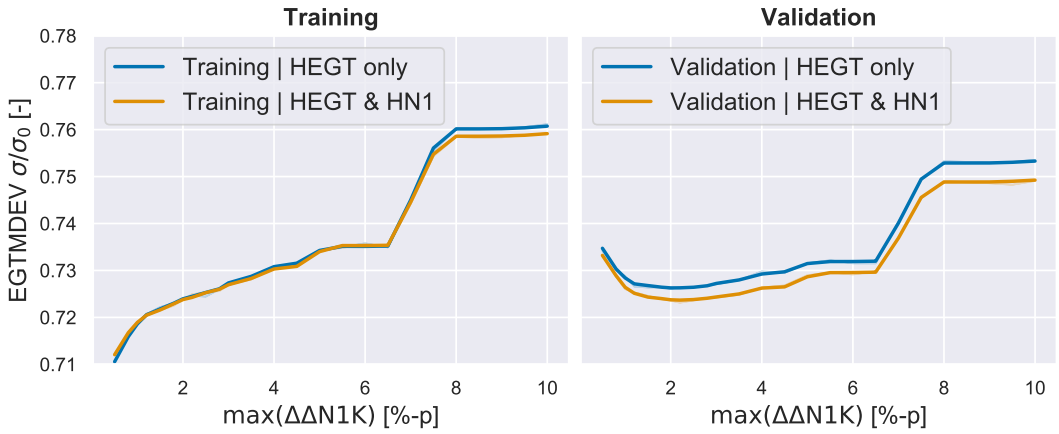

Figure 5.21: Fitting analysis for customised corrections for CF6-80E1: Fleet-average EGTMDEV σ/σ_0 for training and validation set as function of $\max(\Delta\Delta\mathrm{N1K})$

Figure 5.21 gives the results of the fitting analysis, including the results for the alternative problem formulation where both dHEGT/dAH and dHN1/dAH are optimised. Clearly the difference between these formulations is acceptable, especially if the risk of capturing non-physical relationships is reduced.

Concerning the variation of σ/σ_0 from the final case with only dHEGT/dAH included, expectedly the training set value increases with $\max(\Delta\Delta\mathrm{N1K})$. Validation set σ/σ_0 first decreases with $\max(\Delta\Delta\mathrm{N1K})$ due to severe over-fitting for $\max(\Delta\Delta\mathrm{N1K}) < 2$. In both cases σ/σ_0 makes a considerable jump beyond $\max(\Delta\Delta\mathrm{N1K}) > 6.5$%-p. This is contributed to the fact that between 6.5%-p and 8.0%-p the number of rows in the throttle push correction tables jump from 4 to 3 for all installation periods.

The definitive $\max(\Delta\Delta\mathrm{N1K})$ value used for the CF6-80E1 correction customisation was set to 6.5%-p, which should produce good EGTMDEV scatter reduction while minimising the risk of over-fitting. It is possible that part of the observed EGTMDEV-N1K signatures in the data can be contributed to other parameters than N1K itself, which should preferably not be captured by the customised throttle push correction. Simultaneously customising the N1K-, AH- and TT2-corrections should at least avoid that the throttle push correction accounts for AH and TT2 effects.

[7]URL: `https://scikit-learn.org/stable/modules/generated/sklearn.model_selection.KFold.html`

A similar fitting analysis to determine $\max(\Delta\Delta\mathrm{N1K})$ was performed for the CF6-80C2, albeit without the customised AH- and TT2-corrections. This analysis resulted in a wider range of EGTMDEV σ/σ_0 for the same range of $\max(\Delta\Delta\mathrm{N1K})$, which is explained by the fact that in case of the CF6-80C2 small values of $\max(\Delta\Delta\mathrm{N1K})$ enable the throttle push table to also capture AH and TT2 related effects. The definitive $\max(\Delta\Delta\mathrm{N1K})$ value for CF6-80C2 is 3.5%-p. The results revealed questionable drops of assumed dEGT/dN1K at high N1K, probably because high N1K is correlated to high altitude or hot and humid airports. Given the incompleteness of CF6-80C2 data, the results are not included in this report.

5.6. Results of customised corrections for EGT margin

This section provides and discusses the results from the application of the installation-specific N1K-, AH- and TT2-correction customisation from Section 5.5 on the CF6-80E1 OW data. First Subsections 5.6.1, 5.6.2 and 5.6.3 address the AH-, TT2- and N1K-correction related results in terms of the optimised variables as well as the individual effect on EGTM. Subsequently Subsection 5.6.4 handles the combined effect of the corrections on OW EGTM and $\Delta\mathrm{EGTM}_{\mathrm{OW-TC}}$. The adjusted $\Delta\mathrm{EGTM}_{\mathrm{OW-TC}}$ distribution will be presented later in the report in Section 6.1.

It should be noted that as was stated in Subsection 5.5.3, it was decided to perform the correction optimisation based the first 500 OW cycles only. In order to increase the statistical value of the results, CF6-80E1 installation periods without corresponding TC performance data[8] were also included for which the first 500 available snapshots were used. These installation periods account for approximately 50% of the installations included in the correction optimisation for the CF6-80E1 but are evidently not included in any of the $\Delta\mathrm{EGTM}_{\mathrm{OW-TC}}$ distributions.

5.6.1. Humidity correction

Figure 5.22 shows how the new, customised AH-correction affects OW EGTM ($\Delta\mathrm{EGTM}_{\mathrm{AH}}$) for a single, representative CF6-80E1 installation. The net effect on EGTK and EGTM depends on the factor HEGT – a linear function of AH given the customised dHEGT/dAH – and the unshunted EGT it is applied on. Expectedly $\Delta\mathrm{EGTM}_{\mathrm{AH}} = 0$ for AH = 0 g/kg and decreases with AH, in order to correct the measured humid EGTM back to dry EGTM.

The distribution of the optimised dHEGT/dAH values from all CF6-80E1 installations is provided in Figure 5.23. The fleet-average dHEGT/dAH equals 35.0×10^{-5} or 0.035% per g/kg, which corresponds neatly with the 0.0325% per g/kg of the TC AH-correction (if the combined effects of HN1 and HEGT are considered).

Additionally, the dHEGT/dAH distribution has significant variance, only part of which is explained by the engine-to-engine variations that were discussed in Subsection 5.4.3. Other contributors to the scatter that cannot be quantified are: 1) inaccurate AH values because the airport humidity is used for the engine snapshot; and 2) the effects of occasional, unpredictable OW inlet condensation. Additionally, it is predicted that given the strong correlation between AH- and TT2-effects, the optimisation occasionally *smears* TT2-related effects onto the AH-correction. It should however be stated that early results, where dHEGT/dAH was optimised without N1K- and TT2-corrections included, the variance was larger and mean was physically unexplainable low.

Given that the engine-to-engine variation effects on dHEGT/dAH are small, it is recommended for future research to customise a single dHEGT/dAH value for the complete fleet simultaneous with installation-specific N1K- and TT2-corrections using a multi-level optimisation approach.

5.6.2. Temperature correction

The isolated effect of the customised TT2-correction on OW EGTM ($\Delta\mathrm{EGTM}_{\mathrm{TT2}}$) of the same representative CF6-80E1 installation as used for the AH-related effects is provided in Figure 5.24. Given that GE's OW EGTM is also corrected for TT2, $\Delta\mathrm{EGTM}_{\mathrm{TT2}}$ represents the net effect of the customised XT with respect to original XT. Per definition, $\Delta\mathrm{EGTM}_{\mathrm{TT2}}$ = 0°C at TT2 = 30°C (which is the CF6-80E1's $\mathrm{T}_{\mathrm{flat}}$). The customisation has increased XT because the engine is thermally less efficient than the engine or model used for GE's empirically determined XT. Hence the original data was non-conservative for TT2 < 30°C therefore requiring $\Delta\mathrm{EGTM}_{\mathrm{TT2}}$ < 0°C (and vice versa).

[8] The reasons for OW installation periods without coupled TC data are primarily: 1) the corresponding acceptance test was conducted before 2013 and therefore not included in the TC data; and 2) the engine was first installed on an unknown client aircraft and therefore the first available cycles back in the AFR-KLM fleet are not the initial cycles after TC performance testing

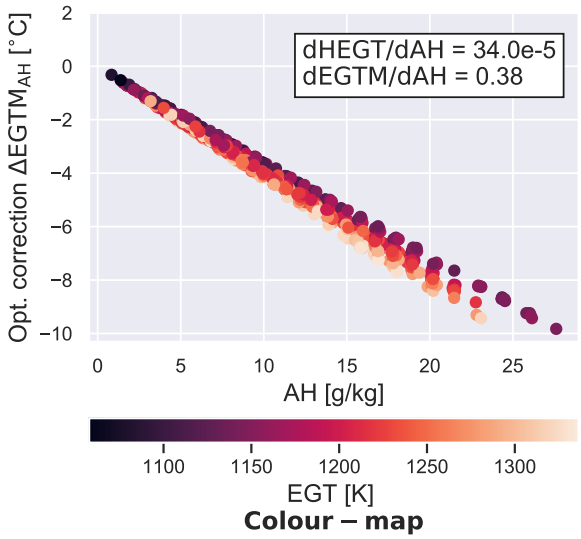

Figure 5.22: Effect of customised AH-correction on EGTM ($\Delta EGTM_{AH}$) as function of AH for a single, representative installation

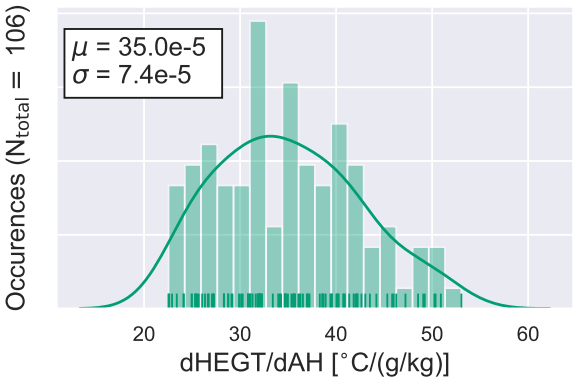

Figure 5.23: Distribution of optimised installation-specific dHEGT/dAH values

The distribution of the optimised XT values of all CF6-80E1 installations is provided in Figure 5.25, including the GE's value ($XT_{official}$) of almost 0.87. Expectedly $\mu(XT) > XT_{official}$ because AFR-KLM's CF6-80E1 fleet is older and has become less efficient overall.

Other than dHEGT/dAH, the width of the almost Gaussian distribution is as expected based on the simulated results in Subsection 5.4.3 because both the data-driven and simulated results predict a maximum engine-to-engine variation of $\max(\Delta EGTM_{TT2})$ of approximately 12°C. The precise XT values are nevertheless subject to the same sources of uncertainty as dHEGT/dAH.

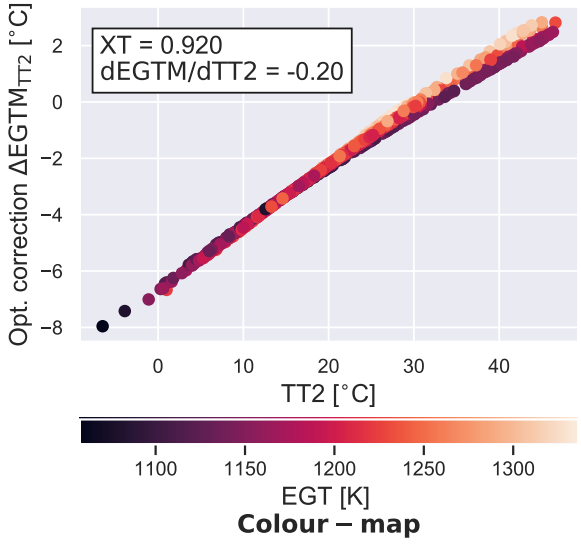

Figure 5.24: Effect of customised TT2-correction on EGTM ($\Delta EGTM_{TT2}$) as function of TT2 for a single, representative installation

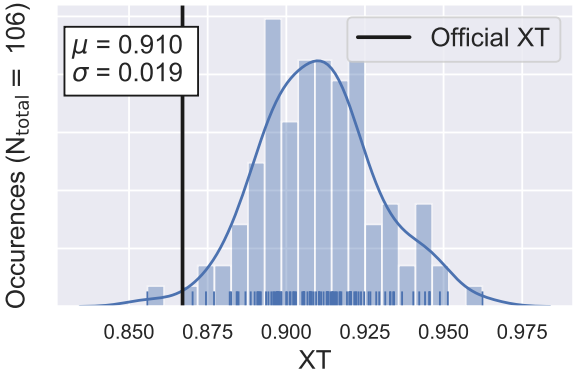

Figure 5.25: Distribution of optimised installation-specific dHEGT/dTT2 values

5.6.3. Throttle setting correction

The isolated effect of the customised N1K-correction is subject to engine-to-engine variation such that no single, representative example can be supplied. Some visual examples of the quadratic spline

based on the customised throttle push tables were already provided in Figure 5.4 in the EGTM domain and Figures 5.5 and 5.6 in the EGTK domain, both in Subsection 5.3.1 starting at page 50.

Upon a second review of those figures it is observed that the splines are not precise fits of the EGTMDEV- and EGTK-N1K data, which is explained by the fact that part of the observed relationship can be contributed to AH and TT2.

For some installations, the customised ΔEGT-ΔN1K trend describes a questionably level of dEGT/dN1K drop-off at high N1K values. As will be discussed in Subsection 5.7.2, those results might be affected by the influence of power off-take (PTO) on EGTM as it was revealed that PTO is correlated to N1K. Given the lower data density at high N1K values, the *optimal* ΔEGT-ΔN1K relation is more sensitive to the unpredictable impact of phenomena such as inlet condensation and thermal effects. The latter will be discussed in Section 6.2.

It is recommended to extend the scope of the customised corrections by including other measurable inputs to EGTM such as PTO and customer bleed. The more parameters are included, the narrower the confidence bounds of the resulting relations will be because the risk of mutual smearing is reduced.

5.6.4. Combined customised corrections

The distribution of the achievement EGTMDEV scatter reduction (σ/σ_0) over all CF6-80E1 installations is provided in Figure 5.26. Expectedly, given the engine-to-engine variations of the underlying customised corrections, σ/σ_0 varies considerably with reductions between 6.2% and 58.6%. Furthermore, Figure 5.27 indicates that $\sigma/\sigma_0 \sim f(\sigma_0)$, which is explained by the fact that σ_0 is a measure of original OW EGTM calculation accuracy and logically larger inaccuracies enable larger improvements.

In the original data fleet-average EGTMDEV σ is 3.8°C, with engine-specific values between 2.2°C and 4.6°C. After application of the customised corrections the values fall within 1.8°C and 2.9°C with a 2.4°C average. Given that the CF6-80E1 TC correlation report mentions an observed $\sigma(\mathrm{EGT})$ of 1.5°C over 6 consecutive correlation tests, the achieved 2.4°C on-wing is certainly noteworthy.

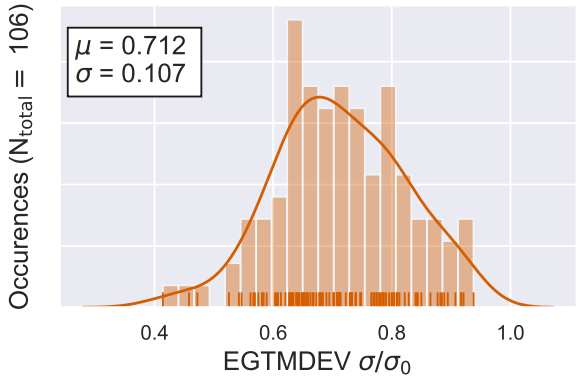

Figure 5.26: Distribution of installation-specific EGTMDEV scatter reduction (σ/σ_0) due to customised corrections

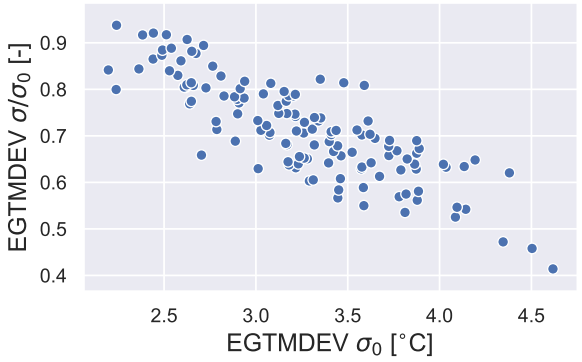

Figure 5.27: Correlation between installation-specific achieved EGTMDEV scatter reduction (σ/σ_0) and initial EGTMDEV scatter (σ_0)

Given that the inaccuracies of the original N1K-, AH- and TT2-corrections typically resulted in non-conservative EGTM values, the distribution of average EGTM reduction ($\Delta\mu(\mathrm{EGTM})$) over all CF6-80E1 installations shown in Figure 5.28 is no surprise. Figure 5.29 shows the $\Delta\mu(\mathrm{EGTM})$ is as expected correlated to the scatter reduction.

Finally, the results from the N1K-, AH- and TT2-correction customisation can also provide insight concerning the contribution of those parameters to the original OW-TC EGTM discrepancy. The isolated contributions to $\mu(\Delta\mathrm{EGTM}_{\mathrm{OW-TC}})$ of the inaccurate or missing N1K-, AH- and TT2-corrections can be derived from Figure 5.30 that provides the distributions for cycles 11-20. The effects of the corrections on $\mu(\Delta\mathrm{EGTM}_{\mathrm{OW-TC}})$ are all negative, which means that the original $\mu(\Delta\mathrm{EGTM}_{\mathrm{OW-TC}})$ was non-conservatively higher due to missing AH- and inaccurate N1K- and TT2-corrections. The combined effect on $\mu(\Delta\mathrm{EGTM}_{\mathrm{OW-TC}})$ is −12.3°C, as can be concluded from Figure 5.31.

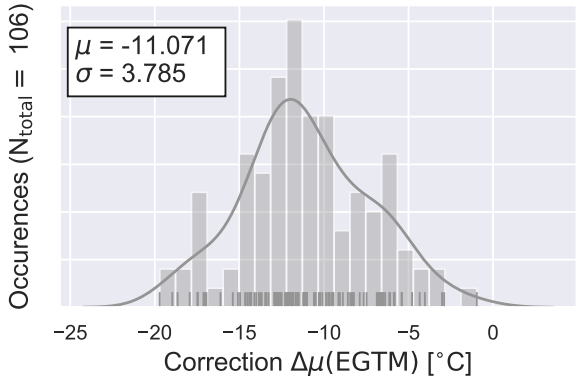

Figure 5.28: Distribution of installation-specific average EGTM change ($\Delta\mu(\mathrm{EGTM})$) due to customised corrections

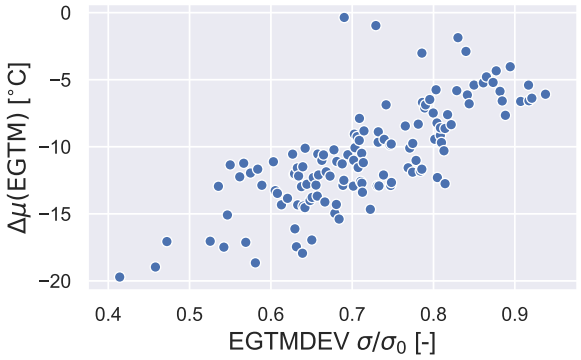

Figure 5.29: Correlation between installation-specific average EGTM change ($\Delta\mu(\mathrm{EGTM})$) and EGTMDEV scatter reduction (σ/σ_0)

The predicted contribution of the inaccurate corrections on $\sigma(\Delta\mathrm{EGTM}_{\mathrm{OW-TC}})$ is 3.7°C based on Figure 5.31, which is smaller than the root sum square of the three individual contributors. This is explained by the fact that the individual contributions do not affect the same snapshots evenly. For example, the original TT2-related error is biggest for low TT2 while the original AH-related error is biggest for high AH and therefore high TT2.

The adjusted $\Delta\mathrm{EGTM}_{\mathrm{OW-TC}}$ distributions will be presented later in the report in Section 6.1.

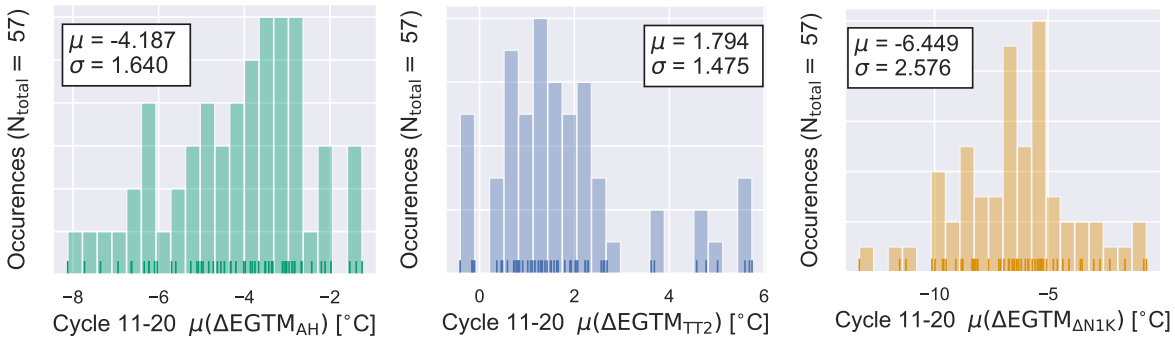

(a) Inaccurate original AH-correction (b) Inaccurate original TT2-correction (c) Inaccurate original N1K-correction

Figure 5.30: Distribution of installation-specific effects of inaccurate original N1K-, AH- and TT2-corrections on cycle 11-20 average EGTM, based on customised corrections results

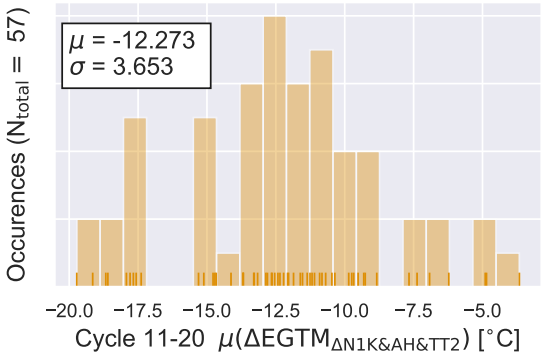

Figure 5.31: Distribution of installation-specific combined effect of inaccurate original N1K-, AH- and TT2-corrections on cycle 11-20 average EGTM, based on customised correction results

5.7. Effects of customer bleed & power extraction on EGT margin

Apart from N1K, AH and TT2, several other OW operation related potential causes for the OW-TC EGTM discrepancy were also briefly investigated. This section discusses the potential influences of customer bleed and power extraction on OW EGTM and hence the OW-TC EGTM discrepancy.

Bleed air extraction for customer bleed and anti-ice functionality is addressed in Subsection 5.7.1. Subsequently the effect of power off-take is discussed in Subsection 5.7.2.

5.7.1. Customer bleed & anti-ice

The extraction of compressed air from the compression system of a turbofan for external usage is called customer bleed, whereas in this research a distinction is made between bleed for anti-icing purposes, referred to as nacelle (NAI) and wing anti-ice (WAI), and pneumatic functionality, referred to as customer bleed (WB). Both categories are discussed in separate paragraphs below based on the adjusted[9] CF6-80E1 data.

Customer bleed

Customer bleed for pneumatic purposes is extracted from the 8th stage – out of 14 total – of the HPC during takeoff, additionally at low power HPC discharge air is extracted when the stage 8 delivery pressure is insufficient. The OW snapshot data includes bleed flow (WB) column, which should equal the total WB in kg/s extracted from the engine.

As was discussed in Subsection 5.1.1, CF6-80E1 OW EGTM calculations include an adjustment for WB ($\Delta\mathrm{EGT}_{\mathrm{WB}}$) that is defined by linear interpolating its value as function of WB. The tabulated relation between $\Delta\mathrm{EGT}_{\mathrm{WB}}$ and WB is almost linear and hence subsequent analyses will assume a constant, linear gradient (dEGTM/dWB).

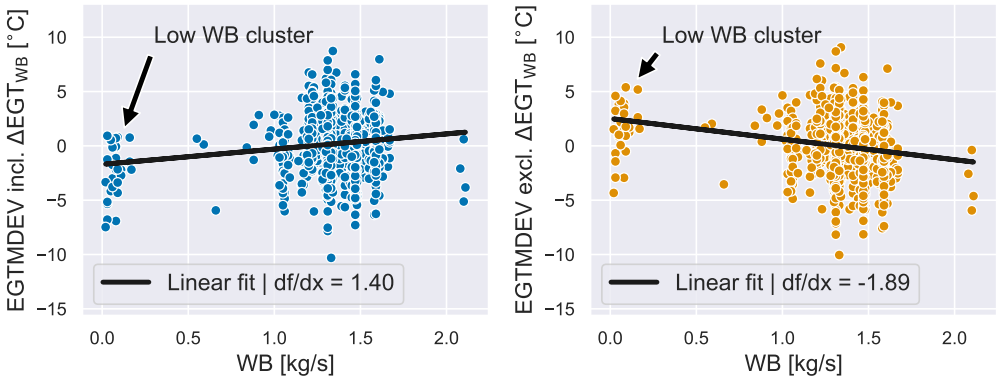

Figure 5.32: Observed correlation between EGTMDEV including $\Delta\mathrm{EGT}_{\mathrm{WB}}$ and WB (left) and correlation between EGTMDEV excluding $\Delta\mathrm{EGT}_{\mathrm{WB}}$ and WB (right) from a single CF6-80E1 installation

Figure 5.32 provides the correlation between EGTMDEV and WB for a single CF6-80E1 install, where a distinction is made between the EGTMDEV including and excluding the contribution of $\Delta\mathrm{EGT}_{\mathrm{WB}}$. The linear gradients are 1.4°C and −1.89°C per kg/s, which reconciles with the known (almost) linear official d$\Delta\mathrm{EGT}_{\mathrm{WB}}$/dWB of 3.36°C per kg/s. It is however concluded that the WB correction over-compensates the physical EGT-WB relationship.

Analogous to previous effect studies, a simulated analysis with the CF6-80C2 model in GSP revealed that dEGT/dWB depends on engine condition. Furthermore WB sensor bias and noise could increase the scatter of dEGTM/dWB in the data. It was however also observed that GSP over-predicted dEGT/dWB by a factor of 3, possibly because the cooling mass fractions in the model are non-physical or because the provided WB values are not in kg/s as supposed to.

Attempts to derive installation-specific dEGTM/dWB values to predict the contribution of WB to OW-TC EGTM discrepancy were hampered by the fact that only 2 installations spanned the *low WB cluster* that is annotated in Figure 5.32 hence resulting in ill-defined linear fitting problems for most installations. Therefore it was decided to assume a generic dEGTM/dWB based on all available data, knowing

[9] *Adjusted data:* data including the application of the customised corrections from Sections 5.5 and 5.6

that this is slightly inaccurate for some engine installations.

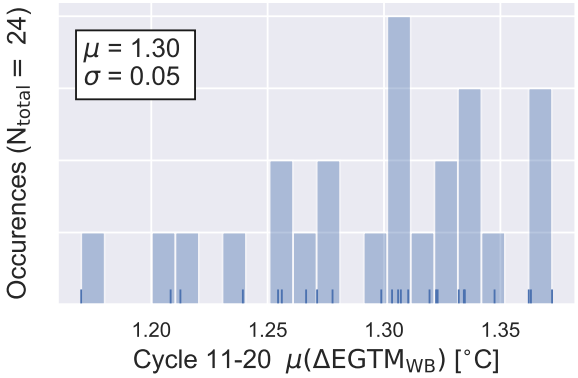

Figure 5.33: Distribution of effects of inaccurate original WB corrections on cycle 11-20 average EGTM over all CF6-80E1

The predict contribution of inaccurate WB corrections to μ and σ of $\Delta\mathrm{EGTM}_{\mathrm{OW-TC}}$ is summarised by the distribution of $\mu(\Delta\mathrm{EGTM}_{\mathrm{WB}})$ over all CF6-80E1 installations for cycle 11-20, as shown in Figure 5.33. The fact that $\mathrm{N}_{\mathrm{total}}$ is only 24 originates from missing WB data, whereby the number of installations with sufficient WB data for cycles 11-20 is limited. For the same reasons the WB correction was not included in the customised correction optimisation described in previous sections.

The primary conclusion to draw from Figure 5.33 is that based solely on the data the predicted contributions of WB to $\mu(\Delta\mathrm{EGTM}_{\mathrm{OW-TC}})$ and $\sigma(\Delta\mathrm{EGTM}_{\mathrm{OW-TC}})$ are 1.3°C and 0.05°C. Therefore customer bleed is not a main root cause for the observed $\Delta\mathrm{EGTM}_{\mathrm{OW-TC}}$ distributions.

Anti-ice bleeds

Considering the wing anti-ice (WAI) effects on OW EGTM, it can directly be concluded that it is not a significant contributor to the OW-TC EGTM discrepancy simply based on the fact that WAI is only active for 0.25% of OW snapshots. Nacelle anti-ice (NAI) is used more frequently depending on the season, as the percentage of affected snapshots is 25% in January and 0.6% in July. When active, HPC stage 11 air is extracted and directed to heat the inlet nacelle or wing leading-edge before disposal. It is unknown if anti-ice mass flow is actively controlled, it is however given that no NAI- or WAI-related measurements are included in the OW data other than an active or inactive boolean.

Current corrections include an fixed adjustment ($\Delta\mathrm{EGT}_{\mathrm{NAI}}$) that is used to correct for the adverse effect of NAI if active. As is observed in Figure 5.34, which provides the distribution of the residual effect of NAI on EGTM (dEGTM/dNAI[10]) over all CF6-80E1 installations, the data suggests that the current correction is insufficiently compensating. Note that only installations with at least 50 active NAI snapshots are included in Figure 5.34.

A theoretical or simulated analysis of NAI effects is not included, primarily because of the black box nature of the system. Nevertheless, utilising the data by combining the dEGTM/dNAI values with the number of NAI-affected snapshots for cycles 11-20 can help predict the approximate contribution of inaccurate NAI corrections on μ and σ of $\Delta\mathrm{EGTM}_{\mathrm{OW-TC}}$ as is shown in Figure 5.35.

Given that the use of NAI is seasonal, installation periods that started in summer months are not impacted by NAI thus explaining the occurrences peak at 0°C. The overall drawn conclusion is that the predicted contributions of inaccurate NAI adjustments to $\mu(\Delta\mathrm{EGTM}_{\mathrm{OW-TC}})$ and $\sigma(\Delta\mathrm{EGTM}_{\mathrm{OW-TC}})$ are -0.12°C and 0.20°C. The precise values should not be taken for granted, as data revealed that a generic dEGTM/dNAI does not capture its sensitivity to operating conditions. Nevertheless NAI is certainly not a main root cause for $\Delta\mathrm{EGTM}_{\mathrm{OW-TC}}$.

5.7.2. Power off-take (PTO)

Mechanical power drawn from the high pressure spool (N2) will adversely affect the engine, as engine has to burn more fuel and run hotter to maintain sufficient core speed to maintain the demanded N1.

[10] $\Delta\mathrm{EGT}_{\mathrm{NAI}}$: given that NAI is either 0 or 1, dEGTM/dNAI is equal to $\mu(\mathrm{EGTMDEV})_{\mathrm{NAI=1}} - \mu(\mathrm{EGTMDEV})_{\mathrm{NAI=0}}$

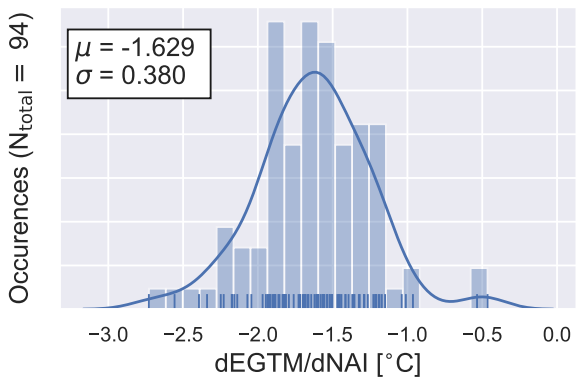

Figure 5.34: Distribution of installation-specific dEGTM/dNAI values from the CF6-80E1 fleet

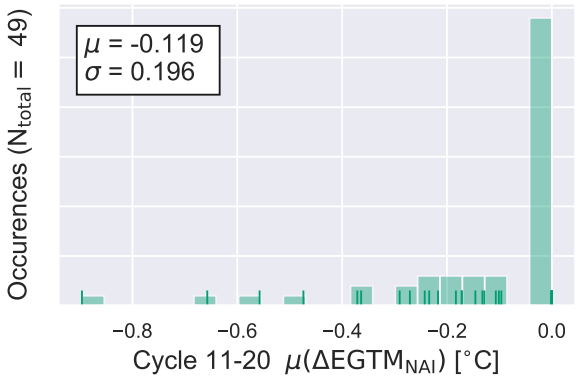

Figure 5.35: Distribution of installation-specific impact of inaccurate original NAI corrections on cycle 11-20 average EGTM values from the CF6-80E1 fleet

The total mechanical power extraction is the sum of the power drawn by the Integrated Drive Generator (IDG) for electrical power and the power drawn by the Engine Driven Pump (EDP) for hydraulic power. Below a data- and simulations-driven analysis of PTO effects is addressed.

Electrical PTO is only available in the *PROGNOS* data which includes 22 CF6-80E1 installations. Distributing all reported PTO values revealed an average of 53 kW with outliers between 24 kW and 80 kW. Hydraulic power is not measured, allegedly because it is presumed negligible by GE. Maximum EDP power is 31.3 kW, but representative values are only 10% of that.

Figure 5.36 plots the simulated results from GSP at ISA conditions with 100% N1 with PTO between 0 kW and 100 kW. Expectedly, $\Delta\mathrm{EGT}_{\mathrm{PTO}}$ increases almost linearly with PTO. Although $\max\left(\Delta\mathrm{EGT}_{\mathrm{PTO}}\right)$ = 2.5°C, the value of $\Delta\mathrm{EGT}_{\mathrm{PTO}}$ at the average OW PTO is between 0.8°C and 1.3°C depending on the engine deterioration case.

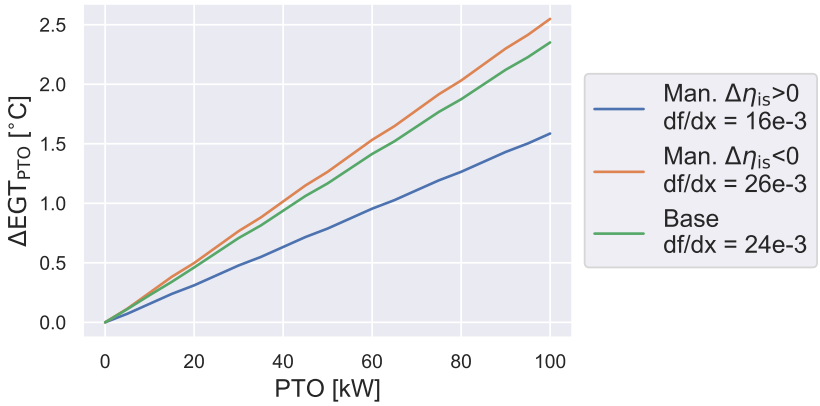

Figure 5.36: Simulated ΔEGT-PTO correlations based on CF6-80C2 GSP model for 3 deterioration cases from Appendix C

A data-driven analysis of PTO revealed that with the adjusted data dEGTM/dPTO ≈ 0°C per kW with negligible scatter of engine-specific dEGTM/dPTO values. A similar analysis with the original EGTMDEV data revealed a non-physically scattered dEGTM/dPTO distribution, albeit with a fleet-average dEGTM/dPTO of -14.7×10^{-3}°C per kW, which reconciles with the simulated gradients.

It was found that the above observations stem from the fact that PTO is weakly correlated to N1K and TT2, therefore the original dEGTM/dPTO is affected by the known EGTM-N1K and -TT2 correlations. Furthermore the adjusted dEGTM/dPTO is negligible because PTO effects have effectively already be accounted for with the customised N1K- and TT2-corrections for OW EGTM. This conclusion also provides at least some explanation for the installations with noteworthy drop-off of dEGT/dN1K at high N1K in their customised throttle push tables.

No meaningful conclusion can be drawn on the contribution of PTO to original μ and σ of $\Delta\mathrm{EGTM}_{\mathrm{OW-TC}}$ because original dEGTM/dPTO is dominated by correlated N1K and TT2 effects. However, concerning the adjusted data the influence of PTO has implicitly mostly be accounted for through the customised N1K- and TT2-corrections such that the adjusted $\Delta\mathrm{EGTM}_{\mathrm{OW-TC}}$ is negligibly impacted by PTO.

6

Comparison of on-wing & test-cell engine performance

So far in-depth data-driven assessments of TC and OW EGTM have been addressed in Chapters 4 and 5, with frequent support of gas turbine theory and GSP simulations for validation. Thereby all potential causes for the observed difference between OW and TC EGTM that originate from inaccurate or incomplete corrections for EGTM have been investigated. Furthermore a method was proposed and tested to customise throttle setting, humidity and temperature corrections to account for engine-to-engine variations and hence significantly reduce OW EGTM scatter.

This chapter continues with the OW and TC EGTM comparison. First of all, an updated overview of the OW-TC differences based on the adjusted data is provided in Section 6.1. Afterwards the additional potential causes for the discrepancy are addressed, starting with the effect of thermal stabilisation and seal run-in in Sections 6.2 and 6.3. Any remaining causes are briefly discussed in Section 6.4. Lastly, Section 6.5 wraps up the research by comparing the observed OW-TC discrepancy distribution with the combined predicted distribution.

6.1. Updated performance discrepancy

The baseline comparison of OW and TC EGTM was performed in Section 2.4 to quantify the scale of the discrepancy problem. Given the adjusted OW data originating from the application of the customised engine installation-specific N1K-, AH- and TT2-corrections and fixing faults, this section will briefly quantify OW-TC EGTM discrepancy ($\Delta\mathrm{EGTM}_{\mathrm{OW-TC}}$) based on that data including comparison with the baseline. As an reminder, the previously defined discrepancy definitions are:

$\Delta\mathrm{EGTM}^{\mathrm{tc}}_{\mathrm{OW-TC}}$ The difference between the cycle 11-20 average OW EGTM and the official TC EGTM.

$\Delta\mathrm{EGTM}^{\mathrm{ow}}_{\mathrm{OW-TC}}$ The difference between the cycle 11-20 average OW EGTM and the OW-method-based TC EGTM. That OW-method-based TC EGTM is calculated by applying the OW EGTM calculations on the official TC measurements, where in case of the adjusted OW data the corresponding TC EGTM is also adjusted by applying the customised OW EGTM calculations.

Figure 6.1 compares the original and adjusted $\Delta\mathrm{EGTM}_{\mathrm{OW-TC}}$ distributions for the CF6-80E1. The left column of histograms belongs to $\Delta\mathrm{EGTM}^{\mathrm{tc}}_{\mathrm{OW-TC}}$ and the right column of histograms belongs to $\Delta\mathrm{EGTM}^{\mathrm{ow}}_{\mathrm{OW-TC}}$. Furthermore Table 6.1 summarises the distributions by the corresponding mean (μ) and standard deviation (σ). The change of $\mu(\Delta\mathrm{EGTM}_{\mathrm{OW-TC}})$ from original to adjusted and the ratio of $\sigma(\Delta\mathrm{EGTM}_{\mathrm{OW-TC}})$ between the adjusted and original values are also included. The key observations and conclusions regarding the table and histograms are:

$\Delta\mathrm{EGTM}^{\mathrm{tc}}_{\mathrm{OW-TC}}$ As expected, $\mu(\Delta\mathrm{EGTM}^{\mathrm{tc}}_{\mathrm{OW-TC}})$ of the adjusted distribution is shifted towards negative values, because the original corrections are non-conservative and the customised corrections accounted for that. Fixing the faults also contributes with -2.0°C to that shift.

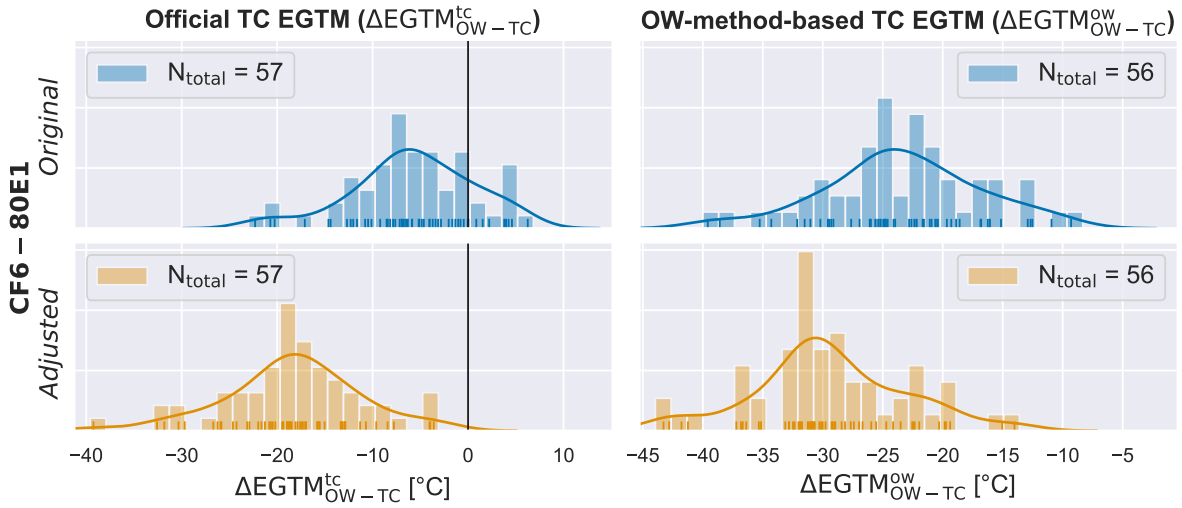

Figure 6.1: Comparison of distributions of baseline and adjusted OW-TC EGTM discrepancy from CF6-80E1 fleet, distinguishing between OW EGTM w.r.t. official TC EGTM (left) and OW-method-based TC EGTM (right)

On the other hand, $\sigma(\Delta EGTM^{tc}_{OW-TC})$ is almost unaffected, which can be explained by the fact that the official TC EGTM values are still calculated with generic corrections that do not capture engine-to-engine variation. As was discussed in Section 4.4, the contribution of the facility modifier (EGTFM) and cowling adjustment (ΔEGT_{cowl}) is almost constant and therefore including EGTMFM and ΔEGT_{cowl} does not positively affect $\sigma(\Delta EGTM^{tc}_{OW-TC})$.

$\Delta EGTM^{ow}_{OW-TC}$

In case of $\Delta EGTM^{ow}_{OW-TC}$ the customised corrections are also used for TC EGTM, which is therefore also adjusted for the non-conservative original corrections. The −7.99°C shift of $\mu(\Delta EGTM^{ow}_{OW-TC})$ is therefore primarily explained by the fact that the cycle 11-20 snapshots are on average recorded at considerably lower N1K than the corresponding TC snapshot and therefore the OW EGTM value is affected more by the application of the customised N1K-corrections. Any adjustments related to fixing the data faults also only affect OW EGTM and hence reduce $\mu(\Delta EGTM^{ow}_{OW-TC})$.

The adjusted data also reduced $\sigma(\Delta EGTM^{tc}_{OW-TC})$ by 10% from 7.04°C to 6.32°C. The predicted contributions of data faults and inaccurate or missing N1K-, AH- and TT2-corrections are 3.0°C and 3.7°C, therefore if normal distribution probability theory[(1)] is assumed, the predicted value for the adjusted $\sigma(\Delta EGTM^{tc}_{OW-TC})$ is 5.2°C. The difference is explained by the fact that those individual contributions are actually not normally distributed.

Table 6.1: Summary of comparison of baseline and updated OW-TC EGTM discrepancy from CF6-80E1 fleet, distinguishing between OW EGTM w.r.t. official TC EGTM (left) and OW-method-based TC EGTM (right)

FAMILY		Official TC EGTM $\Delta EGTM^{tc}_{OW-TC}$ [°C]		OW-method-based TC EGTM $\Delta EGTM^{ow}_{OW-TC}$ [°C]	
		μ	σ	μ	σ
CF6-80E1	*Original*	-3.84	6.89	-21.45	7.04
	Improved	-18.40	7.05	-29.44	6.32
	Difference	**-14.56**	-	**-7.99**	-
	Ratio	-	**1.023**	-	**0.898**

The remainder of this report will focus specifically on $\Delta EGTM^{ow}_{OW-TC}$, which uses the OW-method-based TC EGTM. The primary reason for that decision is that by applying exactly the same EGTM calculations on the OW and TC snapshots, any difference in EGTM can clearly be allocated to physical

(1) *Probability theory:* $Z \sim N(\mu_Z, \sigma_Z^2) \sim N(\mu_X + \mu_Y, \sigma_X^2 + \sigma_Y^2)$ where $Z = X + Y$ and $X \sim N(\mu_X, \sigma_X^2)$ and $Y \sim N(\mu_Y, \sigma_Y^2)$

operational differences. Therefore side-by-side comparison of the observed $\Delta\mathrm{EGTM}^{\mathrm{ow}}_{\mathrm{OW-TC}}$ distribution with the predicted physical contributions of the addressed potential causes is not affected by numerical differences in the underlying methods. The key differences between the official TC and customised OW EGTM calculations are:

- The official TC EGTM calculations are not customised to account for engine-to-engine variations of the physical EGT-N1K, -AH and -TT2 relations.
- The official and customised OW EGTM calculations include the constant factor F_{EGTM} and adjustment C_{EGTM} – discussed in Section 5.1 – while the TC EGTM calculations do not. By comparing OW EGTM with the OW-method-based TC EGTM the contribution of these unexplained terms is eliminated. Given that F_{EGTM} is potentially a safety factor, it is recommended to assess if it can be discarded because the customised corrections are no longer non-conservative.

Obviously using an OW EGTM calculation method for the TC snapshot does mean that the effects of the facility modifier (EGTFM), cowling adjustment ($\Delta\mathrm{EGT}_{\mathrm{cowl}}$) and condensation correction are not included. To this end, a last additional discrepancy definition is proposed that uses an hybrid-method-based TC EGTM and will be referred to as $\Delta\mathrm{EGTM}^{\mathrm{hybrid}}_{\mathrm{OW-TC}}$. The hybrid-method constitutes to the customised OW corrections with the addition of EGTFM, $\Delta\mathrm{EGT}_{\mathrm{cowl}}$ and condensation correction (i.e. CEGT and CN1) from the official TC EGTM calculations.

The distribution of $\Delta\mathrm{EGTM}^{\mathrm{hybrid}}_{\mathrm{OW-TC}}$ is provided in Figure 6.2. The impact of the additional of TC-related terms on the average value is −2.41°C while the standard deviation is as expected unaffected.

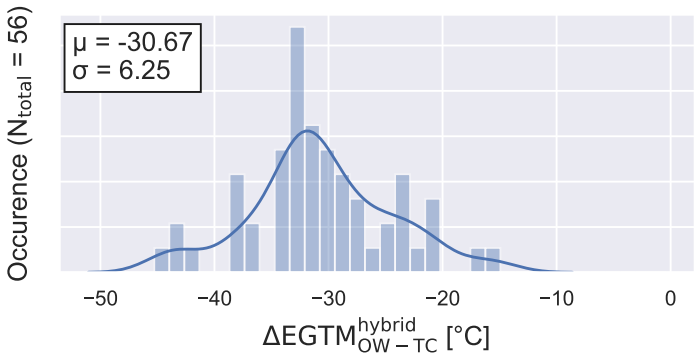

Figure 6.2: Distribution of adjusted OW-TC EGTM discrepancy from CF6-80E1 fleet using the hybrid-method-based TC EGTM

The currently observed average and scatter of $\Delta\mathrm{EGTM}^{\mathrm{ow}}_{\mathrm{OW-TC}}$ and $\Delta\mathrm{EGTM}^{\mathrm{hybrid}}_{\mathrm{OW-TC}}$ are all larger than what can be accounted for based on the potential causes that have been addressed so far. Therefore the subsequent sections will address the remaining potential causes, focusing on thermal effects and seal run-in. Afterwards, in Section 6.5 a final side-by-side numerical comparison of the observed and predicted $\Delta\mathrm{EGTM}^{\mathrm{ow}}_{\mathrm{OW-TC}}$ distribution will be provided.

6.2. Effects of engine thermal-state on EGT margin

While test-cell procedures prescribe to let the turbofan stabilise before recording the official TO snapshot, it is unlikely that the engine will reach thermal equilibrium within the 40s to 60s between commencing takeoff and snapshot recording during OW operation. Therefore the engine thermal-state is potential cause for the OW-TC EGTM discrepancy. This section will substantiate that hypothesis on the basis of continuous data from 2 CF6-80E1 performance acceptance tests.

First Subsection 6.2.1 will address the effect of that stabilisation phase on performance, while Subsection 6.2.2 will discuss the underlying physical causes for the observed EGTM variation.

6.2.1. Thermal effects on performance

Figure 6.3 provides an overview of one of the available continuous data-sets belonging to a CF6-80E1 acceptance test. The ambient conditions are not included but their variation throughout the testing procedure is negligible.

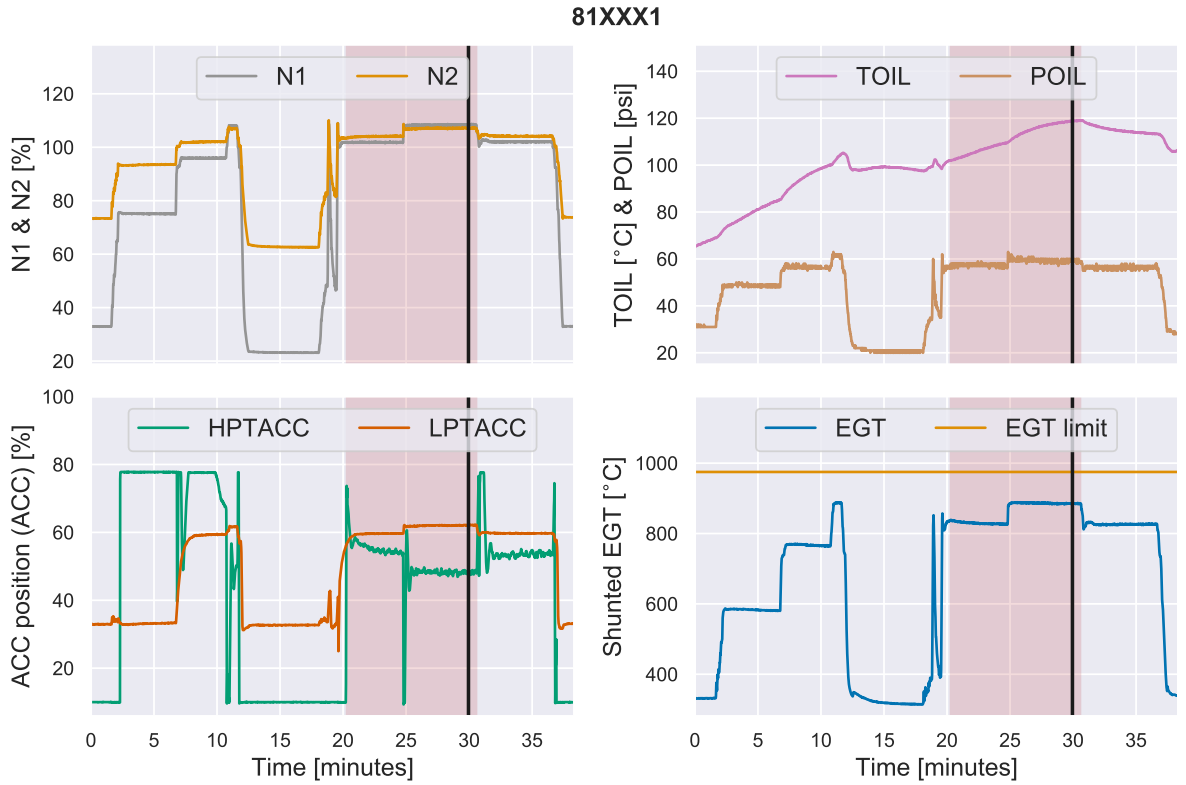

Figure 6.3: Overview of time-dependent variation of key operation and performance parameters during a CF6-80E1 performance acceptance test at KLM's test-cell facility

Focusing on the controls, the initial step-by-step increase of N1 is performed to break in the seals, which is followed with a 5-minute stabilisation at idle. Then an acceleration test is performed and if no abnormalities are observed the official performance testing phase – highlighted pink in Figure 6.3 – is commenced. Subsequently the engine is consecutively stabilised at Maximum Continuous (MC) and TO power for 5 minutes before the actual TO snapshot is recorded, which is indicated by the black line in the figure. The other snapshots are not relevant for this research.

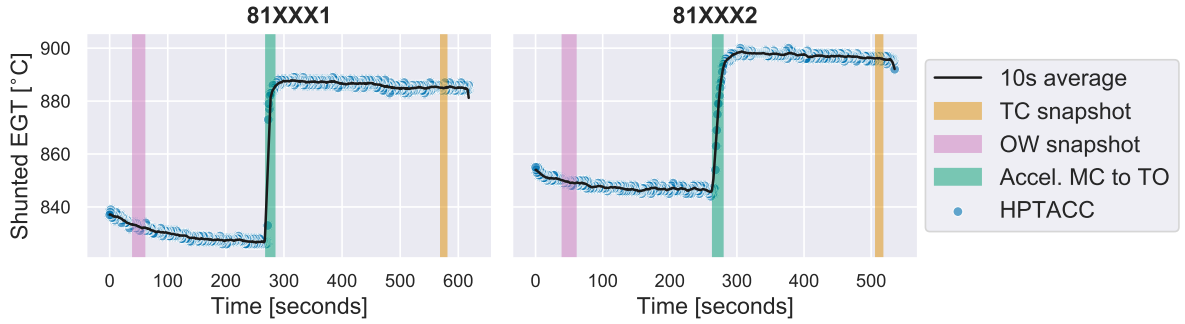

Figure 6.4: Continuous variation of EGT during two separate CF6-80E1 test-run examples performed at KLM's facility

The variation of unshunted EGT during the actual performance testing – corresponding to the highlight timespan in Figure 6.3 – is provided in Figure 6.4, where additionally similar data from the other continuous dataset is plotted on the left. Both the raw 1Hz data and a 10s Simple Moving Average (SMA) are included.

The TO performance snapshot and MC-to-TO acceleration timespans are highlighted. Additionally, the timespan between 40s and 60s after commencing the performance test is highlighted to demonstrate when the OW TO snapshot would hypothetically have been recorded. Please note that

$N1K_{rated,MC}$ = 101.9% and $N1K_{rated,TO}$ = 108.1% such that MC power is also representative for OW takeoff because most snapshots fall between 98% and 105%.

Regarding Figure 6.4, EGT clearly stabilises at MC and TO setting for both examples, where stabilisation is expressed by an exponential time-dependent decrease of EGT. Given that operating conditions and the corresponding corrections are constant, EGTK and EGTM must therefore be time-variant as well.

Visual proof of that conclusion is provided in Figure 6.5, which shows the stabilisation of EGTM during the 10-minute thermal stabilisation. The EGTM values were calculated with the customised OW corrections, such that any variation of EGTM can be assigned to changes of the engine thermal efficiency. Neglecting the non-physical spike during MC-to-TO acceleration, EGTM increases gradually as expected during the stabilisation at both MC and TO power. Therefore proving that the reported EGTM value depends on snapshot-timing.

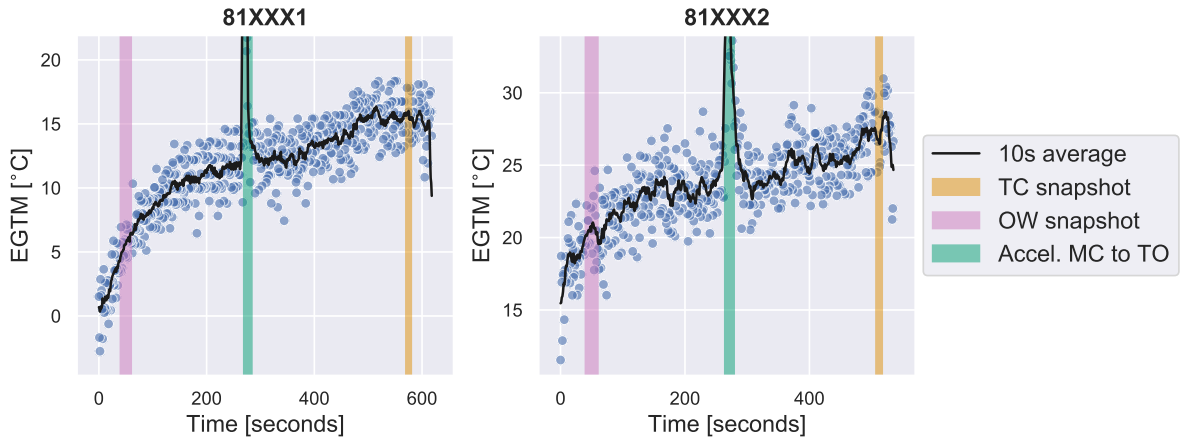

Figure 6.5: Continuous variation of EGTM during two separate CF6-80E1 test-run examples performed at KLM's test-cell facility

As was addressed in Section 4.1, the TC EGT limit ($EGT_{TC\text{-}limit}$) is set lower than the actual redline ($EGT_{redline}$) to account for the different thermal-state and initial OW losses (i.e. seal run-in). For the CF6-80E1, that difference is 15°C.

However, in case of the continuous datasets plotted in Figure 6.5 the differences between recording at OW snapshot-timing and at TC snapshot-timing are approximately 10°C and 7.5°C. Although no statistical conclusions can be drawn from merely 2 examples, it can be concluded that the lack of thermal stabilisation has a significant, unpredictable effect on EGTM.

Additionally, the engine is already pre-heated before the performance testing is commenced due to the seal break-in phase, therefore the impact of the thermal effects is expected to be even larger for OW snapshots. All in all, it is concluded that thermal effects are a main root cause for negative mean and scatter of $\Delta EGTM_{OW-TC}$.

Finally, both of the EGTM-variation plots demonstrate the accuracy of the installation-specific customised N1K-, AH- and TT2-corrections. Despite the 6.2%-p and 50+°C step increase of N1K and EGT during MC-to-TO acceleration, these effects are accurately accounted for such that the corrected performance (i.e. EGTM) is unaffected.

Furthermore it was found that the 10s moving standard deviation of EGTM varied between 1°C and 2°C, which reconciles with the 1.5°C reported in the CF6-80E1 correlation report and is close to the 2.4°C achieved OW with the customised corrections.

6.2.2. Origin of thermal effects

The origin of the thermal effects on cycle thermal efficiency and EGTM is known to originate from variation of turbine tip clearances [24, 83]. The fuel flow increase required to accelerate and maintain the demanded N1 is accompanied by increasing gas path temperatures, particularly those in the hot section after the combustion chamber. The engine's thermal equilibrium is consequently disturbed and its gas path components start to heat up towards the new equilibrium.

The tip clearances depend on the blade tip and casing diameters, which are both subject to thermal expansion during engine heat-up. However the casing diameter will typically expanded more and faster than the blade tip diameter because: 1) the thermal capacity of the thin casings is much smaller than the blade disks; and 2) the casings have a large heat-transfer surface-to-volume ratio while the blade disks – which contribute the most to blade the tip diameter increase – have not. Therefore the turbine tip clearances first increase and subsequently gradually decrease during the heat-up.

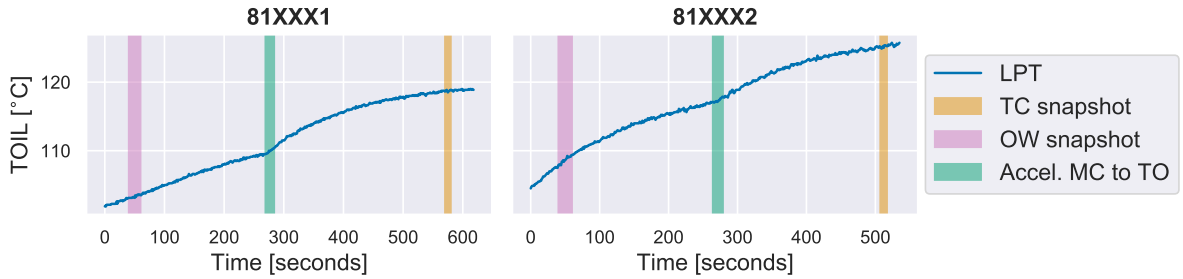

Figure 6.6: Continuous variation of TOIL during two separate CF6-80E1 test-run examples performed at KLM's facility

In order to visualise how the engine's thermal-state stabilises with time, consider Figure 6.6 where the oil temperature (TOIL) serves as a proxy parameter for overall thermal-state and shows a similar asymptotic exponential increase as EGTM.

Extending on the use of TOIL as indicator of the thermal-state of the engine, the distributions of the recorded TOIL for all OW and TC CF6-80E1 snapshots are compared in Figure 6.7. Although certainly not solid proof, as expected the distributions suggest that engines are typically hotter during TC snapshot recording given the difference of μ(TOIL). Additionally the scatter of the OW TOIL distribution is larger, which suggests that the thermal state of the engine during OW snapshot recording is also subject to larger cycle-to-cycle variations.

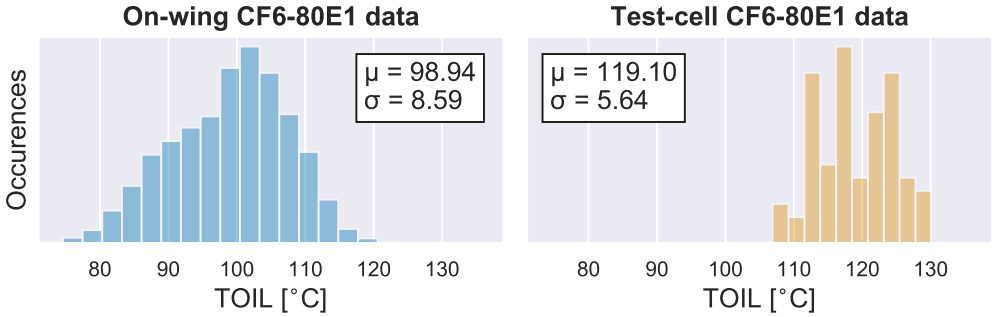

Figure 6.7: Distributions of TOIL values for OW snapshots (left) and official TC snapshots (right) from CF6-80E1 fleet

Modern turbofans – including the CF6-80 family – are fitted with Active Clearance Control, which is used to minimise turbine tip clearances by actively regulating cooling of the HPT and LPT casings for optimal *shrinkage*. Given ACC's finite reaction time and the destructive consequences of *over-shrinking* the casings, it is believed that ACC is only active during cruise when the engine is thermally stable. Unfortunately, the manuals only mention that HPTACC and LPTACC are scheduled – among others – with N1, N2, EGT and ambient conditions.

Active-clearance control potentially contributes to $\Delta\mathrm{EGTM}_{\mathrm{OW-TC}}$ because its scheduling during thermal stabilisation in the test-cell could amplify the aforementioned thermal effects of EGTM. Since no separate TC mode exists for ACC's control-schedule, any potential contribution to $\Delta\mathrm{EGTM}_{\mathrm{OW-TC}}$ needs to be related to the different OW and TC snapshot-timing.

Figure 6.8 plots the time-wise variation of HPTACC and LPTACC from the same continuous TC data. LPTACC is only related to N1 within the figure's time-frame. HPTACC is probably EGT- or N2-controlled, given that its actuator position stabilises with a similar timescale as EGT and N2. This

is further backed by the fact that the OW snapshot EGT, N2 and HPTACC distributions are similarly shaped. Quantifying the precise contribution of HPTACC to the thermal effects is beyond the scope of this research, nevertheless it is expected that the effectiveness of ACC in minimising tip clearances will increase during engine heat-up therefore amplifying the thermal effects.

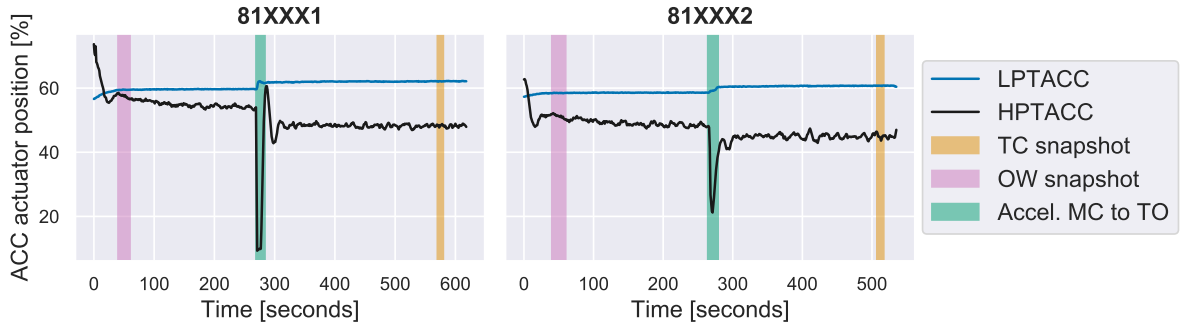

Figure 6.8: Continuous variation of ACC actuator positions during two separate CF6-80E1 test-run examples performed at KLM's facility

To conclude, snapshot-timing differences have been identified to contribute to $\Delta\mathrm{EGTM}_{\mathrm{OW-TC}}$ as the engine's thermal-state is not in equilibrium during OW snapshots. Based on the 2 examples, it can concluded that the thermal effects on EGTM are unpredictable, hence contributing to OW EGTM and $\Delta\mathrm{EGTM}_{\mathrm{OW-TC}}$ scatter. Furthermore it was found that HPTACC position is coupled to the thermal effects during heat-up.

A larger number of continuous datasets need to be analysed to draw statistical conclusions on the contribution of thermal effects to the average and scatter of $\Delta\mathrm{EGTM}_{\mathrm{OW-TC}}$, which will conservatively be assumed to be -8.75°C and 1.25°C based on just these examples.

Finally, it is recommended for future research to use GSP's heat transfer modelling functionality to extend the CF6-80C2 model and subsequently simulate the effects as well. The recent introduction of Continuous Engine Operating Data (CEOD) with newer engine models does open up possibilities for new research on thermal effects as well.

6.3. Effect of seal run-in on EGT margin

The principle of turbomachinery sealing was introduced in Subsection 2.1.2, whereas the related phenomena of seal break-in or run-in was identified as a potential cause for the observed baseline discrepancy in Subsection 3.3.2. The goal of this section is to assess the contribution of seal run-in to the OW-TC EGTM discrepancy.

6.3.1. Seal run-in phenomena & practices

All previously addressed potential root causes resulted from operational differences, while seal run-in is the only potential cause for the discrepancy that results from a difference between TC and OW engine condition. In other words, seal run-in is related to *a change of the engine condition* and all other potential causes are related to *a change of how the engine is used*. The description below discusses how the engine conditions changes due to seal run-in.

A shop visit where at least part of the workscope is tailored to improve the engine's thermodynamic performance, often specifically the performance of the high pressure components, is generally defined as a performance overhaul. Replacement of the abradable honeycomb material used for interstage labyrinth seals if commonly included in performance overhaul workscopes, primarily because it is a relatively straightforward and cost-effective task that is guaranteed to improve performance [24].

When the honeycomb material is replaced, the seal teeth will cut channels in the honeycomb over the first approximately 10 cycles, whereby clearances and leakage flows tend to rapidly increase. Afterwards rubbing between the teeth and honeycomb only happens very occasionally and hence the clearances *stabilise*. Seal run-in is expressed by an initial rapid degradation of EGTM before the rate

of deterioration stabilises. That effect is often amplified by initial deterioration of other parts such as newly applied thermal-coatings.

The official TC EGTM value should preferably be representative of the OW EGTM after seal run-in, such that KLM and its clients can predict the expected time-on-wing. Therefore TC EGTM calculations – already presented in Section 4.1 – use a different EGT limit for TC and OW operation to account for initial losses and thermal effects. That difference is −15°C for CF6-80E1A3. The previous section revealed that up to 10°C of that difference can be allocated to thermal effects. This subsection includes a data-driven assessment of the impact of seal run-in.

6.3.2. Data analysis

The focus of this research on OW-related potential causes for $\Delta\mathrm{EGTM}_{\mathrm{OW-TC}}$ among others stems from the initial lack of data for analysis of thermal and seal run-in effects. Later in the research it was discovered that official TC performance logs include a boolean *seal run-in* parameter that indicates if a seal run-in phase was included in the performance acceptance test. The subsequent analysis is based on the premise that this seal run-in parameter can be used to split the data into installations following performance overhaul, including seal replacement, and less intensive maintenance, excluding seal replacement.

Figure 6.9 once more provides the adjusted distribution of $\Delta\mathrm{EGTM}^{\mathrm{ow}}_{\mathrm{OW-TC}}$ including the effect of the customised corrections for the CF6-80E1, albeit split between installations with (left) and without (right) replaced seals. A distinct difference between $\mu(\Delta\mathrm{EGTM}^{\mathrm{ow}}_{\mathrm{OW-TC}})$ is observed, with as expected lower values for installations with replaced seals and hence seal run-in. The low number of CF6-80E1 installations without replaced seals follows from the fact that its maintenance is typically performance-driven.

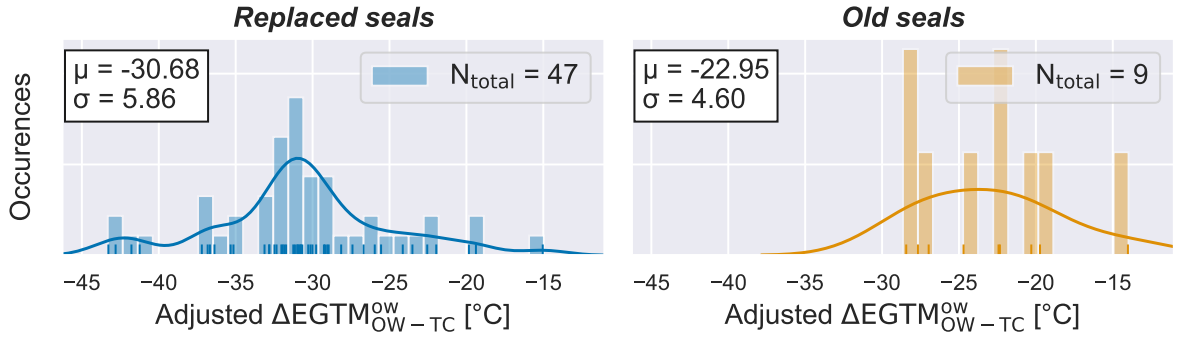

Figure 6.9: Comparison of distributions of updated OW-TC EGTM discrepancy from CF6-80E1 fleet, split between installations with (left) and without (right) seal replacement

The fleet-average effect of seal run-in on initial EGTM degradation is visualised in Figure 6.10 for both the CF6-80E1 and CF6-80C2. Although the statistical value of the CF6-80E1 data is limited, the figure suggests an average difference up to −6°C after 50 cycles whereof the majority can be attributed to the first 10 cycles. Combined with the thermal effects between −7.5°C and −10°C from Section 6.2, these values reconcile with the −15°C difference between OW and TC EGT limit to account for seal run-in and thermal effects.

However, studying installation-specific seal run-in effects reveals their unpredictability. For example, Figure 6.11 shows EGTM degradation of 10 CF6-80E1 installations that did receive seal-replacement. Furthermore the distribution of seal run-in effects for all CF6-80E1 installations is provided in Figure 6.12, where the distributed value is the difference between the cycle 11-20 average and cycle 1 EGTM.

To conclude, the average predicted contribution is −4.4°C, which reconciles with GE's TC and OW EGT limit adjustment if thermal effects are also considered. Based on the distribution in Figure 6.10 it is predicted that the contribution of seal run-in to the scatter of the OW-TC EGTM difference ($\sigma(\Delta\mathrm{EGTM}_{\mathrm{OW-TC}})$) is approximately 4.6°C. Therefore seal run-in is a main root cause for the OW-TC EGTM discrepancy.

For future research on seal run-in it is recommended to assess if the initial EGTM loss can be predicted better by distinguishing different levels of performance overhaul workscopes. If sufficient

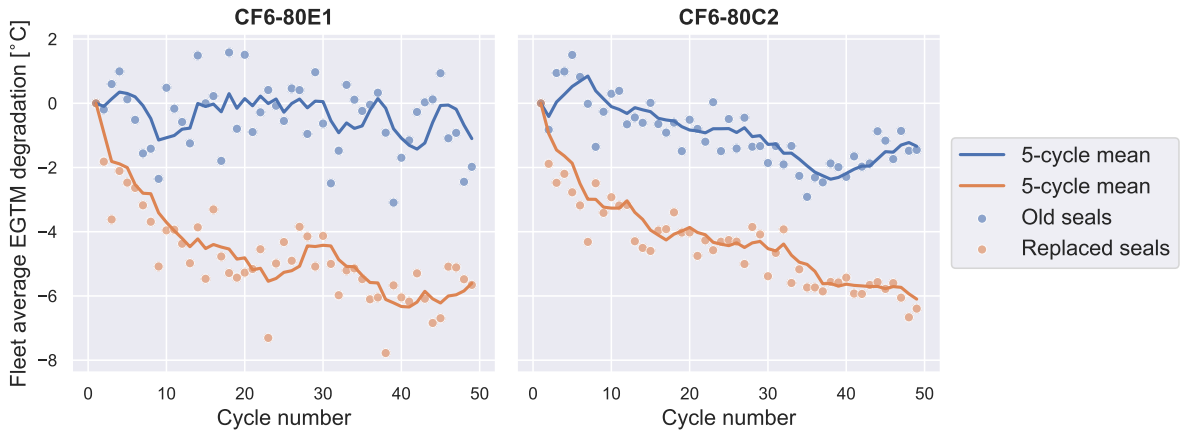

Figure 6.10: Average post-overhaul EGTM degradation of complete CF6-80E1 and CF6-80C2 fleet split between with (left) and without (right) seal replacement

data can be collected, machine-learning could also be used to identify patterns between the seal run-in effects and component or engine workscope-levels.

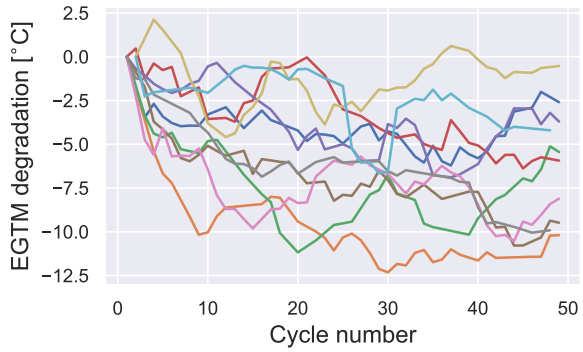

Figure 6.11: Post-overhaul EGTM degradation of 10 example CF6-80E1 installations with replaced seals

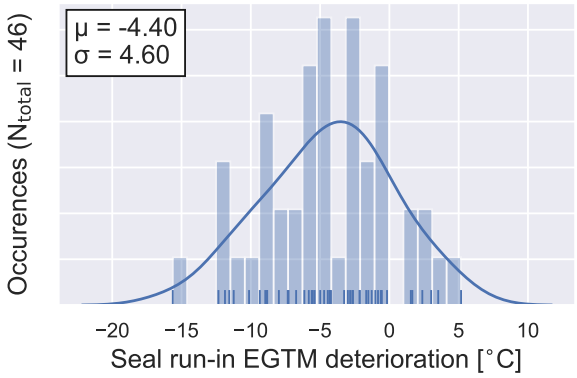

Figure 6.12: Distribution of installation-specific seal run-in EGTM deterioration (cycle 11-20 w.r.t. cycle 1) from CF6-80E1 fleet

6.4. Remaining potential causes

Several of the potential causes for OW-TC EGTM differences mentioned in Section 3.3 have so far not been accounted for, either because the related effects are assumed negligible or because a lack of data. These causes are briefly addressed below.

Unsteady ambient conditions

Given that the OW TO performance snapshot is recorded between 40s and 60s after TO power is selected, the ambient and inlet conditions are unsteady from the perspective of the engine due to aircraft acceleration and climbing. In order to quantify the related effects on engine performance, several N1-controlled transient and steady-state series simulations with the CF6-80C2 GSP model were performed for different representative and extreme TO flight envelopes. This analysis is addressed more elaborately in Appendix D.

With a maximum discrepancy between simulated transient and steady-state EGT of 0.1°C, it was concluded that the transient ambient conditions have negligible impact on the EGTM. The rate-of-change of the inlet conditions is concluded to be negligible compared to the transient reaction-time of the turbofan.

Inlet & flow distortion
Phenomena like inlet lip separation and atmospheric distortion can affect the effective inlet pressure and contribute to the unsteady nature of OW operation. However, experimental and simulated studies of flow distortion have concluded that the influence on gas path temperatures – and hence EGTM – is negligible [38, 54].

Given the use of a bell-mouth inlet during performance testing, the OW inlet geometry is distinctly different. GE accounts for the installation differences with the test-cowling adjustment ($\Delta\mathrm{EGT}_{\mathrm{cowl}}$). The values of that adjustment cannot be validated based on the available data.

In Subsection 5.4.5 on condensation effects it was concluded that the capture ratio (A0/A1) is larger than 1, which is a prerequisite for inlet lip separation and hence separation can affect inlet pressure recovery (PT2/PT0). Since total temperature is theoretically unaffected [41], EGTM is theoretically also unaffected. This is further substantiated by the lack of any correlation between aircraft Mach, PT2 and EGTM in the data.

Sensors
Noise and bias of the EGT and N1 sensors are unlikely to contribute to $\Delta\mathrm{EGTM}_{\mathrm{OW-TC}}$ because the same sensors are used during TC and OW operation, furthermore drift will have negligible effect because the compared snapshots are only a maximum of 21 cycles apart. The specific characteristics of KLM's TC TT2-sensor are accounted for with the facility modifier for EGT (EGTFM).

However aircraft-to-aircraft variation of the TT0-sensors characteristics could affect OW EGTM given that OW inlet temperature corrections are based on the aircraft's TT0 measurements. Quantifying the contribution hereof to $\Delta\mathrm{EGTM}_{\mathrm{OW-TC}}$ is impossible with the currently available data. Given that confidentiality issues make tracking down the required aircraft details a time-consuming process, research on the aircraft TT0-sensors left as an recommendation.

In order to illustrate the considerable potential impact of aircraft-to-aircraft sensor differences consider the following brief examples.

- If a CF6-80E1 takes off at 30°C with an actual 30°C EGT margin, than a -1°C TT0-sensor bias will result in a -2.5°C shift of the reported EGTM based on the average customised temperature correction exponent (XT) of 0.91. Therefore aircraft-to-aircraft and aircraft-to-TC sensors differences can have notable impact on $\mu(\Delta\mathrm{EGTM}_{\mathrm{OW-TC}})$ and $\sigma(\Delta\mathrm{EGTM}_{\mathrm{OW-TC}})$.
- Closer inspection of the correlation testing results in Figure 2.7 on page 2.7 reveals that the EGTK difference between the indoor and outdoor facility maximises at approximately 10°C. Given that this difference is expected to stem primarily from the TT2-sensor differences, it is demonstrate that the TT2-sensor can have a considerable effect on the reported EGTM.

6.5. Discussion of results
At this point all of the potential causes for the OW-TC EGTM differences that were mentioned in Section 3.3 have been addressed. Therefore the objective of this section is to do a side-by-side comparison of the observed and predicted distribution of the OW-TC EGTM differences and conclude whether the observed average value and variance can be accounted for.

This side-by-side comparison will be based on $\Delta\mathrm{EGTM}^{\mathrm{ow}}_{\mathrm{OW-TC}}$ and $\Delta\mathrm{EGTM}^{\mathrm{hybrid}}_{\mathrm{OW-TC}}$ including the application of the customised N1K-, AH- and TT2-corrections from Section 5.5 and the adjustments for data faults from Section 5.2. As a reminder, the definitions of these discrepancies are:

$\Delta\mathrm{EGTM}^{\mathrm{ow}}_{\mathrm{OW-TC}}$ The difference between the cycle 11-20 average OW EGTM and the OW-method-based TC EGTM. That OW-method-based TC EGTM is calculated by applying the customised OW EGTM calculations on the official TC measurements.

$\Delta\mathrm{EGTM}^{\mathrm{hybrid}}_{\mathrm{OW-TC}}$ The difference between the cycle 11-20 average OW EGTM and the hybrid-method-based TC EGTM. That hybrid-method-based TC EGTM is calculated by applying the customised OW EGTM calculations with the addition of the facility modifier (EGTFM), cowling correction ($\Delta\mathrm{EGT}_{\mathrm{cowl}}$) and TC condensation correction (CEGT and CN1) on the official TC measurements.

The distributions of both discrepancy definitions for all CF6-80E1 installations are provided in Figures 6.13 and 6.14. The standard deviation, a measure of the unpredictability of the performance discrepancy, is 6.3°C for both definitions. The average values are −29.4°C and −31.9°C.

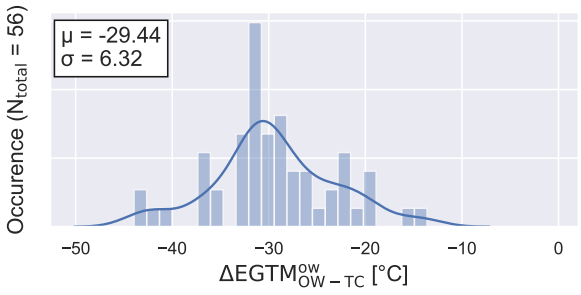

Figure 6.13: Distribution of adjusted OW-TC EGTM discrepancy from CF6-80E1 fleet using the OW-method-based TC EGTM

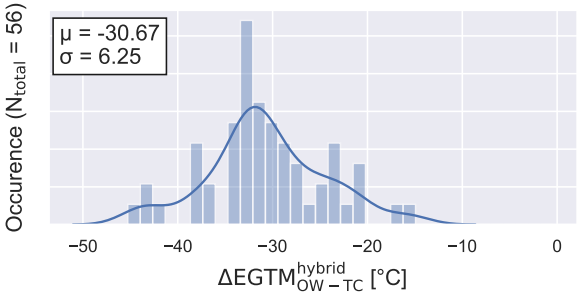

Figure 6.14: Distribution of adjusted OW-TC EGTM discrepancy from CF6-80E1 fleet using the hybrid-method-based TC EGTM

Concerning the predicted discrepancy, below a chronological recap is provided of the conclusions on the contributions of all investigated potential causes including the actual predicted contribution where applicable. Understandably those predicted values are merely indicators of the expected magnitude of the impact on $\Delta\mathrm{EGTM}_{\mathrm{OW-TC}}$ given that scattered nature of the underlying data and limitations of the analysis methods and CF6-80C2 GSP model.

- ***TC condensation:*** As was discussed in Section 4.3, correcting for condensation is non-trivial given the unpredictability. The impact of the official TC corrections on the official TC EGTM is distributed with μ = 1.5°C and σ = 0.6°C. It is unknown if the used method accurately accounts for TC condensation, but if the corrections are inaccurate it is expected that the resulting effects on $\Delta\mathrm{EGTM}_{\mathrm{OW-TC}}$ will be of the same magnitude.

- ***Facility modifier & cowling adjustment:*** The actual combined impact of EGTFM and $\Delta\mathrm{EGT}_{\mathrm{cowl}}$ on TC EGTM was studied in Section 4.4. Within the operating range spanned by the CF6-80E1 acceptance tests included in this research, that impact was revealed to be almost constant such the impact on $\sigma(\Delta\mathrm{EGTM}_{\mathrm{OW-TC}})$ in case on inaccuracies is negligible. Whether the corresponding magnitude accurately captures the average difference between OW and indoor TC operation is unknown and cannot be determined other than comparing indoor and outdoor test results for EGTFM or outdoor and OW test results for $\Delta\mathrm{EGT}_{\mathrm{cowl}}$.

- ***Throttle setting, humidity and inlet temperature:*** The potential effects of N1K, AH and TT2 are accounted for by application of the corresponding engine installation-specific customised OW EGTM corrections as discussed in Section 5.6. Furthermore it was already concluded in Section 6.1 that their combined contribution to the OW-TC discrepancy primarily resulted in a negative shift of the $\Delta\mathrm{EGTM}_{\mathrm{OW-TC}}$ distributions, while the scatter was mostly unaffected.

- ***On-wing inlet condensation:*** As was discussed in Subsection 5.4.5, inlet condensation will occasionally affect OW snapshots if N1K, RH and condensing nuclei density are all high. Nevertheless no systematic correlation between EGTM and RH was identified. Given the small potential impact of condensation based on the TC condensation corrections, it was therefore concluded that OW inlet condensation is not a main root cause for either $\mu(\Delta\mathrm{EGTM}_{\mathrm{OW-TC}})$ or $\sigma(\Delta\mathrm{EGTM}_{\mathrm{OW-TC}})$.

- ***Non-gaseous water ingestion:*** The physical affects of precipitation on EGTM are very complex and unpredictable. It was however concluded in Subsection 5.4.4 that non-gaseous water ingestion has negligible influence on the distribution of $\Delta\mathrm{EGTM}_{\mathrm{OW-TC}}$, because only 6.5% of the OW snapshots is potentially affected by precipitation and no consistent correlation between EGTM of affected and unaffected snapshots could be found.

- ***Power off-take:*** It was revealed in Subsection 5.7.2 that in general the effects of PTO on EGTM were implicitly accounted for by the customised installation-specific corrections due to the underlying correlation of PTO to TT2 and N1K. Therefore PTO only affects cycle 11-20 OW EGTM if the corresponding snapshots include unusual combinations of PTO, TT2 and N1K. Nevertheless contribution to the $\Delta\mathrm{EGTM}^{\mathrm{ow}}_{\mathrm{OW-TC}}$ values will insignificant given that maximum physical effect of PTO on EGTM is in the order of 1°C.

- ***Customer bleed:*** The effects of customer bleed (WB) and Nacelle Anti-Ice (NAI) on $\Delta\mathrm{EGTM}^{\mathrm{ow}}_{\mathrm{OW-TC}}$ were predicted in Section 5.7 based on the installation-specific correlations between EGTMDEV, WB and NAI in combination with the actual WB and NAI values for cycle 11-20. It is predicted that $\mu(\Delta\mathrm{EGTM}_{\mathrm{OW-TC}})$ is shifted by +1.3°C by over-compensating WB-corrections, furthermore the predicted impact on $\sigma(\Delta\mathrm{EGTM}_{\mathrm{OW-TC}})$ is negligible. For NAI the contributions to $\mu(\Delta\mathrm{EGTM}_{\mathrm{OW-TC}})$ and $\sigma(\Delta\mathrm{EGTM}_{\mathrm{OW-TC}})$ are predicted to be -0.1°C and 0.2°C.

- ***Thermal effects:*** Section 6.2 addressed the effect of thermal stabilisation on the reported EGTM using continuous TC data. Given that only 2 continuous datasets were available, the statistical value of the results is limited. Nevertheless, it was revealed that recording a performance snapshot *after* instead of *during* thermal stabilisation results in a 7.5°C to 10.0°C increase of EGTM. Therefore it can at least be concluded that thermal effects contribute to both $\mu(\Delta\mathrm{EGTM}_{\mathrm{OW-TC}})$ and $\sigma(\Delta\mathrm{EGTM}_{\mathrm{OW-TC}})$. Accurately predicting the impact to $\sigma(\Delta\mathrm{EGTM}_{\mathrm{OW-TC}})$ specifically, requires insight in the average thermal state of the engine during the OW cycle 11-20 snapshots. For the subsequent side-by-side comparison a conservative 1.25°C contribution is assumed.

- ***Seal run-in:*** Alternative to all other potential causes, seal run-in and its impact on $\Delta\mathrm{EGTM}_{\mathrm{OW-TC}}$ is related to changes of the engine condition as was discussed in Section 6.3. The initial cycle 1-10 EGTM degradation due to seal run-in varies considerably from engine-to-engine, which is also expected to contribute considerably to $\sigma(\Delta\mathrm{EGTM}_{\mathrm{OW-TC}})$ with a predicted impact of 4.6°C. The impact of seal-run to $\mu(\Delta\mathrm{EGTM}_{\mathrm{OW-TC}})$ is predicted to be -4.4°C.

- ***Unsteady inlet conditions:*** The effect of unsteady inlet conditions, either caused by the changing ambient conditions or inlet-related effects, were not extensively investigated within this research. As is discussed in Section 6.4 their impact on OW-TC EGTM differences is assumed to be negligible based on the literature research and several transient GSP simulations.

- ***Sensors:*** The impact of gas path sensors on $\Delta\mathrm{EGTM}_{\mathrm{OW-TC}}$ is expected to be negligible since the OW and TC snapshots are both recorded with those same sensors and only a maximum of 21 cycles apart. As was briefly illustrated in Section 6.4, the aircraft-to-aircraft differences in terms of the ambient total temperature (TT0) sensor can potentially have considerable impact on OW EGTM and therefore $\Delta\mathrm{EGTM}_{\mathrm{OW-TC}}$. Nevertheless the TT0-sensors were not investigated.

The combined discrepancy distribution based on the above mentioned individual predicted contributions can be predicted by assuming normal distribution probability theory, where the sum of the $\mu(\Delta\mathrm{EGTM}_{\mathrm{OW-TC}})$ contributions and the root sum square (RSS) of the $\sigma(\Delta\mathrm{EGTM}_{\mathrm{OW-TC}})$ contributions represent the combined μ and σ.

Following those calculations, the predicted $\Delta\mathrm{EGTM}_{\mathrm{OW-TC}}$ distribution can be summarised by $\mu \approx -12.0$°C and $\sigma \approx 4.8$°C. Given that most of the contributions are not perfectly normally distributed, the results merely serve as an indicator for the predicted magnitudes.

Regarding the average, the primary contributors are clearly the thermal effects and seal run-in. The predicted -12.0°C is almost consistent with the -15°C difference between the TC and OW EGT limit that GE applies to account for those key contributors. However, the majority of the difference between OW and TC EGTM is still unaccounted for given $\mu(\Delta\mathrm{EGTM}^{\mathrm{hybrid}}_{\mathrm{OW-TC}}) = -31.9$°C.

By checking off all the potential causes that were proven to be insignificant or were already quantified with reasonable accuracy, it can be concluded that the significant gap of approximately -19.9°C must primarily be contributed to the combination of: 1) inaccurate facility modifier (EGTFM); 2) inaccurate cowling adjustment ($\Delta\mathrm{EGT}_{\mathrm{cowl}}$); and 3) inaccurate aircraft TT0-measurements. Furthermore, over-compensation by the TC condensation correction might also contribute slightly, but the maximum

contribution thereof is 1.5°C.

Regarding the standard deviation, the primary contributor is clearly seal run-in. The observed standard deviation of $\Delta\mathrm{EGTM}_{\mathrm{OW-TC}}$ is 6.3°C, therefore a considerable part of the observed scatter is not accounted for given the predicted 4.8°C.

It is expected that aircraft-to-aircraft TT0-sensor differences potentially add considerably because a 1°C TT0-sensor bias can shift the reported OW EGTM with several degrees. Furthermore, the contribution of the thermal effects is expected to be larger than the assumed 1.25°C based solely on two examples. Other causes that can decrease the gap between predicted and observed $\sigma(\Delta\mathrm{EGTM}_{\mathrm{OW-TC}})$ are inaccurate TC condensation corrections, occasional OW condensation effects and PTO.

7

Conclusion & Recommendations

This research stems from the discrepancy between on-wing (OW) and test-cell (OW) turbofan corrected performance indicators observed at KLM Engine Services, despite the extensive corrections used to account for operating conditions and OW- and TC-related installation losses.

The corresponding research objectives are therefore: 1) to identify the root causes for the observed OW-TC corrected performance discrepancy; and 2) to assess the feasibility of reducing OW-TC performance differences by improving and extending the corresponding corrections.

The research is specifically focussed on the Exhaust Gas Temperature (EGT) and its corrected margin (EGTM) of KLM's GE CF6-80E1 turbofan fleet. The resulting research conclusions and the recommendations for further research are addressed in the subsequent sections.

7.1. Conclusions

This conclusions section is structured into paragraphs, starting with the conclusions regarding the definition of OW-TC EGTM discrepancy and the fleet-wide distribution of its values. Then the conclusions on the individual potential causes are addressed followed with the comparison of the combined predicted and observed discrepancy distribution. Lastly the conclusions concerning the feasibility of reducing the OW-TC differences are discussed.

Observed on-wing to test-cell differences

The discrepancy is defined by OW EGTM with respect to TC EGTM, therefore negative values suggest performance loss from TC to OW. It was decided to base the OW-TC EGTM comparison ($\Delta\mathrm{EGTM}_{\mathrm{OW-TC}}$) on: 1) the cycle 11-20 average OW EGTM; and 2) an alternative TC EGTM where the official measurements are corrected with the OW EGTM method. With that definition $\Delta\mathrm{EGTM}_{\mathrm{OW-TC}}$ can be fully attributed to physical or operational differences. Subsequently those differences can be individually analysed and compared with the corresponding corrections included in the official TC EGTM calculations where applicable.

The original distribution of $\Delta\mathrm{EGTM}_{\mathrm{OW-TC}}$ is characterised by a -21.8°C average ($\mu(\Delta\mathrm{EGTM}_{\mathrm{OW-TC}})$) and 7.3°C standard deviation ($\sigma(\Delta\mathrm{EGTM}_{\mathrm{OW-TC}})$). That distribution was also adjusted by the application of customised engine-specific corrections that were developed as part of this research. The updated discrepancy is characterised by $\mu(\Delta\mathrm{EGTM}_{\mathrm{OW-TC}})$ = -29.4°C and $\sigma(\Delta\mathrm{EGTM}_{\mathrm{OW-TC}})$ = 6.3°C.

Analysis of individual causes

Following a thorough literature research, a comprehensive list of potential causes for the discrepancy was composed. Regarding the individual causes the following conclusions were drawn:

- ***Inlet & Flow distortion:*** Inlet pressure recovery and flow distortion do affect engine performance in terms of thrust and compressor stability, nevertheless based on previous research in open literature it is concluded that the impact on EGTM is negligible.
- ***Test-cell inlet condensation:*** The official TC EGTM calculations include a correction for the adverse effects of condensation, which on average adjusts the TC EGTM by -1.5°C. However, it is

concluded that the correction probably occasionally compensates without actual condensation occurring because condensation is unpredictable and prerequisites such as sufficient condensing nuclei concentration are neither measured or used as input for the correction.

- ***Facility modifier (FM) & cowling adjustment*** **($\Delta\mathrm{EGT}_{\mathrm{cowl}}$):** An empirical FM is used to account for operational differences between indoor and outdoor testing. Subsequently performance is theoretically corrected to equivalent OW performance with $\Delta\mathrm{EGT}_{\mathrm{cowl}}$. The accuracy of the magnitude of the adjustments cannot be quantified, but it is concluded that their contribution to $\sigma(\Delta\mathrm{EGTM}_{\mathrm{OW-TC}})$ is case of inaccuracies is still insignificant.

- ***Throttle setting (N1K):*** The official OW EGTM calculations are unable to capture the deterioration-induced engine-to-engine variation of the physical EGT-N1K relation, resulting in undesired, residual EGTM-N1K correlations and non-conservative values. Based on the customised engine-specific corrections that were developed as part of this research, it is concluded that the impact on $\mu(\Delta\mathrm{EGTM}_{\mathrm{OW-TC}})$ was +6.5°C. Application of those custom corrections reduced the impact of N1K on the updated $\mu(\Delta\mathrm{EGTM}_{\mathrm{OW-TC}})$ and $\sigma(\Delta\mathrm{EGTM}_{\mathrm{OW-TC}})$ to negligible levels.

- ***Absolute humidity (AH) and inlet temperature (TT2):*** The official OW EGTM calculations non-conservatively assume dry conditions because humidity is not measured during OW operation. To bypass the missing AH data, airport weather data was successfully merged with OW data. The observed correlation between EGTM and AH in the original data is engine-dependent and considerably weaker than expected based on theory and simulations. It was concluded that the effect of AH is masked by the correlated and opposite impact of inaccurate TT2-correcting due to engine-to-engine variations.

  By application of the proposed customised engine-specific corrections, which include AH- and TT2-related terms, the effects of AH and TT2 on the updated discrepancy distribution were eliminated. It was also concluded that inaccurate TT2 and missing AH-corrections were responsible for a +6.0°C shift of original $\mu(\Delta\mathrm{EGTM}_{\mathrm{OW-TC}})$.

- ***On-wing inlet condensation:*** It was concluded based on simulations that occasional OW inlet condensation is probable, if the prerequisites of high power setting, high ambient relative humidity and sufficient condensing nuclei density are met. Pinpointing the affected snapshots is impossible given the unpredictable nature and the minor impact if condensation occurs. Furthermore, no consistent correlation between relative humidity and EGTM was found in the updated data.

- ***Non-gaseous water ingestion:*** It was concluded that non-gaseous water ingestion has negligible influence on the distribution of $\Delta\mathrm{EGTM}_{\mathrm{OW-TC}}$, because only 6.5% of the OW snapshots is potentially affected by precipitation and no consistent correlation between EGTM of affected and unaffected snapshots could be found. The physical affects of precipitation on EGTM are furthermore very complex and unpredictable.

- ***Power off-take (PTO):*** The contribution of PTO to original $\Delta\mathrm{EGTM}_{\mathrm{OW-TC}}$ is inconsistent due to inaccurate N1K- and TT2-corrections, but based on simulations in the order of -1.5°C. The customised corrections for N1K, AH and TT2 implicitly also account for PTO-related effects due to a correlation between PTO, N1K and TT2. Therefore the impact of PTO on the updated $\Delta\mathrm{EGTM}_{\mathrm{OW-TC}}$ distribution is negligible.

- ***Customer bleed (WB):*** Both customer bleed (WB) and nacelle anti-ice (NAI) are theoretically corrected for, nevertheless due to an over-compensating WB-correction and an under-compensating NAI-correction the combined impact on $\mu(\Delta\mathrm{EGTM}_{\mathrm{OW-TC}})$ is +1.3°C. The contribution to the variance of $\Delta\mathrm{EGTM}_{\mathrm{OW-TC}}$ is negligible.

- ***Thermal effects:*** An OW snapshot is recorded shortly after spooling-up while the TC snapshot is recorded after full thermal stabilisation. Thermal stabilisation is accompanied by an increase of EGTM due to decreasing clearances, which is amplified by the increasing effectiveness of turbine Active Clearance Control. Based on limited continuous TC data, it was concluded that the lack of thermal stabilisation during OW operation contributes to $\mu(\Delta\mathrm{EGTM}_{\mathrm{OW-TC}})$ with up to -10°C and to $\sigma(\Delta\mathrm{EGTM}_{\mathrm{OW-TC}})$ with at least 1.25°C. Given the small dataset, the statistical value of these numbers is limited.

- ***Seal run-in:*** The effectiveness of new seals quickly deteriorates over the initial OW cycles, therefore in contrast to all other potential causes seal run-in effects result from a change of engine condition instead of operational changes. Seal run-in results in a drop of EGTM during the initial OW cycles which is unpredictable and engine-specific. It was concluded that the contribution of seal run-in to $\mu(\Delta\mathrm{EGTM}_{\mathrm{OW-TC}})$ is -4.4°C and to $\sigma(\Delta\mathrm{EGTM}_{\mathrm{OW-TC}})$ is 4.6°C. Therefore seal run-in is without a doubt a main root cause for the performance differences between OW and TC.
- ***Sensors:*** Both OW and TC snapshots are measured with the engine's dedicated sensors, therefore bias, noise or drift of those sensors will not contribute to $\Delta\mathrm{EGTM}_{\mathrm{OW-TC}}$. The exception is the inlet temperature (TT2) sensor. The specific characteristics of the TC TT2-sensor are accounted for by the facility modifier. On-wing TT2-correction is based on sensors at the nose of the aircraft such that bias and drift of those sensors affect OW EGTM and $\mu(\Delta\mathrm{EGTM}_{\mathrm{OW-TC}})$. Aircraft-to-aircraft differences of those sensors will also contribute to $\sigma(\Delta\mathrm{EGTM}_{\mathrm{OW-TC}})$. Although the exact contribution was not quantified, a 1°C TT2-sensor bias changes the reported EGTM with 2.5°C.

Comparison of observed and predicted on-wing to test-cell differences
Given the conclusions on the impact of the individual causes on $\mu(\Delta\mathrm{EGTM}_{\mathrm{OW-TC}})$ and $\sigma(\Delta\mathrm{EGTM}_{\mathrm{OW-TC}})$, the combined predicted $\Delta\mathrm{EGTM}_{\mathrm{OW-TC}}$ distribution was derived on the basis of normal distribution probability theory and compared with the observed values. Since most contributions are not perfectly normally distributed, the resulting values are only indicative.

- The predicted $\mu(\Delta\mathrm{EGTM}_{\mathrm{OW-TC}})$ is -12.0°C, where thermal effects and seal run-in are concluded to be the primary contributors. That magnitude was found to reconcile with the official TC adjustment of -15°C that should account for EGTM losses related to seal run-in and lack of thermal stabilisation. Nevertheless, given that the observed $\mu(\Delta\mathrm{EGTM}_{\mathrm{OW-TC}})$ is -29.4°C it is concluded that much of the average difference is unaccounted for. By including the official effect of facility modifiers, cowling adjustment and TC condensation correction, $\mu(\Delta\mathrm{EGTM}_{\mathrm{OW-TC}})$ is even shifted to -31.9°C. It is expected that the aircraft TT2-sensors, facility modifier and cowling adjustment are responsible for the remaining unexplained gap.
- The predicted and observed $\sigma(\Delta\mathrm{EGTM}_{\mathrm{OW-TC}})$ are 4.8°C and 6.3°C, with seal run-in as most significant contributor. It is first of all expected that the aircraft-to-aircraft TT2-sensor bias differences will contribute to $\sigma(\Delta\mathrm{EGTM}_{\mathrm{OW-TC}})$, which is not included in the current prediction. Also the contribution of thermal effects on $\sigma(\Delta\mathrm{EGTM}_{\mathrm{OW-TC}})$ is expected to be larger than is currently accounted for. Lastly, it is not ruled out that some of the OW-related causes that were deemed insignificant, occasionally have measurable impact on the cycle 11-20 average EGTM.

Reducing on-wing to test-cell differences
The current official OW EGTM calculations are generic and do not take into account engine-to-engine variations stemming from deterioration and maintenance differences. It was concluded that the inherent inability of generic corrections to capture engine-specific aero-thermodynamic trends results in undesired residual correlations between EGTM and the parameters it is corrected for.

Towards achieving the second objective – assessing the feasibility to reduce OW-TC EGTM differences by improving corrections – a part of the research was dedicated to improving OW EGTM calculations. The resulting method is based on the addition of an absolute humidity (AH) correction and data-driven, engine-specific optimisation of throttle (N1K) and temperature (TT2) corrections. The corresponding conclusions are:

- Merging airport weather data with OW TO snapshots is an effective method to circumvent the missing OW absolute humidity sensor. Inaccuracies stemming from the assumptions that absolute humidity (AH) is constant between weather reports and unaffected by the minor altitude differences were concluded to be insignificant.
- Engine-specific aero-thermodynamic behaviour changes during an installation period due to deterioration and OW maintenance, nevertheless it was concluded that shapes of the underlying physical relations is largely preserved. Therefore assuming constant customised corrections per installation period already produced significant EGTM scatter reductions. The final optimisation was performed based on the initial 500 cycles per engine installation. More advanced methods such as cycle-specific corrections were identified, but left for future research.

- It was revealed that the majority of optimised EGT-N1K relations for the N1K correction reconcile with expectations. For some specific installation periods a questionable decrease of the EGT-N1K gradient was observed at high N1K, which was concluded to originate from the snapshots with high N1K and PTO
- The fleet-average optimised humidity correction gradient reconciles with TC EGTM calculations and simulations, but the width of its distribution is beyond the expectations. The increased scatter probably stems from mutual smearing of AH- and TT2-related effects on EGTM because TT2 and AH are strongly correlated.
- The application of the customised corrections achieved a significant 28.8% reduction of OW EGTM standard deviation, with individual installation period results up to 58.6%. That reduction is accompanied by an average decrease of OW EGTM of 11.1°C, explained by the non-conservative inaccurate and missing original corrections. It can be concluded that the customised corrections successfully eliminated EGTM correlations to N1K, AH and TT2.
- The updated OW-TC EGTM discrepancy distribution was shifted by -8.0°C, but its standard deviation was only reduced by 10%. It is concluded that the proposed customised corrections slightly improve OW-TC EGTM comparability. Hence N1K, AH and TT2 are not main root causes for the variance of $\Delta\mathrm{EGTM}_{\mathrm{OW-TC}}$.
- The identified root causes for $\sigma(\Delta\mathrm{EGTM}_{\mathrm{OW-TC}})$ – seal run-in, thermal effects and aircraft sensor bias – are unpredictable given the currently available data. Therefore no corresponding corrections can be composed and further reduction of $\sigma(\Delta\mathrm{EGTM}_{\mathrm{OW-TC}})$ for improved OW-TC EGTM comparability is concluded to be currently infeasible.
- Closing the gap between predicted and observed $\mu(\Delta\mathrm{EGTM}_{\mathrm{OW-TC}})$ is feasible, but requires further investigation of the expected contributors to that gap such as the facility modifier, cowling adjustment and aircraft TT2-sensors.

7.2. Recommendations

Similar to the conclusions, the recommendations are split into paragraphs, first the recommendations concerning the research to identify the root causes for the OW-TC EGTM discrepancy are discussed. Afterwards the recommendations regarding the improvements made to the OW EGTM calculations are addressed.

Identification of causes for on-wing to test-cell differences

- ***CF6-80C2 GSP model:*** The CF6-80C2 GSP model was used extensively to support the analysis of individual causes. At the same time several limitations of the model itself were identified. The corresponding recommendations are:
  - To check the validity of the constant conditions assumption and if needed re-tune the maps with data from an engine and time period with negligible deterioration.
  - To check if the model was tuned with shunted or unshunted EGT values and if needed re-tune with unshunted, physical EGT values
  - To consider replacing the model design point with a CF6-80CB1F instead of CF6-80C2A5 performance test snapshot
  - To consider tuning of engine-specific models, given it was concluded earlier that engine-to-engine variations are significant
  - To include speed line relocating and speed line morphing in the tuning process
  - To identify the origin of the significant over-estimation of customer bleed effects
- ***Test-cell inlet condensation:*** Given the unpredictable nature of the condensation phenomena, current TC condensation corrections are expected to occasionally adjust EGTM non-conservatively. Therefore it is recommended to perform additional research to assess the accuracy of the TC condensation corrections and their impact on $\Delta\mathrm{EGTM}_{\mathrm{OW-TC}}$. For example, side-by-side comparison

of continuous engine data with corresponding video-material of the inlet condensation could help identify relations or signatures.

- ***Facility modifier (FM):*** Although it was established that potential FM inaccuracies will not contribute to $\sigma(\Delta\mathrm{EGTM}_{\mathrm{OW-TC}})$, they are expected to contribute significantly to $\mu(\Delta\mathrm{EGTM}_{\mathrm{OW-TC}})$. In order to assess the accuracy it is recommended to do additional research. Some proposed steps are in-depth TC trending analysis and quantification of the cumulative effect of back-to-back testing. A full re-correlation of KLM's test-cell can eliminate inaccurate FM altogether.
- ***On-wing inlet condensation:*** Accurate corrections are concluded to be infeasible, nevertheless some recommendations to improve assessment of its impact are made. For better statistical analysis of condensation effects, it is recommended to extend the method used for merging weather data with engine data. It is also recommended to assess if the discrepancy between the aircraft's TT2 measurement and nacelle's TT12 measurement could be used to identify if a snapshot is affected by condensation.
- ***Thermal effects:*** The effects of the thermal state of the engine were identified as a main contributor to $\mu(\Delta\mathrm{EGTM}_{\mathrm{OW-TC}})$ and $\sigma(\Delta\mathrm{EGTM}_{\mathrm{OW-TC}})$ based on the limited available continuous TC data. It is therefore recommended to improve the statistical value of the results by extending the number of datasets. Furthermore the introduction of Continuous Engine Operating Data (CEOD) from OW operation with the latest engine types opens up a lot of possibilities to assess and eliminate thermal effects.
- ***Seal run-in:*** Within the scope of this research, seal run-in was briefly studied and identified as an unpredictable contributor to $\mu(\Delta\mathrm{EGTM}_{\mathrm{OW-TC}})$ and $\sigma(\Delta\mathrm{EGTM}_{\mathrm{OW-TC}})$. It is recommended to assess if the initial EGTM loss can be predicted better by distinguishing different levels of performance overhaul workscopes. If sufficient data can be collected, machine-learning could also be used to identify patterns between the seal run-in effects and component or engine workscope-levels.
- ***Sensors:*** No efforts were put on investigation of the characteristics of the aircraft's temperature sensors used for the TT2-correction, primarily because confidentiality issues make tracking down the required details a time-consuming process. Given that the effects of aircraft TT2-sensor bias are expected to contribute to both $\mu(\Delta\mathrm{EGTM}_{\mathrm{OW-TC}})$ and $\sigma(\Delta\mathrm{EGTM}_{\mathrm{OW-TC}})$, it is evidently recommended to assess the precise characteristics of the applicable sensors.

Improved on-wing corrections for EGT margin

- ***EGTM deviation:*** EGTMDEV is defined as the deviation of the current EGTM value to the expected EGTM value, hence eliminating the time-variant effects of deterioration and OW maintenance. It was used extensively during the research to quantify correlations and its standard deviation was used as objective function for the data-driven optimisation of the engine-specific customised corrections. Within this research the expected EGTM value is defined as the 21-cycle, centred Simple Moving Average (SMA). It is recommended to consider more complex definitions such as weighted moving average, exponential moving average or Kalman-filtering.
- ***Temperature correction:*** Similar to the official OW EGTM calculations, the customised TT2-corrections are based on a single correction exponent (XT) over the complete operating range. It recommended to assess if a N1K-dependent XT, for instance using a polynomial, can improve the quality of the correction without over-fitting.
- ***Humidity correction:*** Given the risk of *smearing* physically TT2-related effects onto the custom AH-correction, it is recommended to test the alternative where a single, generic AH-correction gradient is optimised simultaneously with the engine-specific N1K- and TT2-corrections in a multi-level optimisation. Although AH-related effects were proven to dependent slightly on engine-condition, it was concluded that the current results include a questionably wide distribution of optimised AH-correction gradients.
- ***Safety factor:*** The customised corrections were developed as an improvement and extension of current official OW EGTM calculations. Those calculations include two terms with unknown physical meaning that are expected to serve as safety factors, among others because assuming dry

conditions is fundamentally non-conservative. It is recommended to assess the possibility of dropping those terms from the customised corrections because a safety factor is no longer applicable.

- ***Extensions:*** Although the resulting OW EGTM scatter reduction is already significant, the current effort to improve OW EGTM calculations primarily serves as a proof of concept for the potential of engine-specific corrections for on-wing performance monitoring. Therefore it is recommended to extend the scope of the customised corrections by including parameters such as customer bleed flow and power off-take. Not only will OW EGTM scatter be further reduced, the underlying relations will also represent the physical relations more accurately by eliminating the risk of mutual *smearing* of effects.
- ***Adaptive corrections:*** If the custom corrections were to be used for engine condition monitoring – where the accuracy of the most recent reported EGTM value is critical –, it is recommended to develop adaptive custom corrections. By re-evaluating the underlying relations for each new cycle based on a fixed number of previous cycles, the physical significance of the current reported EGTM value is maximised.

Bibliography

[1] IATA. Traveler numbers reach new height. https://www.iata.org/pressroom/pr/Pages/2018-09-06-01.aspx, 2018. Accessed: 2019-09-21.

[2] M. Verbist. *Gas path analysis for enhanced aero-engine condition monitoring and maintenance*. PhD thesis, Delft University of Technology, 2017.

[3] R. Kurz and K. Brun. Degradation in gas turbine systems. *Journal of Engineering for Gas Turbines and Power*, 123(1):70–77, 11 2000. ISSN 0742-4795. doi: 10.1115/1.1340629. URL https://doi.org/10.1115/1.1340629.

[4] S. Ogaji, S. Sampath, R. Singh, and S.D. Probert. Parameter selection for diagnosing a gas-turbine's performance-deterioration. *Applied Energy*, 73:25–46, 09 2002. doi: 10.1016/S0306-2619(02)00042-9. URL https://doi.org/10.1016/S0306-2619(02)00042-9.

[5] L. Marinai, D. Probert, and R. Singh. Prospects for aero gas-turbine diagnostics: A review. *Applied Energy*, 79:109–126, 09 2004. doi: 10.1016/j.apenergy.2003.10.005.

[6] J. Kurzke. Model based gas turbine parameter corrections. *Turbo Expo: Power for Land, Sea, and Air*, Volume 1: Turbo Expo 2003:91–99, 06 2003. doi: 10.1115/GT2003-38234. URL https://doi.org/10.1115/GT2003-38234.

[7] R.N. Parfitt and M. Bristow. Derivation of aerodynamic thrust correction for an indoor gas turbine engine test facility using the first principles anemometer method. *Internation Congress of Aeronautical Sciences*, 25, 09 2006. URL https://www.icas.org/ICAS_ARCHIVE/ICAS2006/PAPERS/543.PDF.

[8] A.J. Volponi. Gas turbine parameter corrections. *Journal of Engineering for Gas Turbines and Power*, 121(4):613–621, 10 1999. ISSN 0742-4795. doi: 10.1115/1.2818516. URL https://doi.org/10.1115/1.2818516.

[9] R.J. Meijer. KLM Engine Services - Test-cell facility operations manual, 2013. Restricted document.

[10] General Electric Aviation. CF6-80C2 engine shop manual, January 2018. Restricted document.

[11] General Electric Aviation. CF6-80E1 engine shop manual, September 2017. Restricted document.

[12] EASA. CF6-80E1 - Type-certificate data sheet IM.E.007. Technical report, EASA, June 2004.

[13] FAA. CF6-80C2 - Type-certificate data sheet E13N1. Technical report, FAA, August 2009.

[14] General Electric Aviation. CF6-80E1 operating instructions (99382, rev. 8), December 2015. Restricted document.

[15] W.P.J. Visser. *Generic analysis methods for gas turbine engine performance*. PhD thesis, Delft University of Technology, 2015.

[16] S. El Bouazzaoui. Modeling of a GSP diagnostic tool for the CFM56-7B engines. Master's thesis, Delft University of Technology, 2008.

[17] C.C. Tonino. Analysis of post-overhaul engine performance at KLM Engine Services. Master's thesis, Delft University of Technology, 2013.

[18] D.M. den Haan. GSP gas path analysis on CF6-80 engines at KLM Engine Services. Master's thesis, Delft University of Technology, 2010.

[19] M.P.R. Van Moorselaar. Gas path analysis on the GEnx-1B at KLM Engine Services. Master's thesis, Delft University of Technology, September 2018.

[20] K. Geris. CFM56-7B post-overhaul performance issues. Master's thesis, Delft University of Technology, 2010.

[21] P. Lironi. CF6-80C2 engine history and evolution. Technical report, GE, 2007.

[22] GE. CF6-80E1: Past, present and future. Technical report, GE, 2006.

[23] P.P. Walsh and P. Fletcher. *Gas Turbine Performance*. Blackwell Science Ltd, 2 edition, 2004. ISBN 0123266505. doi: 10.1037/023990.

[24] R.E. Chupp, R.C. Hendricks, S.B. Lattime, and B.M. Steinetz. Sealing in turbomachinery. *Journal of Propulsion and Power*, 22:313–349, August 2006. doi: 10.2514/1.17778. URL https://ntrs.nasa.gov/search.jsp?R=20060051674. NASA/TM-2006-214341.

[25] T. Rootliep. KLM Engine Services test-cell - CFM56-7B N2 seizures, 2018. Restricted internship report.

[26] M.L. Verbist, W.P.J. Visser, and J.P. van Buijtenen. Experience with gas path analysis for on-wing turbofan condition monitoring. *Journal of Engineering for Gas Turbines and Power*, 136(1): 011204–1 – 011204–8, 2014. ISSN 0742-4795. doi: 10.1115/1.4025347.

[27] A.J. Volponi. Gas turbine engine health management: Past, present and future trends. *Journal of Engineering for Gas Turbines and Power*, 136(05):051201–1 – 051201–20, 2014. ISSN 0742-4795. doi: 10.1115/GT2013-96026. URL http://proceedings.asmedigitalcollection.asme.org/proceeding.aspx?doi=10.1115/GT2013-96026.

[28] N. Aretakis, I. Roumeliotis, A. Alexiou, C. Romesis, and K. Mathioudakis. Turbofan engine health assessment from flight data. *Journal of Engineering for Gas Turbines and Power*, 137(4):041203–1 – 041203–8, 2015. ISSN 0742-4795. doi: 10.1115/1.4028566. URL http://gasturbinespower.asmedigitalcollection.asme.org/article.aspx?doi=10.1115/1.4028566.

[29] S. Ackert. Engine maintenance management - Managing technical aspects of leased assets. Technical report, Jackson Square Aviation, 2015.

[30] S. Krause. Further investigation of engine performance loss, in particular exhaust gas temperature margin, in the CF6-80C2 jet engine and recommendations for test cell modifications to record additional criteria. Master's thesis, Hamburg University of Applied Sciences, August 2011.

[31] A. Giampaolo. *Gas Turbine Handbook: Principles and Practices*. The Fairmont Press, 3 edition, 2006. ISBN 0-88173-515-9.

[32] C. Justin, E. Garcia, and D. Mavris. Aircraft valuation: A network approach to the evaluation of aircraft for fleet planning and strategic decision making. *AIAA Aviation Technology, Integration, and Operations (ATIO) Conference*, 10, September 2010. doi: 10.2514/6.2010-9061. URL https://arc.aiaa.org/doi/abs/10.2514/6.2010-9061.

[33] M.W. Wiseman and T.H. Guo. An investigation of life extending control techniques for gas turbine engines. *Proceedings of the 2001 American Control Conference. (Cat. No.01CH37148)*, 5:3706 – 3707, June 2001. doi: 10.1109/ACC.2001.946211.

[34] General Electric Aviation. KLM Airlines test cell correlation for CF6-80E1 model engines, April 2006. Restricted document.

[35] SAE Aerospace. RP741B - Turbofan and turbojet gas turbine engine test cell correlation. Technical report, SAE, 2002.

[36] SAE Aerospace. ARP5758 - Trend analysis for maintaining correlation of gas turbine engine test cells. Technical report, SAE, 2011.

[37] SAE Aerospace. AIR5026A - Test cell instrumentation. Technical report, SAE, 2011.

[38] SAE Aerospace. AIR1419 - Inlet total-pressure-distortion considerations for gas-turbine engines. Technical report, SAE, 1983.

[39] CFM International. CFM56-7B engine shop manual, July 2018. Restricted document.

[40] H.I.H. Saravanamuttoo, G.F.C. Rogers, and H. Cohen. *Gas Turbine Theory*. Pearson Education, 5 edition, 2001. ISBN 9780130158475.

[41] J. Kurzke and I. Halliwell. *Propulsion and Power*. Springer International Publishing, 2018. ISBN 9783319759777. doi: 10.1007/978-3-319-75979-1.

[42] J.J. Ballough. AC43-207 - Correlation, operation, design, and modification of turbofan & jet engine test cells. Technical report, FAA, 2002.

[43] P.A. Beishuizen. Improving compressor maps of the GE CF6-80C2 engine. Master's thesis, Delft University of Technology, 2012.

[44] J. Bird and W. Grabe. Humidity effects on gas turbine performance. *Turbo Expo: Power for Land, Sea, and Air*, 2: Aircraft Engine; Marine; Microturbines and Small Turbomachinery, June 1991. doi: 10.1115/91-GT-329. URL https://doi.org/10.1115/91-GT-329.

[45] J.B. Young. Condensation in jet engine intake ducts during stationary operation. *Journal of Engineering for Gas Turbines and Power*, 117(2):227 – 236, 1995. URL http://www.asme.org/about-asme/terms-of-use.

[46] AGARD. AR-332 - Recommended practices for the assessment of the effects of atmospheric water ingestion on the performance and operationability of gas turbine engines. Technical report, AGARD, 1995.

[47] H. Hanachi, J. Liu, A. Banerjee, and Y. Chen. Effects of humidity condensation on the trend of gas turbine performance deterioration. *Journal of Engineering for Gas Turbines and Power*, 137(12): 122604–1 – 122604–11, 2015. ISSN 0742-4795. doi: 10.1115/1.4030815.

[48] K. Mathioudakis and T. Tsalavoutas. Uncertainty reduction in gas turbine performance diagnostics by accounting for humidity effects. *Journal of Engineering for Gas Turbines and Power*, 124(10): 801 – 808, 2002. ISSN 07424795. doi: 10.1115/1.1470485.

[49] B.D. Fishbeyn and N.V. Pervyshin. Determination of the effect of atmospheric humidity on the characteristics of a turbofan engine. *News of Institutions of Higher Learning - Aeronautical Engineering*, 2:112 – 118, December 1967. Title, journal and content translated to English by I. Heenan from Foreign Technology Division.

[50] J.C. Samuels and B.M. Gale. Technical note 2119 - Effect of humidity on performance of turbojet engines. Technical report, NACA, June 1950.

[51] Challenge of measuring inlet humidity on combustion turbines. https://www.vaisala.com/en/case/challenge-measuring-inlet-humidity-combustion-turbines, 2012. Accessed: 2019-01-08.

[52] T. Nikolaidis. *Water ingestion effects on gas turbine engine performance*. PhD thesis, Cranfield University, 2008.

[53] T. Nikolaidis and P. Pilidis. The effect of water ingestion on an axial flow compressor performance. *Proceedings of the Institution of Mechanical Engineers, Part G: Journal of Aerospace Engineering*, 228(3):411–423, 2014. ISSN 20413025. doi: 10.1177/0954410012474421.

[54] J. Kurzke. Effects of inlet flow distortion on the performance of aircraft gas turbines. *Journal of Engineering for Gas Turbines and Power*, 130(7):041201–1 – 041201–7, 2008. ISSN 07424795. doi: 10.1115/1.2901190.

[55] A.F. El-Sayed and M.S. Emeara. Aero-engines intake: A review and case study. *Journal of Robotics and Mechanical Engineering Research*, 1(3):35–42, 2016. ISSN 20594909. doi: 10.24218/jrmer.2016.15.

[56] S. Farokhi. *Aircraft Propulsion*. John Wiley & Sons Ltd, 2 edition, 2017. ISBN 9781118806777.

[57] F.S. Mirza-Baig and H.I.H. Saravanamuttoo. Off-design performance prediction of turbofans using gasdynamics. *International Gas Turbine and Aero-Engine Congress and Exposition*, 91-GT389 (6):1 – 8, 1991.

[58] N.U. Rahman and J.F. Whidborne. A numerical investigation into the effect of engine bleed on performance of a single-spool turbojet engine. *Proceedings of the Institution of Mechanical Engineers, Part G: Journal of Aerospace Engineering*, 222(7):939–949, 2008. ISSN 09544100. doi: 10.1243/09544100JAERO389.

[59] A.J. Yuhas and R.J. Ray. Effects of bleed air extraction on thrust levels of the f404-ge-400 turbofan engine. *AIAA Joint Propulsion Conference*, 28(7):1 – 12, 1992.

[60] K. Mathioudakis and A. Tsalavoutas. Effects of anti-icing system operation on gas turbine performance and monitoring. *Proceedings of ASME Turbo Expo: Power for Land, Sea, and Air*, 3:1 – 8, 2001.

[61] A.B. Evans. Contractor report 179447 - The effects of compressor seventh-stage bleed air extraction on performance of the F100-PW-220 afterburning turbofan engine. Technical report, NASA, 1991.

[62] J.D. Brooks. A methodology for capturing the impacts of bleed flow extraction on compressor performance and operability in engine conceptual design. Master's thesis, Georgia Institute of Technology, 2015.

[63] S.L. Koutz, R.V. Hensley, and F.E. Rom. Technical note 2202 - Effect of heat and power extraction on turbojet-engine performance III - Shaft-power extraction. Technical report, NACA, 1950.

[64] J.W. Bird, J.D. MacLeod, and M.F. Mulligan. Investigation of engine thrust correlation methods for enclosed test cells. *Turbo Expo: Power for Land, Sea, and Air*, Volume 2: Aircraft Engine; Marine; Microturbines and Small Turbomachinery, June 1991. doi: 10.1115/91-GT-068. URL https://doi.org/10.1115/91-GT-068. V002T02A002.

[65] G.L.B. Ramos. Study of a test cell for commercial jet engines. Master's thesis, Instituto Superior Tecnico Lisbon, July 2016.

[66] M. Marx, M. Kotulla, A. Kando, and S. Staudacher. Comparison and synthesis of performance and aerodynamic modeling of a pass-off turbofan engine test cell. *Turbo Expo: Power for Land, Sea, and Air*, Volume 1: Aircraft Engine; Fans and Blowers; Marine, June 2015. doi: 10.1115/GT2015-43525. URL https://doi.org/10.1115/GT2015-43525. V001T01A025.

[67] A. Al-Alshaikh. An experimental and numerical investigation of the effect of aero gas turbine test facility aspect ratio on thrust measurement. Master's thesis, Cranfield University, August 2011.

[68] H.I.H. Saravanamuttoo. AR-245 - Recommended practices for measurement of gas path pressures and temperatures for performance assessment of aircraft turbine engines and components. Technical report, AGARD, 1990.

[69] Y.G. Li. Performance-analysis-based gas turbine diagnostics: A review. *Proceedings of the Institution of Mechanical Engineers*, 216(July):363–377, 2002.

[70] L.A. Urban. *Gas Turbine Engine Parameter Interrelationships*. Hamilton Standard Division of United Aircraft Corporation, 1 edition, 1967.

[71] A. Stamatis, K. Mathioudakis, and K.D. Papailiou. Adaptive simulation of gas turbine performance. *Journal of Engineering for Gas Turbines and Power*, 112(2):168–175, April 1990. ISSN 0742-4795. doi: 10.1115/1.2906157. URL https://doi.org/10.1115/1.2906157.

[72] T.U.J. Grönstedt. Identifiability in multi-point gas turbine parameter estimation problems. *Turbo Expo: Power for Land, Sea, and Air*, Volume 2: Turbo Expo 2002, Parts A and B:9–17, June 2002. doi: 10.1115/GT2002-30020. URL https://doi.org/10.1115/GT2002-30020.

[73] H. Asgari, X. Chen, and R. Sainudiin. Considerations in modelling and control of gas turbines — a review. *International Conference on Control, Instrumentation and Automation*, 2:84–89, Dec 2011. doi: 10.1109/ICCIAutom.2011.6356635.

[74] N. Aretakis, K. Mathioudakis, and A. Stamatis. Nonlinear engine component fault diagnosis from a limited number of measurements using a combinatorial approach. *Journal of Engineering for Gas Turbines and Power*, 125(7):642 – 650, 2003. ISSN 07424795. doi: 10.1115/1.1582494.

[75] J. Kurzke and C. Riegler. A new compressor map scaling procedure for preliminary conceptional design of gas turbines. *Turbo Expo: Power for Land, Sea, and Air*, Volume 1: Aircraft Engine; Marine; Turbomachinery; Microturbines and Small Turbomachinery, May 2000. doi: 10.1115/2000-GT-0006. URL https://doi.org/10.1115/2000-GT-0006. V001T01A006.

[76] S. Van Vuuren. Humidity effects on turbo-fan performance in an MRO context. Master's thesis, Delft University of Technology, December 2019.

[77] B. Lambiris, K. Mathioudakis, A. Stamatis, and K. Papailiou. Adaptive modeling of jet engine performance with application to condition monitoring. *Journal of Propulsion and Power*, 10(6): 890–896, 1994. doi: 10.2514/3.23828. URL https://doi.org/10.2514/3.23828.

[78] P.T. Tsilingiris. Thermophysical and transport properties of humid air at temperature range between 0 and 100°c. *Energy Conversion and Management*, 49(5):1098 – 1110, May 2008. ISSN 0196-8904. doi: https://doi.org/10.1016/j.enconman.2007.09.015. URL http://www.sciencedirect.com/science/article/pii/S0196890407003329.

[79] A.L. Buck. New equations for computing vapor pressure and enhancement factor. *Journal of Applied Meteorology*, 20(12):1527–1532, 1981. doi: 10.1175/1520-0450(1981)020<1527:NEFCVP>2.0.CO;2. URL https://doi.org/10.1175/1520-0450(1981)020<1527:NEFCVP>2.0.CO;2.

[80] W. Brutsaert. On a derivable formula for long-wave radiation from clear skies. *Water Resources Research*, 11(5):742–744, October 1975. doi: 10.1029/WR011i005p00742. URL https://agupubs.onlinelibrary.wiley.com/doi/abs/10.1029/WR011i005p00742.

[81] A.D. Culf, J.H.C. Gash, and M.V.K. Sivakumar. Daily patterns of dew-point temperature in a semiarid climate. *Agricultural and Forest Meteorology*, 68(1):107 – 111, March 1994. ISSN 0168-1923. doi: https://doi.org/10.1016/0168-1923(94)90072-8. URL http://www.sciencedirect.com/science/article/pii/0168192394900728.

[82] Radiocommunications Sector. P.8365-6 - Test bed calibration trending brochure. Technical report, International Telecommunication Union, December 2017.

[83] S.B. Lattime and B.M. Steinetz. Turbine engine clearance control systems: Current practices and future directions. *2002 NASA Seal/Secondary Air System Workshop*, 1:113–134, September 2003. URL https://ntrs.nasa.gov/search.jsp?R=20040000621. NASA/CP—2003-212458/VOL1.

[84] Gangoli, a.r. Delft University of Technology Brightspace, 2019. Accessed: 2019-03-11.

[85] CFM56 trend interpretation presentation. Technical report, CFMI, 2005.

[86] Y G Li, P Pilidis, and M A Newby. An adaptation approach for gas turbine design-point performance simulation. *Journal of Engineering for Gas Turbines and Power*, 128(10):789 – 795, 2006. ISSN 07424795. doi: 10.1115/1.2136369.

[87] M Draper, H Howard, and Y Piet. PPR 1474 - Test bed calibration trending brochure. Technical report, Rolls-Royce, 2007.

A

Test-cell calculations for corrected thrust (FNK)

Demonstrating that sufficient corrected thrust (FNK) is delivered by the engine is the primary objective of performance acceptance testing. Furthermore the delivered thrust margin (FNM), which is the difference between measured FNK and the minimum rated thrust (FNK_{rated}), is used to determine the fan speed modifier (N1MOD) that the engine will be installed with.

That N1MOD slightly lowers the physical fan speed (N1) for a given indicated fan speed (N1i) such differential thrust between engines is eliminated. Given that effective the rated fan speed (N1K) is adjusted, a non-zero N1MOD level is accompanied by an EGTM adjustment as well. Given that the N1MOD level is constant over a full install period and applies to the both OW and TC EGTM, it does not contribute to OW-TC EGTM differences.

Nevertheless, for the interested reader this appendix addresses the official TC FNK calculations in similar fashion as Section 4.1 on the official EGTK, EGTM and N1Kc calculations.

Similarly to the definitions of N1Kc and N1K from Subsection 4.1.3, there is the option to distinguish the *fully* and *basic* corrected thrust. Since there is no use for the basic corrected thrust, only the fully corrected thrust is addressed and referred to as FNK. The definition for FNK is provided in Equation A.1.

$$\mathrm{FNK} = \mathrm{FN_{net}} \cdot \left(\frac{1}{\delta_{2,\mathrm{SD}}} \right) \cdot \mathrm{HFN} \cdot \mathrm{FNFM} + \Delta\mathrm{FN_{cowl}} + \Delta\mathrm{FN_{\Delta N1K}} \tag{A.1}$$

Where:

FN_{net} The net measured thrust, which is defined as the net force exerted by the engine along its own centreline. Thrust load cell calibration defines the numeric conversion of the strain gauge measurements to FN_{net} [37].

HFN The Absolute Humidity (AH) correction factor, defined as a function of AH by linearly interpolating HFN for the measured AH in the AH correction factor table. Since that humidity decreases thrust, the correction to dry conditions increases FNK (i.e. HFN > 1 if AH > 0). Thrust is not corrected for condensation effects because it is not affected by effective TT2. As is mentioned and substantiated in Section 4.2, it is concluded that the effects of AH on FNK are primarily accounted for via the FNK throttle push correction ($\Delta\mathrm{FNK_{\Delta N1K}}$). The contribution of HFN is negligible compared to the AH-related additional $\Delta\mathrm{FNK_{\Delta N1K}}$.

FNFM The thrust facility modifier, defined as a polynomial function of FNK excluding the contribution of FNFM, $\Delta\mathrm{FN_{cowl}}$ and $\Delta\mathrm{FN_{\Delta N1K}}$. The coefficients of the polynomial function are determined empirically similarly as discussed for EGTFM in Subsection 4.1.1. Theoretically FNFM should always be larger than one because it corrects for the indoor testing related drag forces, which is confirmed by all correlation reports at KLM ES.

$\mathbf{\Delta FN_{cowl}}$ The test cowling adjustment, defined as a function of N1Kc by linearly interpolating $\Delta \mathrm{FN}_{\mathrm{cowl}}$ for the actual N1Kc in the test cowling correction factor table. Where FNFM corrects for facility-specific effects to enable comparability between indoor and outdoor testing, the test cowling correction corrects for test cowling effects to enable comparison with OW operation. The magnitude of $\Delta \mathrm{FN}_{\mathrm{cowl}}$ increases with N1Kc.

$\mathbf{\Delta FN_{\Delta N1K}}$ The throttle push adjustment, defined as a function of ΔN1K by linearly interpolating values at the actual N1Kc and $\mathrm{N1K}_{\mathrm{rated}}$ in the throttle push correction table and determining the difference. The throttle push correction principle is already discussed in Subsection 4.1.1 for $\Delta \mathrm{EGT}_{\Delta \mathrm{N1K}}$. Intuitively FNK increases with N1Kc, therefore if N1Kc < $\mathrm{N1K}_{\mathrm{rated}}$ then $\Delta \mathrm{FN}_{\Delta \mathrm{N1K}} > 0$ and vice versa.

B

Reverse-engineering of on-wing EGT margin calculations

The correction equations and tables for OW EGTM calculations are considered confidential by GE and therefore not disclosed to their clients. Therefore considerable efforts were made to reverse-engineer the unknown equations and tables based on the data.

This appendix first of all discusses the overall methodology and subsequently provides an accessible example to visualise the method.

Methodology

The reverse-engineering problem is equivalent to curve fitting and can be formulated as an error minimisation problem. The Root Mean Square Error (RMSE) was chosen to serve as the minimisation objective function, defined according to Equation B.1 where N_{data} equals the number of data points, and EGTM_{RE} and $\text{EGTM}_{\text{official}}$ are the reverse-engineered and official EGTM.

$$\text{RMSE} = \sqrt{\sum_{1}^{N_{\text{data}}} \frac{\left(\text{EGTM}_{\text{RE},i} - \text{EGTM}_{\text{official},i}\right)^2}{N_{\text{data}}}} \tag{B.1}$$

Given that the to-be determined EGTM calculations are deterministic, perfect fit (RMSE = 0) is theoretically possible if the mathematical formulation of the fitting function is compatible with the actual EGTM equations. The chosen formulations of EGTK, EGTKHD and EGTM were all based on the TC EGTM calculations covered in Section 4.1 of the main report, although all humidity-related terms were discarded for the absence of corresponding measurements.

The initial curve-fitting results indicated residual correlations between the error and parameters like the status of anti-ice bleed systems. Therefore the mathematical formulation of the EGTM equations and the related empirical correction tables were iteratively adjusted to eliminate error correlations and hence improve the overall fitting quality.

The next section shows the tuning process of the throttle push (EGT-N1K) correction table for OW EGTM as an example. As is shown in Subsection 5.1.2 in main report, the final formulation also includes a constant correction factor and adjustment that were needed to achieve RMSE $\approx$ 0, but are unexplained from a physical perspective.

The actual minimisation problem was programmed in Python and solved with a gradient-based SLSQP algorithm from the optimisation library from the SciPy-package(1). The scale of the problem is demonstrated by the length of the design vector, which exceeds 40 variables for the CF6-80E1 including adjustments for various bleed systems, the temperature correction exponent (XT) and an array of EGT values for the throttle push correction table.

The final results converged to RMSE values in the order of 1×10^{-5} and are can therefore be considered the mathematical equivalent of the unknown official calculations. It is not guaranteed that the

(1)URL: `https://docs.scipy.org/doc/scipy/reference/generated/scipy.optimize.minimize.html`

GE's official EGTM calculations have the exact same formulation. Some adjustments can be applied either in the EGKT, EGTKHD or EGTM equation, which results in slightly different values in the underlying tables, among others due to application of the SF on EGTKHD and EGTM.

Example: throttle push correction table

The throttle push correction is used to adjust the measured EGT from actual to rated N1K ($N1K_{rated}$). The throttle push correction is based on tabulated combinations of N1K and EGT. The adjustment ($\Delta EGT_{\Delta N1K}$) is derived by evaluating EGT at the rated and observed N1K using linear interpolation on the table and subsequently adding the difference to EGTK. That difference represents how much the engine is expected to heat up if it were accelerated to exactly $N1K_{rated}$.

Focussing on reverse-engineering the throttle push corrections, the variables were: 1) the N1K values in the table; and 2) the corresponding EGT values in the table. The former were iteratively adjusted, while the latter are part of the design vector passed to the SLSQP algorithm. Since the absolute EGT values could not be reverse-engineered, it was decided to tabulate the adjustment $\Delta EGT_{\Delta N1K}$ itself directly with respect to N1K. An equality constraint was used to assure a zero adjustment at $N1K_{rated}$.

Table B.1 shows the final results in terms of the N1K and optimised adjustment values in the reverse-engineered throttle push table for CF6-80C2 (with $N1K_{rated}$ = 103.3%). Intuitively, $\Delta EGT_{\Delta N1K}$ is positive if N1K < $N1K_{rated}$ and vice versa.

In order to demonstrate the iterative process of tuning the formulation of the EGTM calculation equations and tables based on previous interim results, Table B.1 also includes a column with the optimised $\Delta EGT_{\Delta N1K}$ values from interim results where the table formulation was incomplete because the row with N1K = 102% was still missing. Because the official $\Delta EGT_{\Delta N1K}$-N1K relation is slightly non-linear, the missing row makes it impossible to exactly reproduce the official calculations and the resulting RMSE is in the order of 1×10^3 higher.

Figure B.1 demonstrates how the fact that N1K = 102% was not yet included in the reverse-engineered throttle push table was recognised. By plotting the errors for the interim results with respect to N1K, it is observed that the errors are correlated to N1K. Furthermore the relation between the residual errors and N1K behaves as a linear-spline – because the throttle push table is based on linear interpolation – with *tipping points* at the even N1K percentages. The only missing even N1K percentage in the interim table formulation is 102%, therefore it was concluded that it should be included as well.

Table B.1: Reverse-engineered throttle push table for CF6-80C2

N1K [%]	**$\Delta EGT_{\Delta N1K}$ [°C]**	
	Final	*Interim*
92	116.96	116.99
94	92.08	92.12
96	69.73	69.77
98	49.35	49.40
100	30.34	30.35
102	12.13	–
104	-5.84	-5.89
106	-24.17	-24.11
108	-43.42	-43.39
110	-64.17	-64.13
RMSE	2.5e-5	2.2e-2

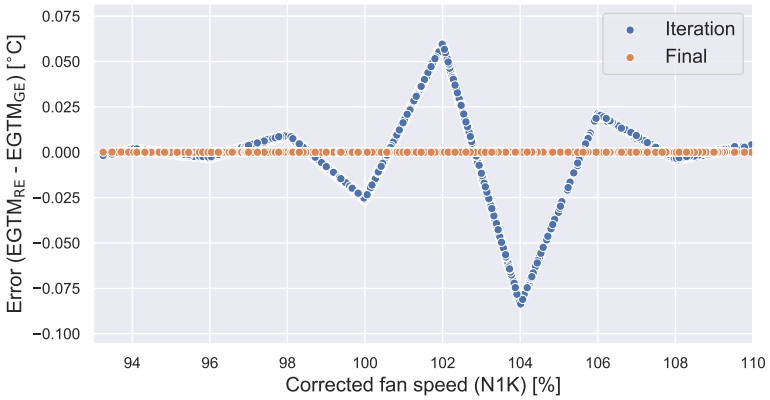

Figure B.1: Effect of incorrect throttle push table formulation – with N1K = 102% missing – on fitting error w.r.t. N1K for CF6-80C2

C

Simulated deteriorated cases

This appendix addresses the simulated deterioration cases that were used in Chapter 5 of the main report. The exact definitions of all cases are provided in Table C.1.

Table C.1: Simulated deterioration case definitions used in Chapter 5

Case	Fan core & booster		HPC		HPT		LPT	
	$\Delta\eta_{\text{is}}$	$\Delta\dot{m}_c$	$\Delta\eta_{\text{is}}$	$\Delta\dot{m}_c$	$\Delta\eta_{\text{is}}$	$\Delta\dot{m}_c$	$\Delta\eta_{\text{is}}$	$\Delta\dot{m}_c$
Baseline	0%	0%	0%	0%	0%	0%	0%	0%
Manual $\Delta\eta_{\text{is}} > 0$	1%	0%	2%	0%	2%	0%	2%	0%
Manual $\Delta\eta_{\text{is}} < 0$	-1%	0%	-2%	0%	-2%	0%	-2%	0%
Random 1	-1%	-2%	0%	0%	1%	-2%	-2%	-4%
Random 2	-1%	-2%	-3%	-6%	-3%	-6%	1%	2%
Random 3	-1%	-2%	1%	2%	-2%	4%	1%	-2%
Random 4	-1%	-2%	-1%	-2%	1%	2%	1%	-2%
Random 5	-2%	-4%	2%	4%	-1%	2%	-2%	-4%
Random 6	1%	2%	-3%	-6%	2%	4%	-2%	-4%
Random 7	1%	2%	2%	4%	-2%	-4%	-3%	6%
Random 8	-1%	-2%	-3%	-6%	-3%	-6%	0%	0%
Random 9	0%	0%	-2%	-4%	-3%	6%	0%	0%
Random 10	-1%	-2%	-2%	-4%	-2%	-4%	1%	-2%

The two noteworthy categories are:

- ***Random cases:*** 10 random cases were randomly generated in order demonstrate the effect of engine-to-engine variation on physical relations. The range and logic used for the component-level deterioration levels were based on previous research [2, 19].
- ***Manual cases:*** 2 manual cases were chosen by the author with either only positive or negative $\Delta\eta_{\text{is}}$. These cases were used to isolate the effect overall thermodynamic efficiency on physical relations by representing a consistently good or bad engine.

Although the range of assigned deterioration levels was based on previous research, it is not guaranteed that all engine-level combinations of deteriorated components are representative. For example, some cases might include a good compressor and bad turbine in terms of thermodynamic efficiency. The objective of the cases is primarily to demonstrate *if* and not *how much* physical relations depend on engine condition.

D

Unsteady inlet conditions

This appendix addresses a simulated study on the effects of unsteady inlet conditions due to aircraft acceleration and climbing. Given that the concluded impact of these effects is understandably negligible, the analysis was omitted to an appendix. The objective of the analysis described below was to proof that the effects of the changing ambient conditions is negligible.

First representative TO flight paths need to be defined, by specifying combinations of timestamp, altitude and Mach number values. In the left of Figure D.1 a scatter-plot of radar altitude (h_{radar}) with respect to Mach number (M0) for Schiphol Airport snapshots is provided. Note that h_{radar} is not included in the data and was calculated using the reported pressure altitude (h_{ISA}) and METAR altimeter setting.

Concerning the CF6-80C2 data there is a clear distinction between snapshots taken during the ground and after lift-off, despite the common believe that all snapshots are taken after lift-off. A typical rotation speed (V_r) for a Boeing 747-400 is 160 kts, or M0 = 0.24 in ISA conditions, which is in agreement with the data. The steep h_{radar}-M0 gradient for the snapshots with M0 > 0.25 can be explained by the common practice to initially climb at constant indicated airspeed (IAS) and hence almost constant Mach number. A typical speed for the initial climb (V_2) of a 747-400 is 180 kts, which corresponds to M0 = 0.28 in ISA conditions.

The CF6-80E1 data consist of a single cluster with narrower Mach number range. Clearly the A330 is able to lift-off at lower Mach numbers, which might also be contributed to the triangular flights the A330 is used for. A triangular flight, such as Amsterdam-Cartagena-Bogota-Amsterdam, often includes a short flight leg with a low TakeOff Weight (TOW) and therefore low takeoff speed, short ground run and steep initial ascend.

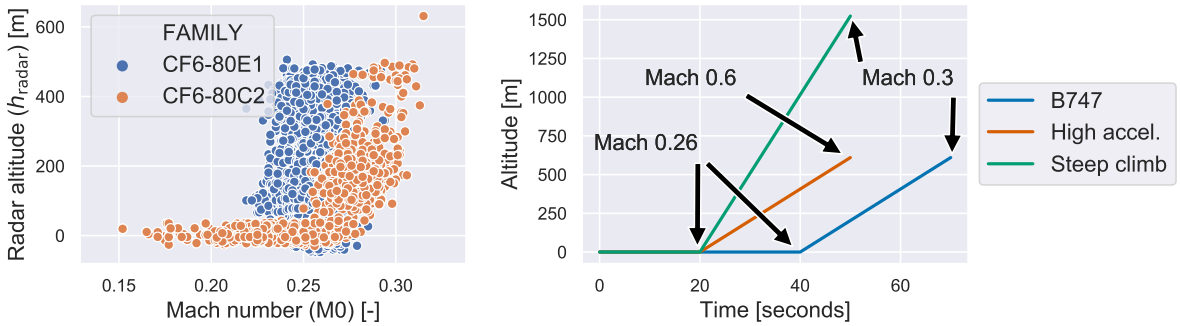

Figure D.1: Scatter-plot of h_{radar}-M0 relation for OW snapshots (left) and schematic visualisation of flight path definitions for transient analysis (right)

Based on the above analysis three to-be simulated flight paths were defined, which are visualised in the right of Figure D.1.

- ***B747:*** The baseline case, which should represent a typical 747-400 takeoff, consist of a 40s ground run towards M0 = 0.26, followed by an initial climb of 30s at a relatively high Rate Of Climb (ROC) of 4000 ft/min towards h_{radar} = 610 m (2000 ft) at M0 = 0.3.
- ***Steep climb:*** The first alternative represents a takeoff with very low TOW and an exceptionally high ROC of 10,000 ft/min, hence the aircraft accelerates to M0 = 0.26 in 20s and subsequently climbs towards 1524 m (5000 ft) at M0 = 0.3 in just 30s.
- ***High acceleration:*** The second alternative also represents a low TOW takeoff, followed with exceptional high acceleration. There is a 20s ground run with lift-off at M0 = 0.26, followed with a 30s acceleration to M0 = 0.6 at 610 m (2000 ft).

Given the three takeoff flight path cases, their definitions were used for three transient analysis in GSP with the baseline CF6-80C2 model. Other inputs included an ISA atmosphere – both its sea-level conditions as well as its variation of pressure and temperature during climbing – and a constant 100% N1.

The variation of simulated EGT for all three cases is provided in the left of Figure D.2. During the initial ground run EGT increases due to the increasing total inlet temperature (TT2). After lift-off EGT is also affected by the decreasing static ambient temperature (TS0). Regarding the representative *B747* case, the effects of climbing and acceleration almost cancel each other. For the high acceleration case the growing ram effect outweighs the TS0 decrease and vice versa for the steep climb case.

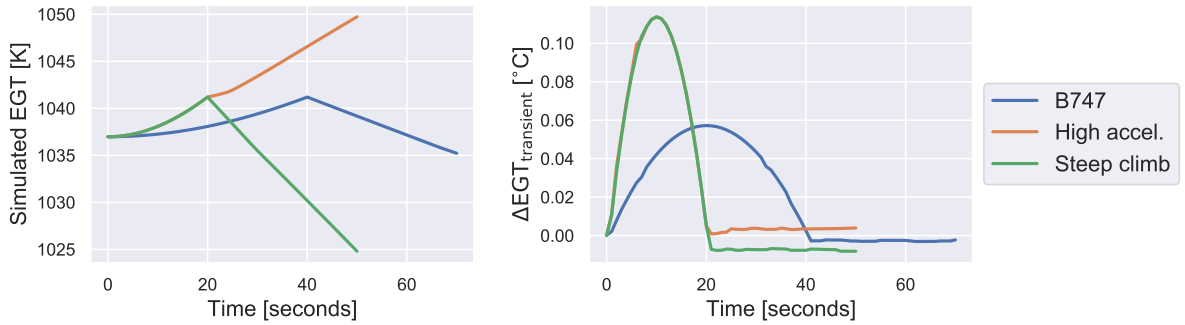

Figure D.2: Simulated transient time-dependent variation of EGT (left) and $\Delta\text{EGT}_{\text{transient}}$ (right), defined w.r.t. the steady-state EGT at equivalent operating conditions, for the TO flight paths defined in Figure D.1

.

In order to actually quantify the potential EGTM error induced by the transient conditions, an additional steady-state series simulation was performed for each flight path. These runs were programmed to simulate the engine performance for the exact same range of operating conditions as the transient analysis. Comparison of the steady-state series and transient results subsequently reveals the magnitude of the errors arising by assuming the snapshot to be taken in steady-state.

The results of that analysis are provided in the right of Figure D.2, where $\Delta\text{EGT}_{\text{transient}}$ is defined as the difference between the transient and steady-state EGT at each Mach and time combination. The first and foremost conclusion to be drawn from the plot is that the effects are negligibly small compared to the known OW EGTM scatter. Therefore, the unsteady operating conditions in terms of the aircraft climbing and acceleration are not a cause for the OW-TC EGTM discrepancy.

Physically the rate of change of the operating conditions is insignificant compared to the dynamic response time constant of the turbofan engine. The was also backed by inspection of the HPC and LPC performance map, where it was found that the transient and steady-state analysis operating points almost coincide. The latter means that the isentropic efficiency of those components and the engine as a whole is also the same.

The small variation of $\Delta\text{EGT}_{\text{transient}}$ can be attributed to the fact that the transient engine slightly lags the changing operating conditions because it cannot react instantaneously.